T NO. UMTA-MA-06-0025-75-13

VIBRATION PREDICTION MODEL FOR FLOATING - SLAB RAIL TRANSIT TRACK

J.E. Manning
D.C. Hyland
G. Tocci

AUGUST 1975
FINAL REPORT

Prepared for

U.S. DEPARTMENT OF TRANSPORTATION
URBAN MASS TRANSPORTATION ADMINISTRATION
Office of Research and Development
Washington DC 20590

TECHNICAL REPORT STANDARD TITLE PAGE

1. Report No.	2. Government Accession No.	3. Recipient's Catalog No.
UMTA-MA-06-0025-75-13		

4. Title and Subtitle	5. Report Date
VIBRATION PREDICTION MODEL FOR FLOATING-SLAB RAIL TRANSIT TRACK	August 1975
	6. Performing Organization Code

7. Author(s)	8. Performing Organization Report No.
J.E. Manning, D.C. Hyland, and G. Tocci	DOT-TSC-UMTA-75-17

9. Performing Organization Name and Address	10. Work Unit No.
Cambridge Collaborative, Inc.* 238 Main Street Cambridge MA 02142	UM504/R6747
	11. Contract or Grant No. DOT-TSC-643
	13. Type of Report and Period Covered Final Report July 1973 - June 1975
12. Sponsoring Agency Name and Address U.S. Department of Transportation Urban Mass Transportation Administration Office of Research and Development Washington DC 20590	14. Sponsoring Agency Code

15. Supplementary Notes

*Under contract to: U.S. Department of Transportation, Transportation Systems Center, Kendall Square, Cambridge MA 02142

16. Abstract

This report presents the theoretical development of a model to predict the vibration reduction by floating-slab tracks in subway tunnels. Data from a field study of a floating-slab track in New York City are also presented. The report is one of three reports prepared by Cambridge Collaborative under the UMTA Urban Rail Supporting Technology Program, dealing with noise and vibration control for urban rail transit track and elevated structures. The theoretical model described here allows for the prediction of the force transmissibility--the ratio of the amplitudes of the force on the tunnel floor and the force on the rail. Data from the field study support the use of a simple single-degree-of-freedom oscillator for predicting the vibration reduction due to the particular floating slab track that was studied. The theoretical model developed here allows predictions to be made for a more general case.

17. Key Words	18. Distribution Statement
Vibration, Mass Transit, Subway Noise, Rail Noise, Community Noise, Vibration Analysis	DOCUMENT IS AVAILABLE TO THE PUBLIC THROUGH THE NATIONAL TECHNICAL INFORMATION SERVICE, SPRINGFIELD, VIRGINIA 22161

19. Security Classif. (of this report)	20. Security Classif. (of this page)	21. No. of Pages	22. Price
Unclassified	Unclassified	142	

Form DOT F 1700.7 (8-69)

PREFACE

This report has been prepared by Cambridge Collaborative, Inc. (CC), under Contract DOT-TSC-643 as part of the Urban Rail Supporting Technology Program managed by the Transportation Systems Center, Cambridge, Massachusetts, under the sponsorship of the Rail Technology Division, Urban Mass Transportation Administration, Washington, D.C.

The authors express their gratitude to Dr. Leonard Kurzweil of TSC who provided much assistance and encouragement during preparation of this report.

The work described includes extensive field measurements on a floating-slab track section near the Parsons Boulevard Station on in IND line of the New York City Transit Authority. The measurements would not have been possible without the cooperation of the NYCTA. In particular we wish to thank Mr. Anthony Paolillo who made all of the necessary arrangements for the many hours of measurements and gave us many useful suggestions for our work.

TABLE OF CONTENTS

CONTENTS (Concluded)

LIST OF FIGURES

FIGURES (Concluded)

1. INTRODUCTION

Recent years have seen a renewed interest in urban rail transit systems for public transportation. In part this interest has come about because of the many environmental problems associated with other non-rail transit systems. However, environmental problems are also associated with rail transit systems. This report focuses on one problem of particular concern: vibration and low frequency noise in buildings near underground transit lines. A second problem of concern, noise near elevated rail transit structures, is dealt with in another report prepared by Cambridge Collaborative, Inc., for the Department of Transportation [1].

1.1 Background

As systems manager for the U.S. Urban Mass Transportation Administration (UMTA) Rail Systems Supporting Technology Program, the Transportation Systems Center (TSC) is conducting research, development and demonstration efforts directed towards the introduction of improved technology in urban rail systems applications. As part of this program, TSC is conducting analytical and experimental studies directed towards noise and vibration reduction in urban rail systems.

The UMTA Rail Noise Abatement effort will bring together and improve existing and new elements into a unified technology consisting of: design criteria for establishing goals, noise control theory, design methods, test procedures, and appropriate documentation. The program has been organized into four concurrent and interrelated parts which will be closely coordinated with each other by TSC. They are:

1. Assessment of Urban Rail Noise and Vibration Climates and Abatement Options;
2. Test and Evaluation of State-of-the-Art Urban Rail Noise Control Techniques;
3. Wheel/Rail Noise and Vibration Control Technology;
4. Track and Elevated Structure Noise and Vibration Control Technology.

This report is a result of work performed under part 4 of the program and deals with the development and engineering use of a model for predicting the effectiveness of floating-slab track in reducing the vibration and noise transmitted to buildings near subway tunnels. Results of field measurements for a length of floating-slab track on the New York City transit system are also presented.

1.2 Program Objectives

In an effort to reduce the vibration transmitted from

subway tunnels, a number of techniques have been suggested and tried [2]. The most successful of these has been to isolate the vibrations of the rail from the tunnel floor by means of resilient rail fasteners and floating-slab track. Although the floating-slab tracks appear to be more effective than resilient rail fasteners in preventing the transmission of vibration, past installations have been so expensive that their use may not be cost effective.

The goal of the work presented in this report is to develop a model for predicting the performance of floating-slab track. It is hoped that by developing a basic understanding of these devices, the transit industry can implement less expensive and equally effective designs.

1.3 State-of-the-Art in Floating-Slab Track Design

Within the present state-of-the-art floating-slab tracks are designed according to a simple single-degree-of-freedom model shown in Fig. 1.1. The resonance frequency of the model is set to equal the rigid body resonance of the floating slab on its supports.

The damping is determined from the damping properties of the slab supports. As seen in Fig. 1.2 this simple model

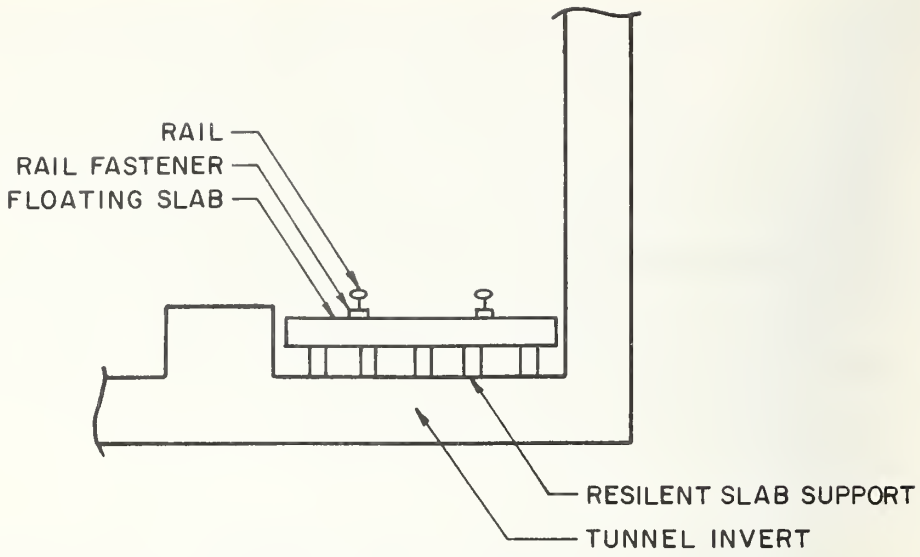

a) TYPICAL FLOATING SLAB INSTALLATION

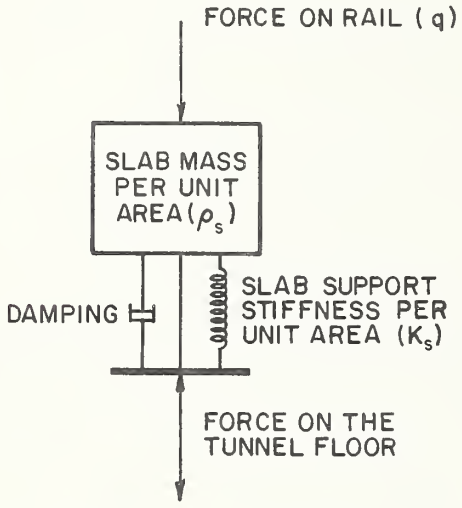

b) SINGLE DEGREE OF FREEDOM SYSTEM

FIG. 1.1 SIMPLE MODEL USED TO PREDICT FLOATING SLAB VIBRATION REDUCTION

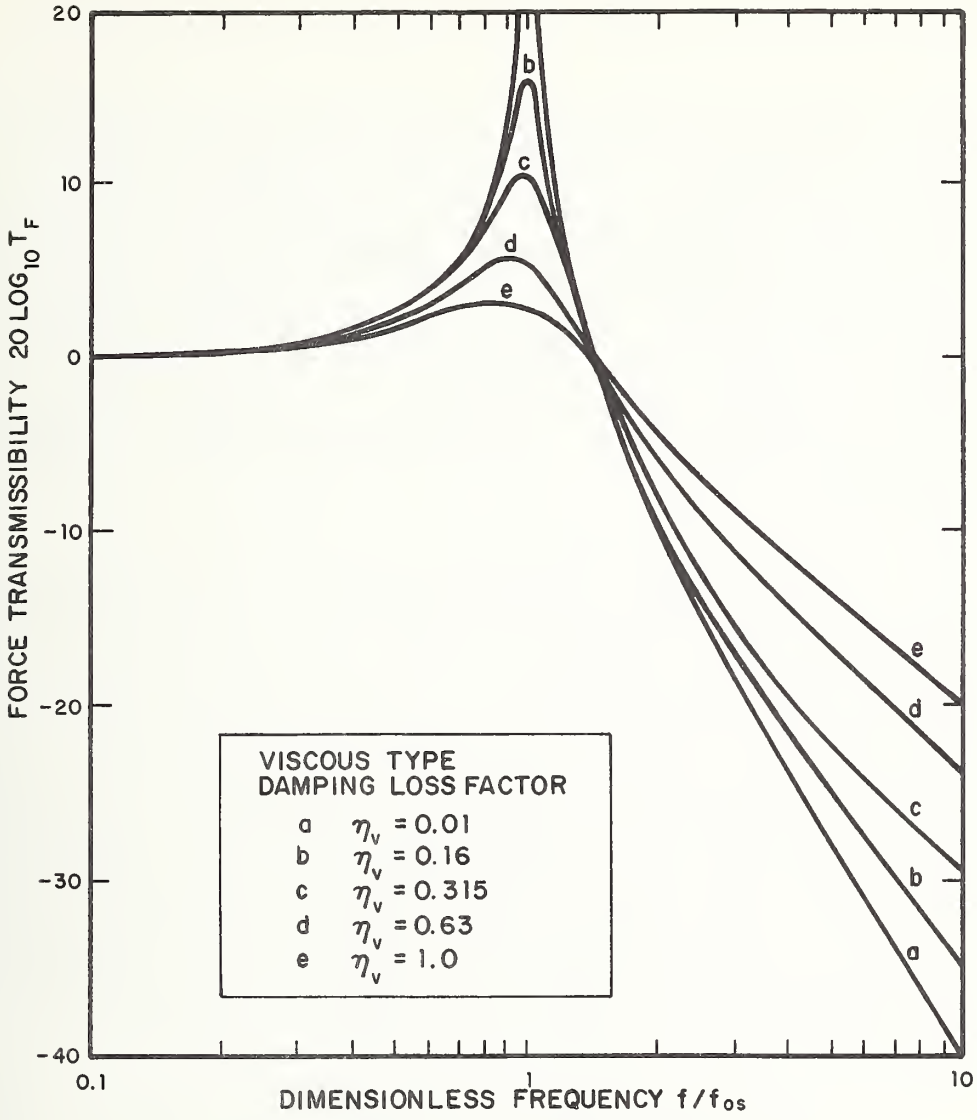

PARAMETERS

T_F FORCE TRANSMISSIBLITY, RATIO OF THE AMPLITUDES OF THE FORCE ON THE RAIL AND THE FORCE ON THE TUNNEL FLOOR;

f_{os} RESONANCE FREQUENCY OF THE SLAB ON ITS SUPPORTS, $f_{os}^2 = K_s/\rho_s$;

η_v VISCOUS DAMPING LOSS FACTOR (FOR SOLID TYPE DAMPING, δ_s, LET $\eta_v = \delta_s \, f_{os}/f$);

$\eta_v = 2\zeta$ WHERE ζ IS 100 TIMES THE PERCENT OF CRITICAL DAMPING VALUE

FIG 1.2 FORCE TRANSMISSIBILITY FOR THE SINGLE DEGREE OF FREEDOM SYSTEM

predicts that the forces applied to the tunnel floor are effectively reduced at frequencies well above the resonance frequency and are increased at frequencies near the resonance frequency. A design tradeoff must be made in selecting the damping. High damping reduces the force amplification at the resonance frequency but at the expense of higher frequency performance.

Most floating slab designs have set the resonant frequency in the range 10 to 30 Hz. The objective has been to set the resonance frequency as low as possible within material and static displacement constraints. One problem has been to find resilient materials that can withstand the high static loads and severe environmental conditions associated with transit systems. Most designs make it difficult to replace the slab supports so that their life must be very long.

The single-degree-of-freedom model does not take into account the flexibility of the slab or effects of using a resilient rail fastener between the rail and the slab. In spite of this neglect the performance predicted by the simple model for a floating slab track in New York City agrees reasonably well with measured data that we have taken. We believe this to be a fortuitous result for the particular slab design that was studied. A more realistic model may be required for other designs.

In this report we develop a new model that takes into account the flexibility of the slab and the effects of resilient rail fasteners. The model can be used to study both long continuous slabs and resiliently supported ties.

1.4 Summary of Results

The prediction model developed in this report allows the determination of the reduction in the dynamic forces applied to the tunnel floor. A method to calculate the response of the tunnel to the applied forces has not been found and should be the subject of future work. Similarly, methods to calculate the transmission of tunnel vibration through the ground to neighboring buildings have not been developed as part of the work carried out in this report. However, in spite of these limitations the authors believe that the reduction in the dynamic forces acting on the tunnel floor is a good measure of performance and can be used to compare different floating-slab designs.

The prediction model indicates that the ratio of slab support stiffness to slab mass should be as small as possible within imposed limitations on maximum allowable deflections during the passby of a fully loaded train. The slab performance at the rigid body resonance of the slab on its supports is governed by the damping of the supports, with lightly-damped supports giving

poor performance. However, a tradeoff exists in selecting the support damping, since high values of damping cause the performance above the rigid body resonance to decrease.

The role of slab support damping at frequencies above the rigid body slab resonance is varied. For very low values of damping performance of the slab is poor because of the excitation of lightly damped bending waves in the slab. For somewhat higher values of support damping the bending wave motion of the slab is reduced to a minimum value determined largely by the slab mass. Finally, for large values of damping the forces transmitted to the tunnel floor increase as shown by the simple prediction chart in Fig. 1.2

At high frequencies, above the rigid body resonance of the rail on its fasteners, it is possible for the free bending wavespeed in the rail and the slab to coincide. This coincidence effect reduces the performance of the slab at these frequencies and should be avoided.

The field study results support the general conclusions of the prediction model. They show that the floating slab has a detrimental effect at and near the rigid body slab resonance. For the particular system studied the vibration levels of the tunnel are increased by the floating slab approximately 10 dB

in the one-third octave band centered on the rigid body resonance frequency. Above this resonance frequency the performance of the slab improves rapidly with increasing frequency. For this particular slab, the support damping appears to be sufficiently high that the vibration due to free bending waves in the slab is not important in determining the slab performance.

We conclude from this study that floating ties can be just as effective as long floating slabs. The floating ties prevent the occurrence of coincidence effects and eliminate free bending wave response of the track support--both beneficial effects with regard to reducing the dynamic forces transmitted to the tunnel floor. On the other hand, the floating ties allow the static deflection during a train passby to be larger and thereby increase the maximum stresses on the rail.

1.5 Organization of the Report

The report is organized into three basic sections. In Section 2 we describe the mathematical formulation of the prediction model. The basic approach is presented and predictions applicable to a high and low frequency regime are developed. In Section 3 we present the results of a field study of the performance of a length of floating-slab track on the New York City transit property. Finally, in Section 4, we summarize the results and show how they can be applied to the practical engineering design of floating-slab track.

2. MATHEMATICAL FORMULATION

2.1 Introduction

This section presents the mathematical formulation of a model to predict the dynamics of floating-slab track systems and the influence of design parameters on their effectiveness in reducing vibration transmission from trains to subway floors and hence to neighborhood buildings.

The rationale for the "floated track slab" is similar in philosophy to a vibration isolation method used in industrial situations which involves mounting vibrating machinery on an inertia block, a reinforced concrete block resiliently mounted on a floor. In a recent study [3], Bender summarizes the significant differences between the floated slab system and a conventional inertia block. However, his work is principally directed toward the investigation of acoustic radiation from the rail-slab system. This is accomplished by a detailed consideration of the separate behaviors of rail and slab and a qualitative analysis of the effects of dynamic coupling by assuming the various system elements to be cascaded.

The present effort is primarily devoted to an understanding of the vibration transmission properties of the floated slab system. In addition, the results of the previous study [3] have been extended by removing certain approximations and

restrictive assumptions. More specifically, our effort provides a detailed examination of the dynamic coupling between rail and slab and an approximate solution to the fully coupled equations of motion including a Bernoulli-Euler plate formulation for the slab and visco-elastic damping associated with rail fasteners and slab supports. The results are also shown to apply to floated tie systems. We shall evaluate appropriate measures of the force transmitted to the floor of the subway tunnel and the acoustic radiation from the slab. Guidelines for optimizing the vibration isolation performance are presented.

2.2 Basic Formulation

The floated slab system consists of rails resiliently fastened to a concrete slab which is in turn mounted on the tunnel floor by resilient pads. The basic physical model to be adopted for this analysis along with definitions of the pertinent parameters are presented in Fig. 2.1. Representative values of these parameters are given in Appendix A.

For the purpose of developing guidelines for floated slab design it is deemed sufficient to examine the interaction of the slab with a single rail excited by the motion of one wheel of the rail vehicle. To provide a basis for more refined analysis it is assumed initially that both rail and slab are infinite

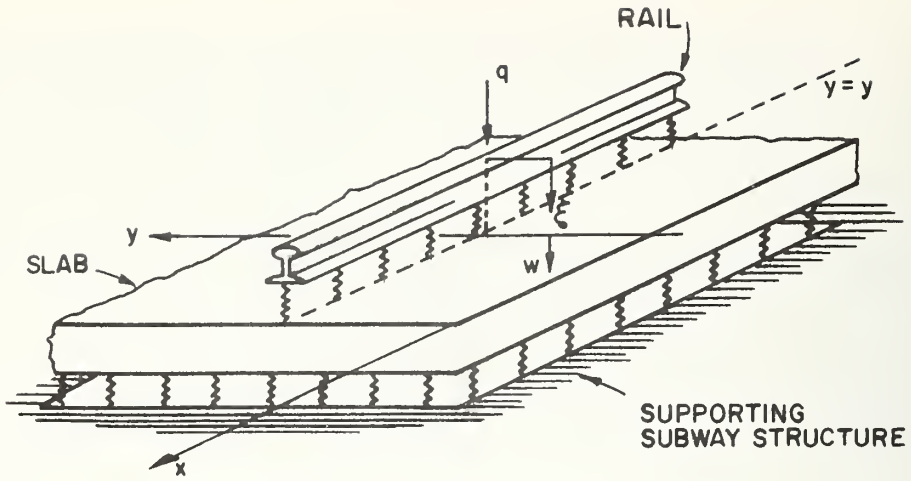

ρ_r = rail mass per unit length

E_r = modulus of elasticity of the rail material

I_r = moment of inertia of the rail

ρ_s = slab mass per unit area

E_s = modulus of elasticity for the slab material

I_s = moment of inertia for the slab

D = slab flexural rigidity per unit width

h = slab thickness

L = slab width

y_o = position of rail fasteners on the slab

q = applied force due to rail-rail interaction

K_r^* = visco-elastic stiffness modulus for rail fasteners per unit length of rail

K_s^* = visco-elastic stiffness modulus of slab supports per unit area of slab

For harmonic response:

$$K_r^* = K_r (1 - j\delta_r), \quad K_s^* = K_s (1 - j\delta_s)$$

where δ_r and δ_s are the solid type damping loss factors and $j = \sqrt{-1}$.

FIG. 2.1 SLAB GEOMETRY AND DEFINITIONS OF PARAMETERS

along the track and that the slab is of constant rectangular cross-section and homogeneous material properties. In Section 2.10 the analysis is extended so that it can be applied to floating-tie tracks. Also, only the vertical motions of rail and slab are considered. Damping is accounted for in the formulation by idealizing the slab mounts and rail fasteners by continuous viscoelastic supports.

In all practical instances, the train speed is much smaller than the wave speed of vibrations transmitted down the rail and slab. Thus, the force due to wheel/rail interaction may be modeled by a stationary, vertical point force located at the origin of the x coordinate [4].

The fluid loading of rail and slab due to the acoustic space is neglected so that system dynamics are calculated in vacuo. In some cases of practical interest, however, the effective stiffness of air enclosed under the slab must be included in calculating the stiffness of the slab supports.

Finally, the dynamic interaction of the slab with the tunnel floor is neglected in this analysis. That is, the tunnel floor is taken to be a rigid support. This assumption is rather restrictive as it requires the tunnel floor impedance to be much larger over all frequencies than the impedances of all other system components. However, it is anticipated that once a determination of actual tunnel floor impedance has been made, the present results can be suitably extended so that the tunnel floor vibration can be predicted.

The specific analytical idealizations used here in order to make the analysis tractable are summarized below.

System Element	Analytical Model
Rail.....	Bernoulli-Euler beam
Slab.....	Bernoulli-Euler plate with edges Y=0,L assumed stress free.
Rail fasteners and slab mounts..	Continuous, viscoelastic supports with frequency independent loss factors, i.e., for harmonic response these are modeled with complex elastic moduli.
Wheel-Rail interaction.....	Point force on the rail at x=0. The force time histories are assumed stationary random processes.

Results are derived for two kinds of power spectral densities of the existing excitation at the wheel/rail contact points: (i) a flat spectral density and (ii) the spectrum arising from the micro-roughness model of wheel-rail interaction [5].

Before presenting the picture of rail and slab response developed under the above assumptions, we shall discuss the dynamic characteristics of various individual system elements and outline our general approach.

2.3 Characteristics of Individual Rail and Slab Motions

Some appreciation of the overall response characteristics can be obtained by considering the unforced and undamped motion of (1) the rail on its fasteners with the slab treated as rigid and (2) the slab on its mounts without the rail and fasteners. We shall call those two systems the uncoupled rail and uncoupled slab, respectively.

First, consider the free, undamped motion of the uncoupled rail. The rail displacement in this case, $\xi(t,x)$, is in the form of sinusoidal bending waves,

$$\xi(t,x) = e^{j(k_x x \pm \omega t)} \tag{2.1}$$

where the wave number, k_x, is related to radian frequency, ω, through the dispersion relation,

$$k_x^4 = k_r^4 \tag{2.2a}$$

where the wavenumber for freely propagating waves in the rail, k_r, is

$$k_r^4 = \kappa_1 \left[\left(\frac{\omega}{\omega_{or}}\right)^2 - 1\right] \tag{2.2b}$$

and ω_{or}, the natural frequency of the rail moving as a rigid body on its fasteners, is given by

$$\omega_{or} = \sqrt{K_r/\rho_r} \tag{2.2c}$$

and the parameter κ_1 is given by

$$\kappa_1 \equiv \frac{K_r}{E_r I_r} \tag{2.2d}$$

where K_r is the effective rail fastener stiffness per unit length of rail and $E_r I_r$ is the bending stiffness of the rail. This dispersion relation is shown in Fig. 2.2 for three different values of fastener stiffness. Clearly the character of the rail motion depends on the value of ω relative to ω_{or}. For $\omega > \omega_{or}$, free bending waves can propagate down the rail, while for $\omega < \omega_{or}$, propagating bending waves cannot exist. Finally for $\omega = \omega_{or}$ the rail oscillates as a rigid body on its fasteners.

The situation in the case of the slab is more complicated. The free motion of the slab $w(t,x,y)$ may be expressed as a combination of motions of the form

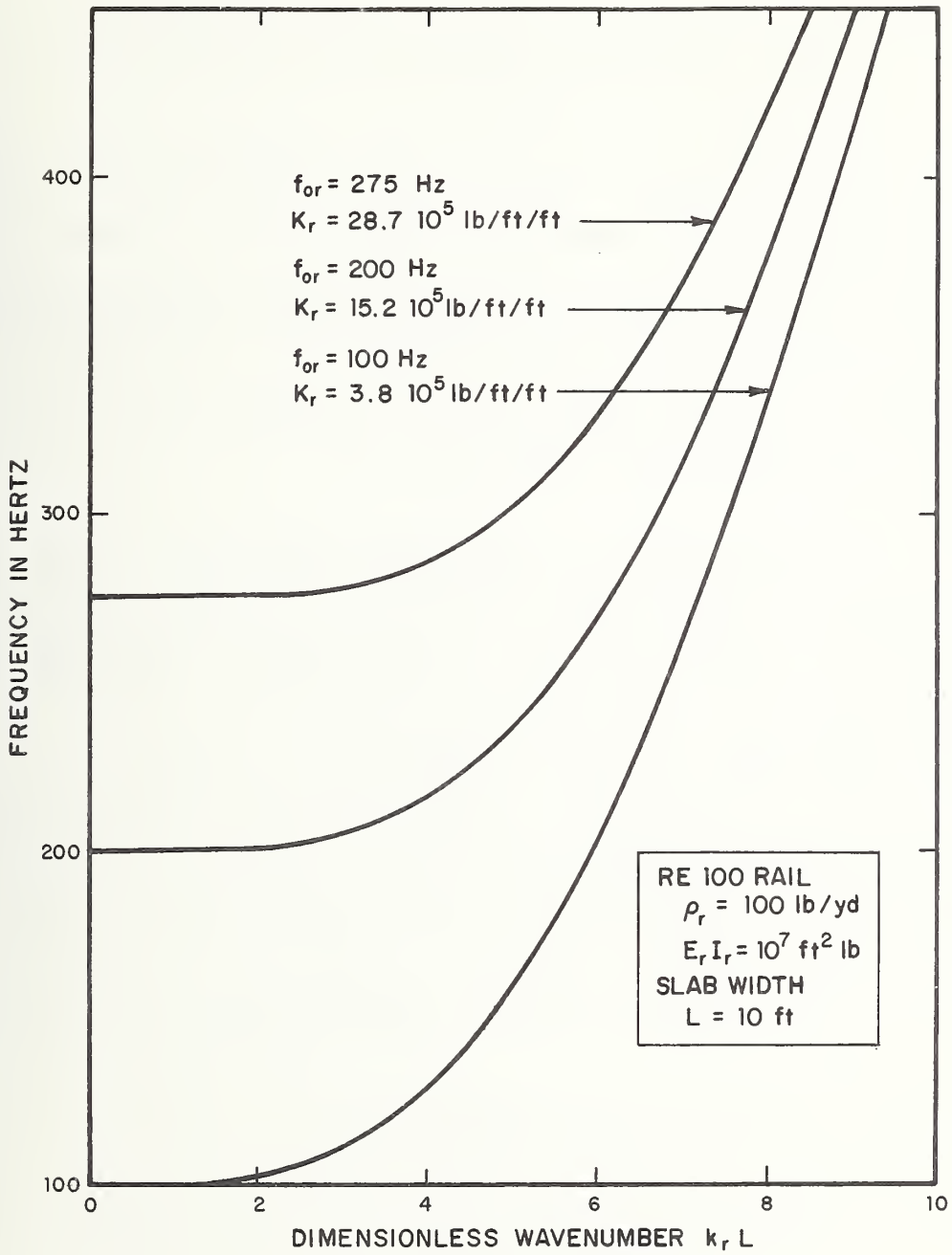

FIG. 2.2 RAIL DISPERSION CURVES FOR THREE VALUES OF FASTENER STIFFNESS

$$w = e^{j(k_x x \pm \omega t)} \psi_n(y, k_x) \tag{2.3}$$

where the ψ_n (n=1,2,...) are the cross-wise normal modes of the slab displacement. Each mode is seen to propagate along the slab as a sinusoidal wave. These mode shapes depend upon the wavenumber k_x and the Poisson ratio, μ, as well as upon y. However, for μ small, as is typical of concrete ($\mu \simeq .15$), the ψ_n's are approximately independent of μ.

Furthermore, for each slab normal mode, the wavenumber and frequency must be related by a distinct dispersion relation. For the values of parameters given in Appendix A, they are given to within 2% accuracy by:

$$\alpha L = (k_x L)\left[1+(\gamma_n/k_x)^4\right]^{\frac{1}{4}}$$

$$\gamma_n = \begin{cases} 0, & n = 1 \\ \dfrac{n\pi}{L}\left[\left(1-\dfrac{1}{2n}\right)^4 + 2\left(\dfrac{k_x L}{n\pi}\right)^2\right]^{\frac{1}{4}}, & n>1 \end{cases} \tag{2.4}$$

where α is related to the frequency by

$$\alpha^4 = (\omega_{os}/\omega_{or})^2 \kappa_2 \left(\frac{\omega^2}{\omega_{os}^2} - 1\right) \tag{2.5a}$$

where ω_{os}, the natural frequency of the slab moving as a rigid body on its resilient pads, is given by

$$\omega_{os} = \sqrt{\frac{K_s}{\rho_s}} \tag{2.5b}$$

and the parameter κ_2 is given by

$$\kappa_2 = \left(\frac{\omega_{or}}{\omega_{os}}\right)^2 \frac{K_s}{D} \tag{2.5c}$$

where K_s is the effective stiffness of the slab supports per unit area of the slab and where D is the bending stiffness of the slab, per unit width, $D = E_s h^3/12$.*

Equations 2.4 are shown in Fig. 2.3 (using the values given in Appendix A) along with the rail dispersion curves given earlier. As in the case of the rail, there is a cutoff frequency for each slab mode, below which that mode cannot propagate freely down the slab. These cutoff frequencies, ω_{ns}, (n=1,2...) are given approximately by

$$\frac{\omega_{ns}^2}{\omega_{os}^2} = 1 + \begin{cases} 0 \; ; & n = 1 \\ \dfrac{\omega_{or}^2}{\omega_{os}^2} \; \dfrac{1}{\kappa_2}\left(\dfrac{\pi}{L}\left(n - \dfrac{1}{2}\right)\right)^4 \; ; & n > 1 \end{cases} \tag{2.6}$$

*In this relation we have neglected the small effect of Poisson coupling which acts to increase the bending stiffness in a plate by a factor $(1-\mu^2)^{-1}$ where μ is Poisson's ratio.

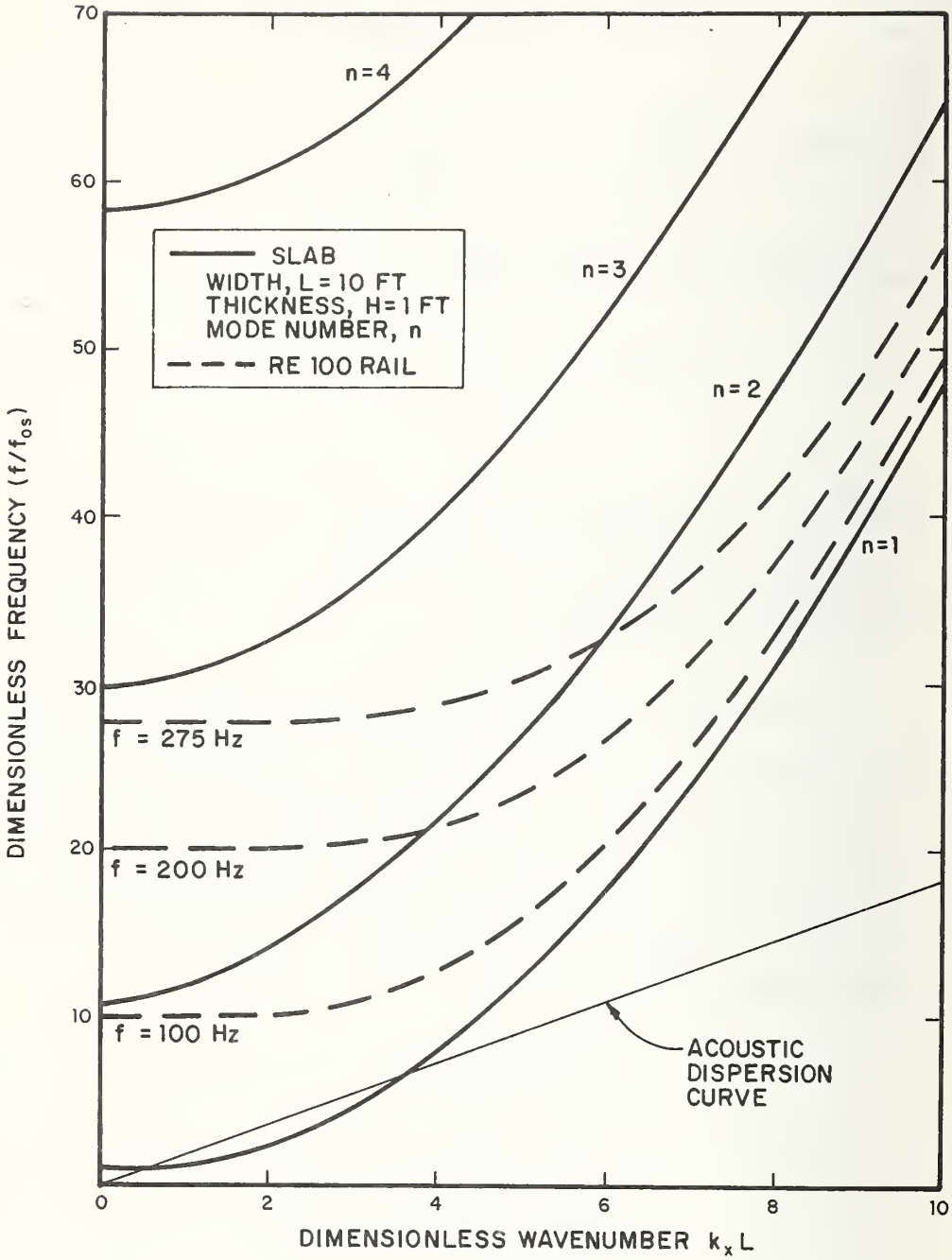

FIG. 2.3 DISPERSION CURVES FOR THE FIRST FOUR CROSS MODES OF A CONCRETE SLAB

$\psi_n(y,k_x)$ gives the cross-sectional shape of the displacement associated with the n^{th} mode and is a function of k_x. The first mode shape, ψ_1, merely represents a rigid body translation of the slab cross-section. As shown in Figs. 2.4 and 2.5 the higher mode shapes depend upon k_x. These plots show the second and third mode shapes for very low to very high wavenumbers. These functions have been normalized to -1 at the slab free edge. It is seen that for very low wavenumbers, $\psi_n(n>1)$ is approximately the n^{th} mode shape of a free-free beam on an elastic foundation, while for very large wavenumbers, ψ_n approaches the limit

$$\psi_n \simeq - \cos n\pi \frac{y}{L}, \quad n = 2, 3,... \tag{2.7}$$

Contrary to what has been stated in Ref. [3] the slab modes are orthogonal. That is:

$$\int_0^L \psi_n(y,k_x)\psi_m(y,k_x)dy = 0 \tag{2.8a}$$

for $n \neq m$. This is demonstrated in Appendix B. Furthermore the modes can be so defined that their norm is L. Thus, we may write

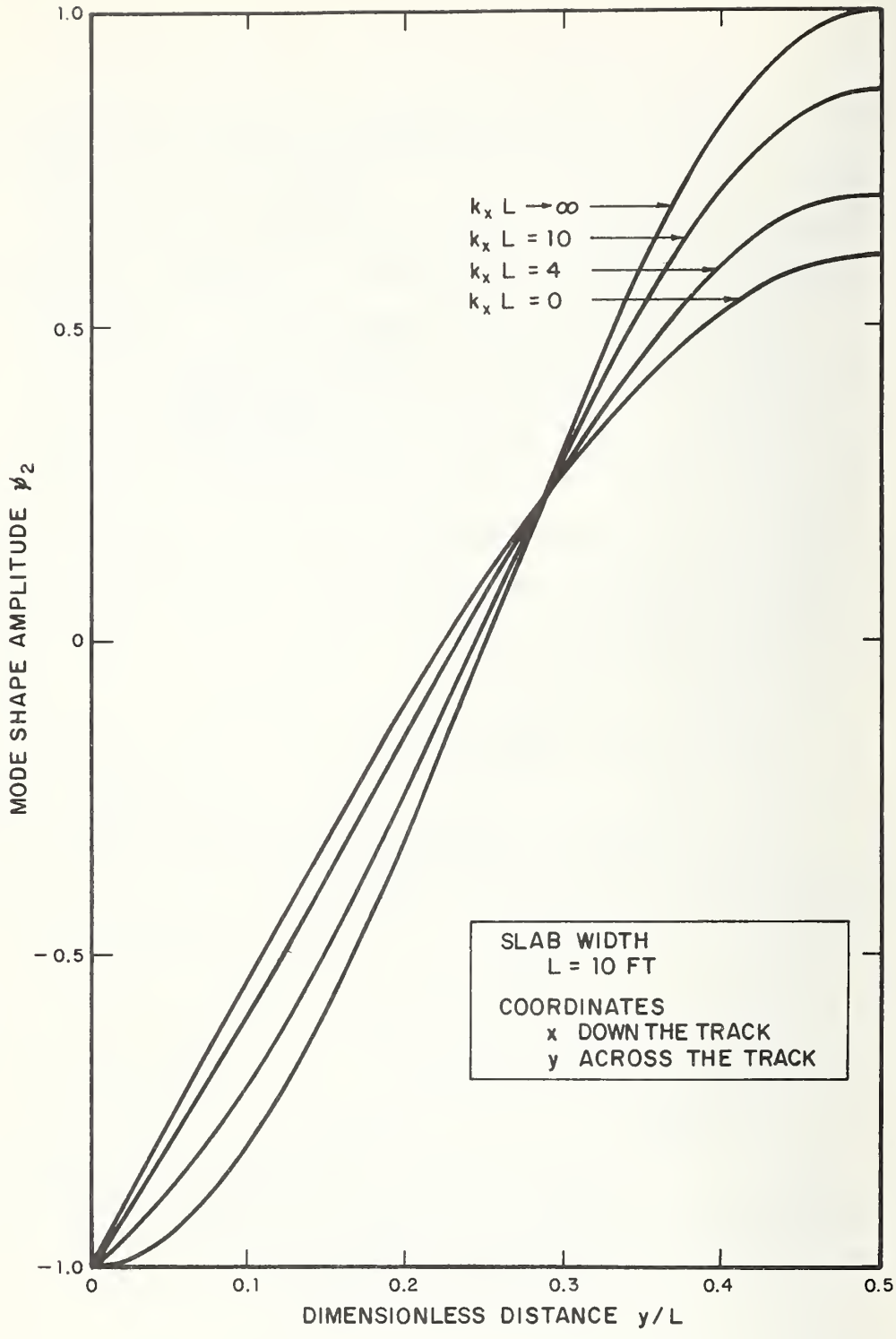

FIG. 2.4 SECOND SLAB MODE SHAPE

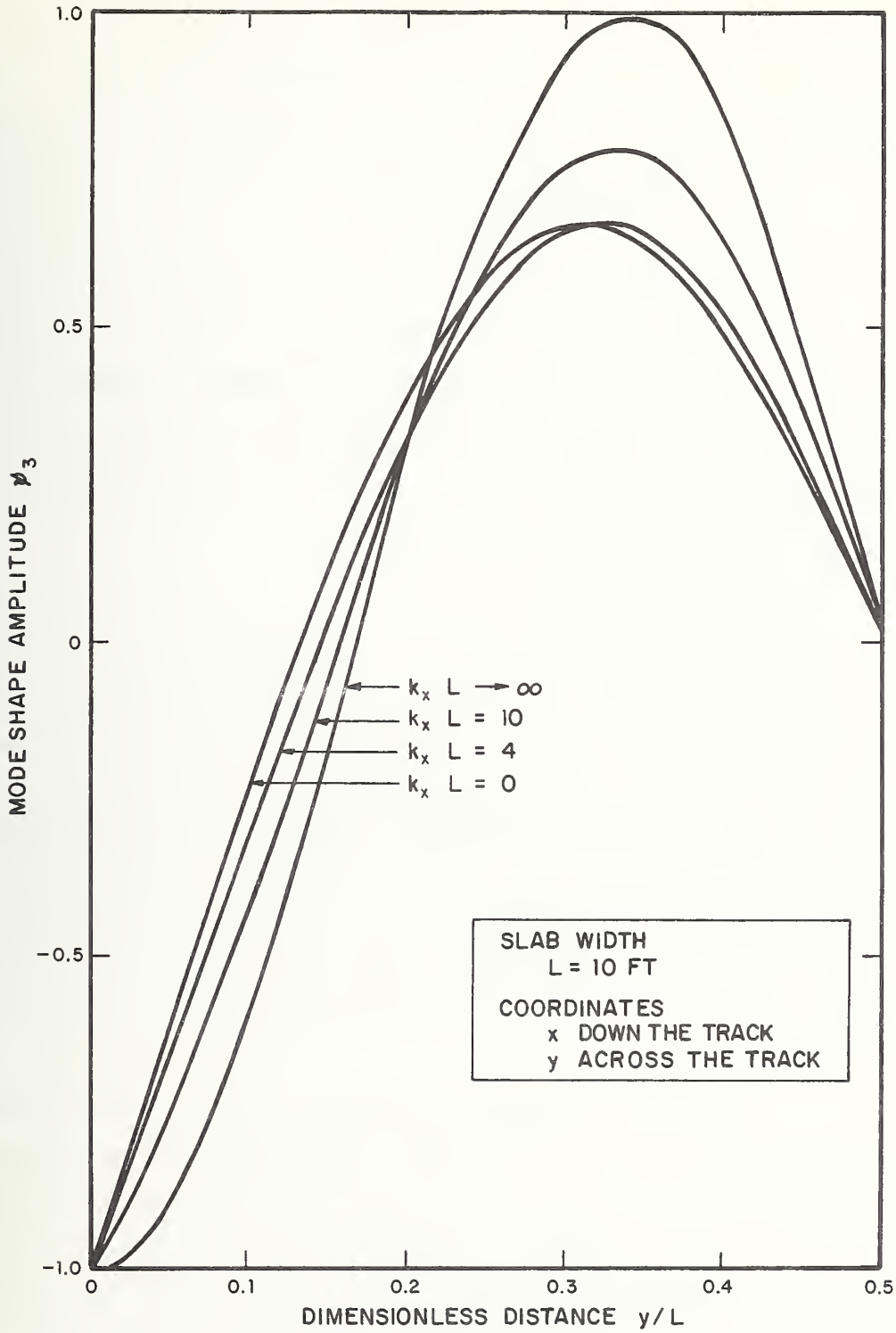

FIG. 2.5 THIRD SLAB MODE SHAPE

$$\int_0^L \psi_n \psi_m dy = \begin{cases} L, & n=m \\ 0, & n \neq m \end{cases} \tag{2.8b}$$

The slab mode shapes defined above may be used to synthesize the actual forced and damped motion of the slab, since in general the slab displacement may be expressed as a combination of functions multiplied by appropriate weighting factors.

The dispersion curves of uncoupled rail and slab can give a qualitative picture of the actual response. In particular, for cases wherein the dispersion curves of rail and slab neither cross nor approach one another very closely, the system elements can be cascaded. That is, the forced rail motion is calculated assuming the slab rigid and the slab motion is taken to be the response of the uncoupled slab to forcing by the rail motion through the fastener stiffness.

When rail and slab dispersion curves cross, however, a cascade analysis is not valid. This condition is called structural wave coincidence, since at the particular frequency at which it occurs, the wavelength of free bending waves of both rail and slab are the same. At the coincidence frequency the system components are very tightly coupled and a detailed

analysis of the coupling dynamics must be carried out. In the following we outline an analysis that does just this.

2.4 Rail-Slab Interaction and Total System Response

Now consider the dynamics of the slab fully coupled to the rail. Our basic approach is as follows.

The slab displacement can be expressed as a combination of its normal modes:

$$w(x,y,t) = \sum_{n=1}^{\infty} w_n(x,t)\ \psi_n(y) \tag{2.9}$$

where the w_n are the modal coordinates of the slab motion. The next step is to express both slab and rail displacements as a combination of components, each of which represents a displacement varying sinusoidally with x at a given wavenumber. The mathematical statement is:

$$\xi(x,t) = \frac{1}{2\pi} \int_{-\infty}^{\infty} dk_x\ e^{-jk_x x}\ \tilde{\xi}\ (k_x,t) \tag{2.10}$$

$$w(x,y,t) = \frac{1}{2\pi} \int_{-\infty}^{\infty} dk_x\ e^{jk_x x}\ \tilde{w}(k_x,y,t) \tag{2.11}$$

Or, on substituting Eq. 2.9 into Eq. 2.11, we get

$$w(x,y,t) = \sum_{n=1}^{\infty} \psi_n(y) \left[\frac{1}{2\pi} \int_{-\infty}^{\infty} dk_x \, e^{jk_x x} \, \tilde{w}_n(k_x,t)\right] \tag{2.12}$$

$\tilde{\xi}$ and $\tilde{w}$ are seen to be the Fourier transforms of ξ and w with respect to x. These quantities might also be termed the wavenumber components of rail and slab motion.

Eq. 2.12 can be interpreted as first a decomposition of the slab displacement into its normal modes and then a resolution of each modal coordinate into its wavenumber components.

The solution procedure is to obtain $\tilde{\xi}(k_x,t)$ and the $\tilde{w}_n(k_x,t)$ in terms of the exciting force, q(t), and then to determine $\xi(k_x,t)$ and $w_n(x,t)$ for all values of n by calculating inverse Fourier transforms.

Substitution of Eqs. 2.10 and 2.12 into the partial differential equations of motion results in an infinite set of coupled ordinary differential equations for $\tilde{\xi}(k_x,t)$ and $\tilde{w}_n(k_x,t)$, the y dependence being completely eliminated. The substitution procedure is discussed in Appendix C. It comes about that for a given k_x, the wavenumber components

of the rail and slab modes behave as the displacements of a system of coupled mechanical oscillators, one oscillator being associated with each slab mode and with the rail response. To a good approximation these oscillators are coupled together only by spring forces arising from the stiffness of rail fasteners and slab supports.

The analogy which comes out of our analysis is shown in Fig. 2.6 where only the first two slab modes are considered. For all k_x, the rail oscillator is excited by the driving force on the rail, q(t), while the slab mode oscillators are only indirectly excited by their coupling to the rail. As the figure illustrates, each slab mode oscillator is not only connected to the rail oscillator, but is coupled to all the other slab oscillators.

For a given k_x, the resonant frequencies of the uncoupled oscillators are given simply by the dispersion curves of the uncoupled rail and slab. It should be noted that all parameters shown in Fig. 2.6 are functions of the wavenumber and are always different for different wavenumbers. Not shown, but implicit in the figure, is the frequency independent viscoelastic damping associated with the springs K_r, K_{s_1}, K_{s_2}, etc.

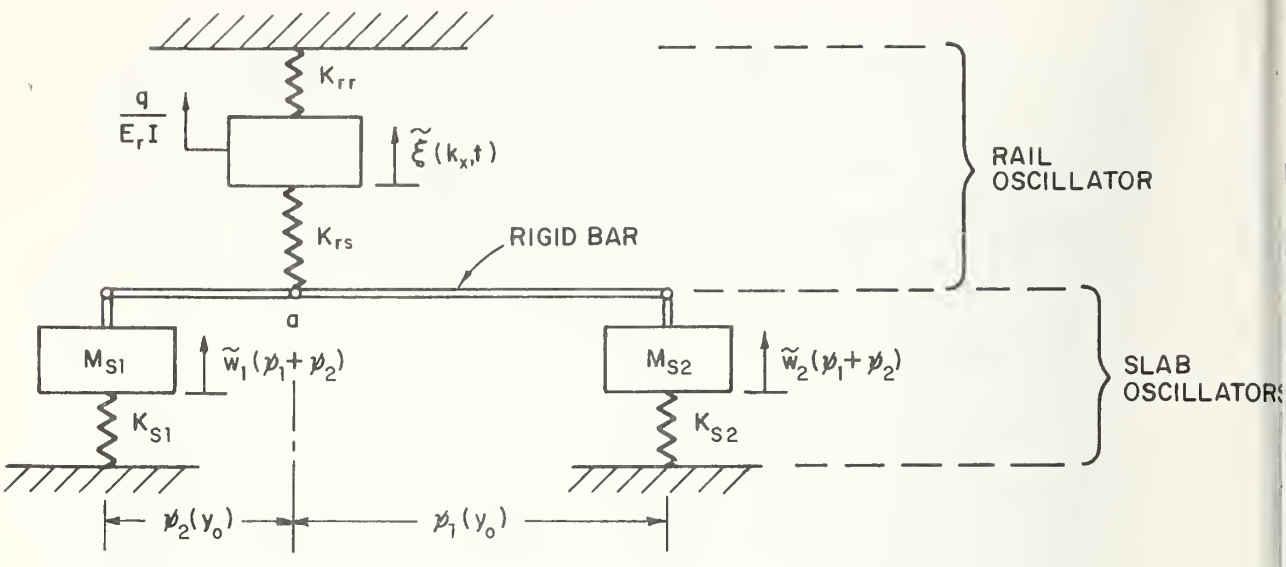

All masses and stiffnesses are functions of k_x:

$$M_r = \frac{\kappa_1}{\omega_{or}^2}, \quad M_{s1} = M_{s2} = \frac{\kappa_1}{\beta\omega_{or}^2} \frac{1}{(\psi_1+\psi_2)^2}$$

$$k_{rr} = k_x^4, \quad k_{rs} = \kappa_1^*$$

$$k_{s1} = \frac{1}{(\psi_1+\psi_2)^2} \frac{\kappa_1}{\kappa_2\beta} \left(k_x^4 + \frac{\omega_{os}^2}{\omega_{or}^2} \kappa_2^*\right)$$

$$k_{s2} = \frac{1}{(\psi_1+\psi_2)^2} \frac{\kappa_1}{\kappa_2\beta} \left(k_x^4+\gamma_2^4 + \frac{\omega_{os}^2}{\omega_{or}^2} \kappa_2^*\right)$$

where for harmonic response

$$\kappa_1^* = \kappa_1(1 - j\delta_r), \quad \kappa_2^* = \kappa_2(1 - j\delta_s).$$

The rigid connecting bar is free to rotate about pivot a and to translate vertically.

FIG. 2.6 MECHANICAL OSCILLATOR ANALOGY FOR THE FLOATED SLAB SYSTEM

First, let us consider the free motion of this composite system. It is found that the free motion of each oscillator is a combination of the normal modes of the total coupled system (i.e., those motions in which all displacements vary sinusoidally with the same frequency). The frequency of each mode, when considered as a function of k_x yields a distinct dispersion curve. A typical situation is shown schematically in Fig. 2.7, which shows two such curves along with the uncoupled rail and slab dispersion curves. For $k_x << k_{xc}$ (k_{xc} being the coincidence wavenumber), the lower frequency mode nearly coincides with the uncoupled slab while the higher mode follows the rail. For $k_x >> k_{xc}$ the correspondence is reversed. At $\omega=\omega_c$ the two dispersion curves have a minimum separation along the k_x axis equal to Δ_n, where

$$\Delta_n = 2\sqrt{\kappa_1\kappa_2\beta}\ \psi_n(y_o) \tag{2.13a}$$

where κ_1 and κ_2 are defined in Eqs. 2.2d and 2.5c, β is the ratio of rail mass per unit length to the slab mass per unit length,

$$\beta \equiv \frac{\rho_r}{L\rho_s} \tag{2.13b}$$

and $\psi_n(y_o)$ is the value of the n^{th} slab mode shape at the rail

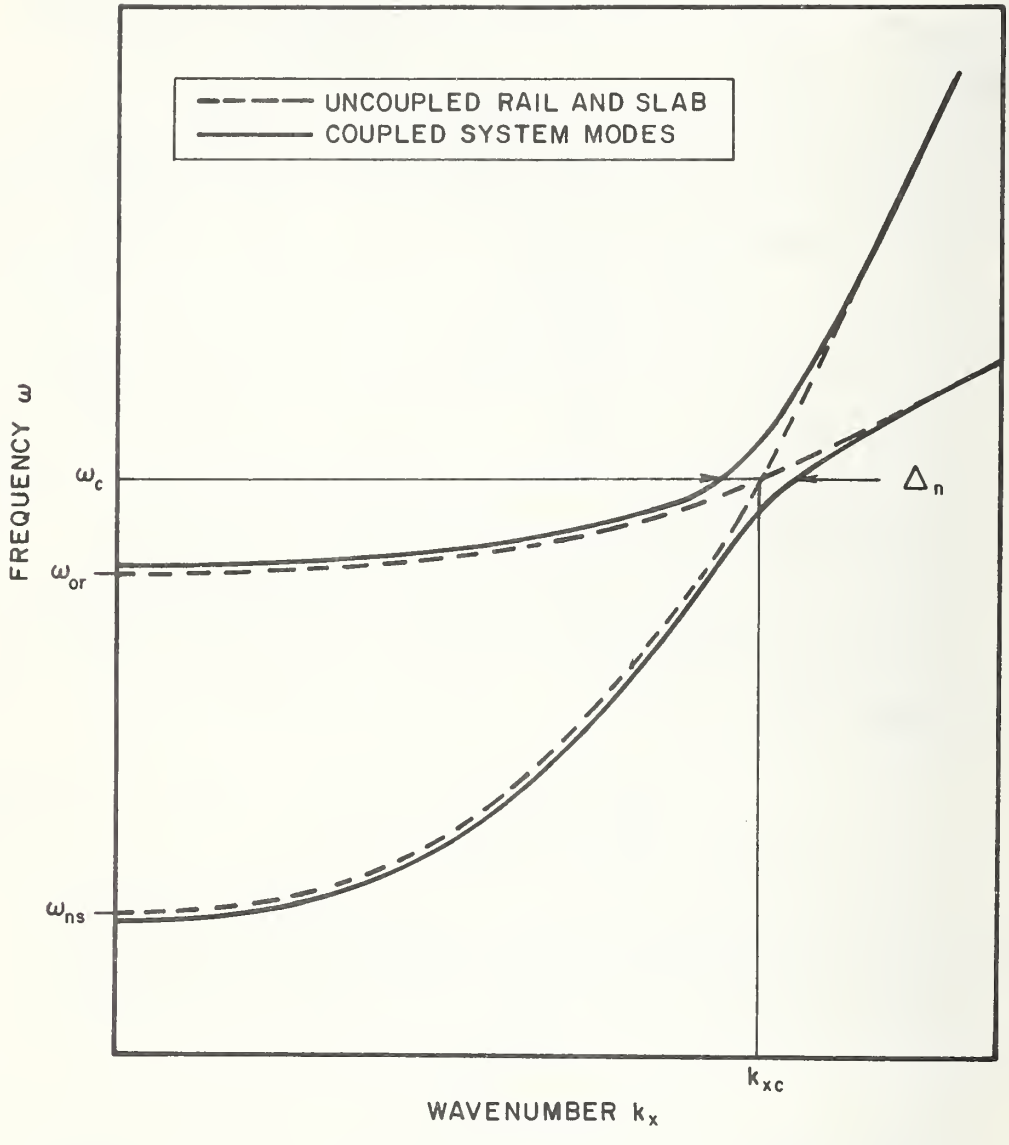

FIG. 2.7 COUPLED MODE DISPERSION CURVES

position. The minimum separation, Δ_n, is, in fact, a measure of the effects of coupling forces between the rail and the n^{th} slab mode. It should be noted that since we have lumped all damping into the coupling stiffnesses which are small in comparison with bending forces, the damping band-width of each oscillator is always smaller than the coupling. This is a basic condition for the validity of many of the results presented here.

Returning to our coupled oscillator analogy, note that at wavenumber coincidence the rail and slab behave as identical, lightly coupled oscillators. Thus, since, as judged from the typical values given in Appendix A , Δ_n is quite small, the overall amplitude of forced response is likely to be relatively large at the coincidence frequency.

Now consider the response to a harmonic point force excitation of the rail

$$q(t) = \hat{q}\, e^{-j\omega t} \tag{2.14}$$

where we shall take $\hat{q}$ to be constant over frequency during this discussion. The resulting wave number components of rail and slab modes are also harmonic with the same frequency:

$$\tilde{\xi}(k_x,t) = \hat{\xi}(k_x,\omega)\ e^{-j\omega t} \tag{2.15a}$$

$$\tilde{w}_n(k_x,t) = \hat{w}_n(k_x,\omega)e^{-j\omega t},\ n = 1,2,... \tag{2.15b}$$

When these relations are placed in the infinite set of coupled oscillator equations, the exact solutions for $\hat{\xi}(k_x,\omega)$ and $\hat{w}_n(k_x,\omega)$ can be determined. Finally, the inverse spatial Fourier transforms of $\hat{\xi}$ and $\hat{w}_n$ can be obtained approximately to give the spatial distribution of response

$$\xi(x,t) = \tilde{\tilde{\xi}}(x,\omega)\ e^{-j\omega t} \tag{2.16a}$$

$$w_n(x,t) = \tilde{\tilde{w}}_n(x,\omega)\ e^{-j\omega t},\ n = 1,\ 2,... \tag{2.16b}$$

where $\tilde{\tilde{\xi}}$ and $\tilde{\tilde{w}}_n$ are the spatial Fourier transforms of $\hat{\xi}$ and $\hat{w}_n$.

The spatial distributions of rail and slab motion have been obtained in this way under the assumption that only the first slab mode is significantly excited. This restriction leaves out the effects due to participation of higher modes, but nevertheless adequately illustrates the salient aspects of response.

The resulting expressions for $\tilde{\tilde{\xi}}(x)$ and $\tilde{\tilde{w}}_1(x)$ are extremely lengthy and not relevant to the actual design of floating track slabs, so we shall merely summarize the qualitative results here. The expressions are given in Appendix C.

(a) For $\omega < \omega_{os}$, ω_{or} no bending waves propagate, the displacements of rail and slab consisting of near-field components only. For $\omega_{os} < \omega < \omega_{or}$ the near field of the rail excites the far field of the slab. Above ω_{or} and ω_{os}, the far fields of both rail and first slab mode consist of two component waves propagating at the rail free bending wave speed and at the slab wave speed. As long as ω is not within a damping bandwidth of ω_{or} or ω_{os}, the role of damping is limited to the attenuation of bending waves.

(b) For $\omega = \omega_{os}$ the overall amplitudes of both rail and slab reach a resonant maximum, limited primarily by the damping in the slab supports and secondarily by damping in the rail fasteners and the slab itself. The shape of the response consists essentially of a nearfield with maximum value at the driving point extending a large distance from the driving point. Smaller bending wave components, propagating at the rail wave speed also exist. For $\omega = \omega_{or}$, these remarks also apply if the roles of rail and slab

are interchanged.

(c) For a structural wave coincidence occurring at the driving frequency the maximum response of the rail occurs at the driving point while the slab response is very small there (of order $\Delta_1/|k_r|^4$, where k_r is allowed to be complex to allow for damping in the rail fasteners. For moderate distances from the driving point, the far field components of response are approximately:

$$\frac{\tilde{\tilde{\xi}}_1}{\hat{q}} \simeq \frac{1}{4E_r I} \frac{j}{|k_r|^3} e^{j|k_r|x} \cos\left[\frac{\Delta_1}{8|k_r|^3} x\right] \qquad (2.17a)$$

$$\frac{\tilde{\tilde{w}}_1}{\hat{q}} \simeq \frac{-1}{4E_r I} \frac{1}{|k_r|^3} e^{j|k_r|x} \sqrt{\frac{\beta\kappa_2}{\kappa_1}} \sin\left[\frac{\Delta_1}{8|k_r|^3} x\right] \qquad (2.17b)$$

The bending waves are thus modulated sinusoidally, the modulation of rail and slab being out of phase. This is essentially a "beating" phenomenon where the distance between successive "beats" is $\frac{8\pi}{\Delta_1}|k_r|^3$. Energy is continually being passed from rail to slab and back again as the bending waves propagate down the track. For distances sufficiently large that vibration attenuation due to damping becomes significant, Eqs. 2.17 are no longer valid. At these

distances "beating" subsides, the vibration amplitudes reach a steady state and rail and slab motions eventually come to be in phase.

The amplitudes of response to a harmonic driving force can easily be used to obtain the driving point impedance of the rail, $z_r(\omega)$. Again, this has been obtained by assuming interaction of the rail with the first slab mode only. Neglecting terms of the order of the damping gives:

$$z_r(\omega) = \frac{j}{\omega} E_r I_r (k_r^4 - \alpha^4 + \beta\kappa_2 \psi_1^2(y_o) - 2\lambda) \frac{4|\alpha|^3 |k_r|^3}{a|\alpha|^3 + b|k_r|^3} \tag{2.18}$$

where

$$a = (k_r^4 - \alpha^4 + \kappa_2 \beta \psi_1^2 - \lambda) \begin{cases} \sqrt{2}; & k_r^4 < 0 \\ j-1; & k_r^4 > 0 \end{cases} \tag{2.19a}$$

$$b = -\lambda \begin{cases} \sqrt{2}, & \alpha^4 < 0 \\ j-1, & \alpha^4 > 0 \end{cases} \tag{2.19b}$$

$$\lambda = \frac{1}{2} \left[(k_r^4 - \alpha^4 + \beta\kappa_2 \psi_1^2) - \sqrt{(k_r^4 - \alpha^4 + \kappa_2 \beta \psi_1^2)^2 + 4\kappa_1 \beta_2 \psi_1^2} \right] \tag{2.19c}$$

where ψ_1 denotes $\psi_1(y_o)$.

As can be seen from Fig. 2.8, which shows $|z_r|^2$ plotted versus frequency for a typical case, the magnitude of the rail impedance shows a resonant minimum at ω_{os} as well as at ω_{or}. On the whole, z_r is very close to the driving point impedance of the uncoupled rail, except within a narrow region centered about ω_{os} where its magnitude drops off sharply. When interaction with higher slab modes is accounted for, z_r is found to have resonant minima at each slab mode cutoff frequency and to be close to the uncoupled rail impedance elsewhere.

To conclude this section on overall system response and the solution procedure, consider the response to a stationary random excitation. In this case response spectra may be immediately obtained in terms of the harmonic response and the excitation spectrum. For example, the power spectral densities of rail and slab displacements at fixed locations are:

$$S_\xi(\omega;x) = \left|\frac{\tilde{\xi}(x,\omega)}{\hat{q}}\right|^2 S_q(\omega) \tag{2.20}$$

$$S_w(\omega;x,y) = \left|\sum_{n=1}^{\infty} \psi_n(y) \frac{\tilde{w}_n(x,\omega)}{\hat{q}}\right|^2 S_q(\omega) \tag{2.21}$$

where S_ξ and S_w are the spectral densities of rail response at x and the slab response at x and y, respectively, and S_q is the spectral density of the driving force.

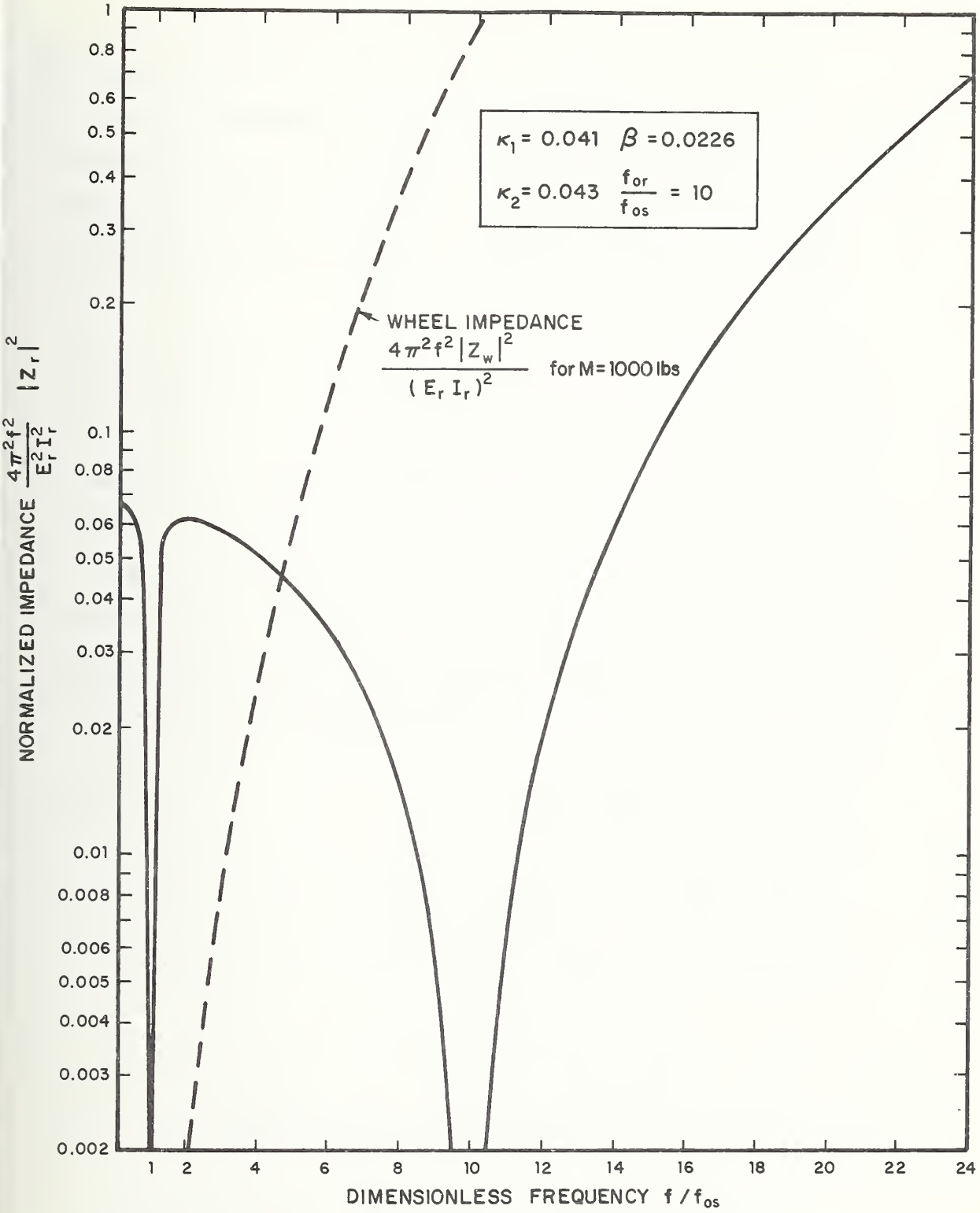

FIG. 2.8 DRIVING POINT IMPEDANCE OF THIS RAIL

Although the spectra of the rail and slab responses at a particular point are of some interest academically, they do not form a convenient basis for engineering design and will not be calculated in this report. Instead we will develop and use a measure of the total dynamic force acting on the tunnel floor.

2.5 Force Transmitted to the Tunnel Floor

Of major concern is the extent to which the floated slab system isolates the subway tunnel from the dynamic forces imparted to the rail due to passage of a rail vehicle. The pressure (force per unit area) on the tunnel floor at location (x,y) is related to the displacement of the slab, w(x,y,t) and the effective spring constant of the slab supports.

$$F(x,y,t) = K_s w(x,y,t) \tag{2.22}$$

Of course, the ultimate question concerns the vibration of the tunnel floor produced by F(x,y,t). Although the response characteristics of the subway tunnel are as yet unknown, it is still clear that, to some approximation, the vibration isolation effectiveness of floated slab systems can be optimized by making a suitable measure of transmitted pressure as small as possible.

The effectiveness of conventional vibration isolation

is usually measured by the force transmissibility which is the magnitude of the ratio of force transmitted to a floor or support to a sinusoidal force on the isolation system. A similar measure of vibration isolation effectiveness might be defined for the floated slab.

One possible definition of force transmissibility is the ratio of the force per unit area on the tunnel floor under the driving point to the force on the rail. On closer inspection, however, this proves inadequate since it fails to account for the effects of the spatially distributed nature of the slab response. For example, there can be different frequencies at which the slab response at the driving point is the same but at one frequency the response is limited to a small area near the driving point, whereas at the other, the response extends over a very large region. Also, as noted in the last section, the slab response at the driving point is nearly zero at coincidence. Thus, this measure of transmissibility would be very small even though the overall force on the tunnel is significant over a great distance. The same remarks might be made concerning any similar measure based on the tunnel floor force at only one location on the slab.

A better but still inconvenient alternative can be obtained by considering the mechanical oscillator analogy presented above. Just as was done for the slab displacement, the forces on

the tunnel floor may be separated into the portions attributable to each slab mode and each of these may be decomposed into their wavenumber components, i.e., for a sinusoidal force on the rail:

$$F(x,y,t) = \sum_{n=1}^{\infty} \frac{1}{2\pi} \int_{-\infty}^{\infty} dk_x \, e^{jk_x x} \, \psi_n(y) \hat{F}_n(k_x,\omega) \, e^{-j\omega t} \qquad (2.23)$$

where $\hat{F}_n$ is the contribution from the k_x^{th} wavenumber component of the n^{th} slab mode. Placing Eq. 2.22 into Eq. 2.23 and comparing with Eq. 2.12, it is seen that

$$\hat{F}_n(k_x,\omega) = K_s(1-j\delta_s)\hat{w}_n(k_x,\omega) \qquad (2.24)$$

where the slab support damping factor, δ_s, has been included by allowing the stiffness K_s to be complex, $K_s = K_s(1-j\delta_s)$. Eq. 2.24 together with Eq. 2.23 relates the tunnel floor force directly to the coupled oscillator analogy. Thus, a transmissibility can be defined for each slab mode oscillator at a given wavenumber by

$$T_{n,k_x}(\omega) = \left| \frac{\hat{F}_n}{\hat{q}} \right| \qquad (2.25)$$

and the effectiveness of the slab might be gauged by considering this function for each slab mode and wavenumber.

Fig. 2.9 shows the transmissibility for the first slab mode at zero wavenumber for rails with a range of fastener stiff-

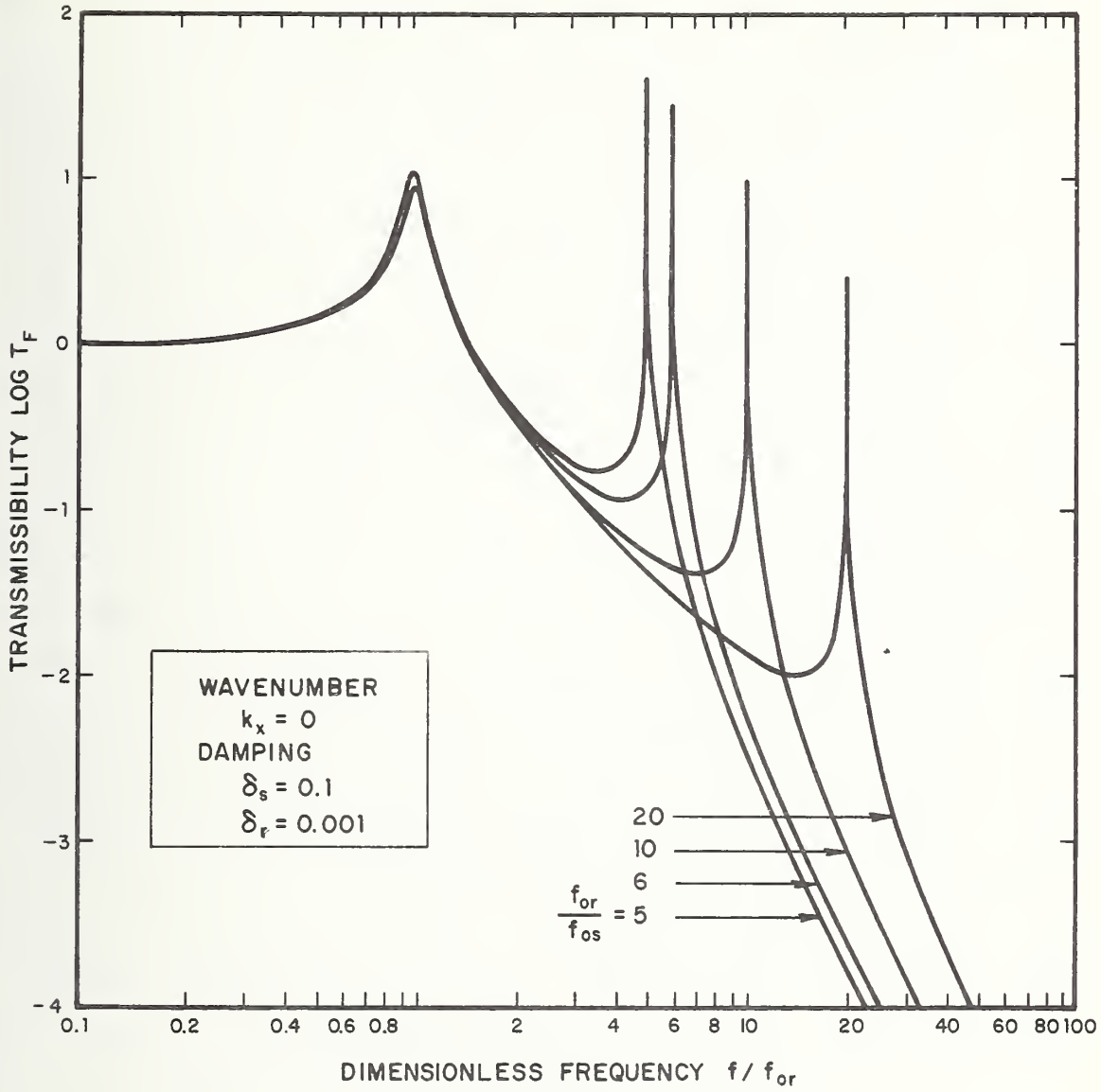

FIG. 2.9 CONSTANT WAVENUMBER TRANSMISSIBILITY CURVES FOR THE FIRST SLAB MODE

nesses. The first slab mode shape is just a constant over the cross-section and the zero wavenumber component is that part of the slab displacement consisting of a rigid body motion all along its length. Hence this plot shows a transmissibility arrived at by conventional vibration isolation theory modeling the slab as a rigid mass. Moreover, the result indicated by these plots -- that force transmission (above slab resonant frequency) decreases with increasing fastener stiffness is just what would be obtained with a conventional isolation system. Thus, if the coupled oscillators of Fig. 2.6 behaved in the same fashion for all wavenumbers, the situation would be simple indeed. Unfortunately this is not the case, as can be seen from Fig. 2.10. The figure shows Eq. 2.25 for the second slab mode and the intermediate rail dispersion curve of Fig. 2.3 plotted for various wavenumbers. As the wavenumber increases from zero, the distance between peaks is completely altered. Moreover, for $k_x L=4$ (at which a coincidence occurs) the peak at $\frac{\omega}{\omega_{os}} \simeq 20$ is some 5 dB above what it is for $k_x L=0$. Eq. 2.25 thus gives different measures of transmissibility for each wavenumbe component of force. Hence, it can be concluded that the above measure of slab effectiveness is also inconvenient. What is needed is an overall measure of the tunnel floor force. To define such a quantity, we begin by considering the case of random excitation. Clearly in this case the spectrum of the tunnel floor force, $S_F(s,y,\omega)$, is a valid measure of the force at each location on the slab. But $S_F(x,y,\omega)$ varies considerably with x and y and so does

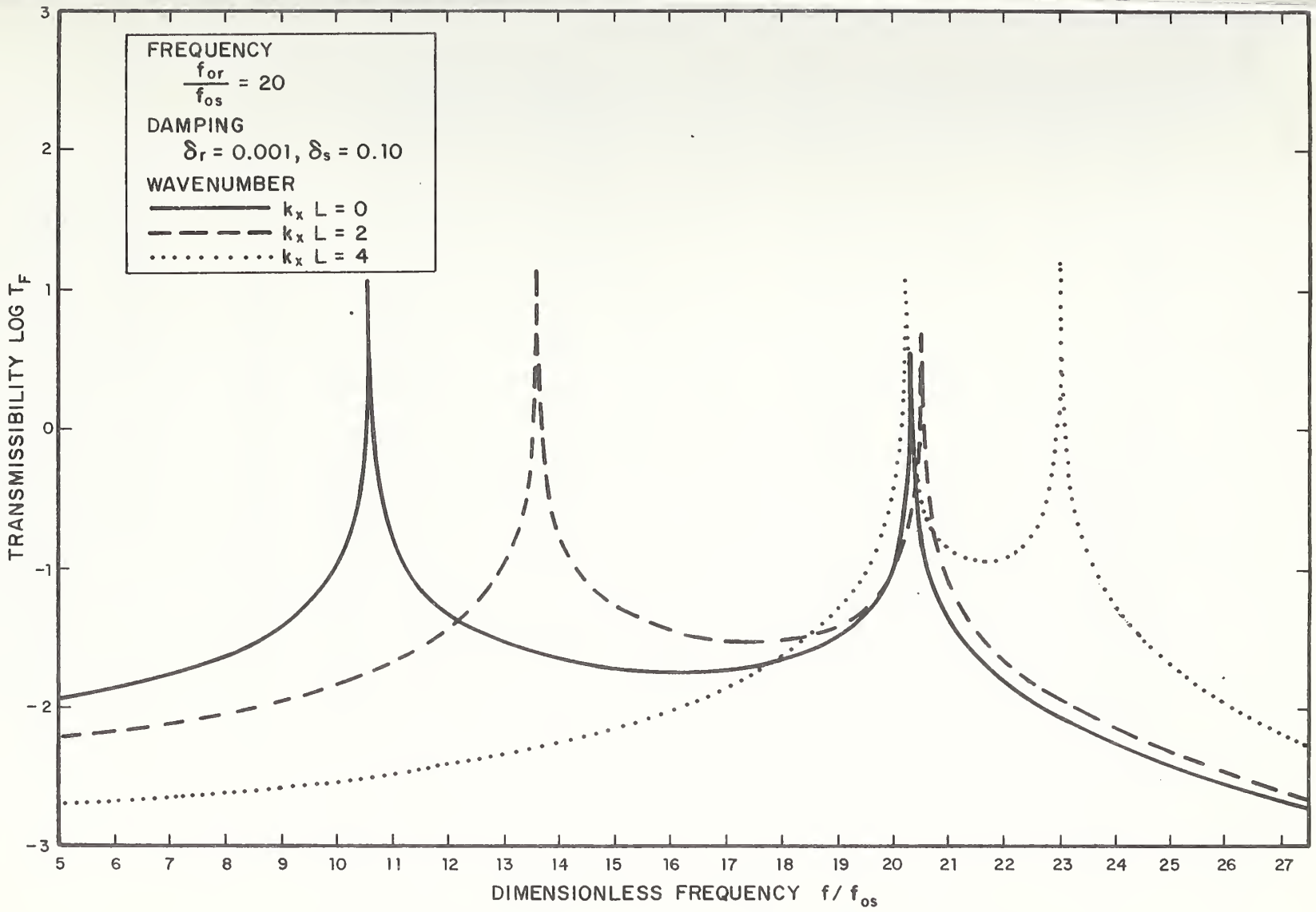

FIG. 2.10 CONSTANT WAVENUMBER TRANSMISSIBILITIES FOR THE SECOND SLAB MODE AT VARIOUS WAVENUMBERS

not provide a single measure of slab performance as a whole at a given ω.

An overall measure of force on the tunnel is the integral of S_F over the whole slab area, i.e.,

$$\Pi_F(\omega) = \int_{-\infty}^{\infty} d_x \int_0^L dy \quad S_F(s,y,\omega) \tag{2.26}$$

We shall call Π_F the integrated spectrum of the tunnel floor force. Using Eqs. 2.24 and 2.21 and the orthogonality relations for the ψ_n, we obtain:

$$\Pi_F(\omega) = \sum_{n=1}^{\infty} \Pi_{F_n}(\omega)$$

$$\Pi_{F_n}(\omega) = K_s^2(1 + \delta_s^2)\, L\, S_q(\omega) \int_{-\infty}^{\infty} dx \quad \left| \frac{\tilde{w}_n(x,\omega)}{\hat{q}} \right|^2 \tag{2.27}$$

Π_F has the advantage that it includes the effects of far field slab response, i.e., it is large when the region over which the slab response is significant becomes large.

By Parsevals' theorem the integration over x can be changed to one over k_x. Thus,

$$\Pi_{F_n}(\omega) = K_s^2(1+\delta_s^2)\, L\, S_q(\omega)\, \frac{1}{2\pi} \int_{-\infty}^{\infty} dk_x \left| \frac{\hat{w}_n(k_x,\omega)}{\hat{q}} \right|^2 \tag{2.28}$$

$$= \frac{1}{2\pi} \int_{-\infty}^{\infty} dk_x \; S_{F_n}(k_x,\omega)$$

where $S_{F_n}(k_x,\omega)$ is the spectral density of the n^{th} oscillator response at wavenumber k_x. Π_F is thus, in a sense, the average of all such spectra over all wavenumbers. Note that when Π_F is divided by $S_q(\omega)$ it gives a measure of overall dynamic force transmissibility.

Finally, it will be seen that the integrated spectrum of the force on the tunnel floor is closely related to an approximation for the total acoustic power radiated by the slab.

2.6 Calculation of the Integrated Spectrum

The procedure for calculating the integrated spectrum of the force per unit area acting on the tunnel floor depends on the values of the damping loss factors for the slab and its supports. For small values of damping we need consider only the resonant response of the slab modes of vibration. Calculations for this case are presented in Section 2.6.1. For larger values of damping contributions from non-resonant slab response must also be included in calculation of the integrated spectrum. The calculations for large damping are presented in Section 2.6.2.

2.6.1 Light Damping

The integrated spectrum has been calculated from Eq. 2.28

under the assumption that the damping loss factors of each constant k_x oscillator are much smaller than the coupling loss factors between oscillators. It is worthwhile to discuss at some length the approximation used in the calculation. The integrand

$$\left|\frac{\hat{w}_n(k_x,\omega)}{\hat{q}}\right|^2$$

is a positive function over the whole k_x - ω plane. For light damping this function has large maxima near the dispersion curves of the coupled system normal modes. Thus, the integrand can be thought of as a distribution of mass in the k_x - ω plane, with large maxima near the dispersion curves of the coupled system normal modes. If damping is small then most of the contribution to the integral comes from the regions near the modal dispersion curves. The subsequent procedure for calculating the lightly damped response is illustrated in Fig. 2.11. First the "spectral mass" in the interval $[k_x, k_x + dk_x]$ attributable to the peaks at each dispersion curve is calculated. This can be done by relatively simple integrations over ω. Next, the spectral masses are lumped onto the corresponding dispersion curves, i.e., the integrand is treated as a set of line densities concentrated solely on the dispersion curves. Finally, these spectral masses are placed within the intervals $d\omega_1$ and $d\omega_2$ in the manner indicated in the figure. The result is a spectral distribution which is correct only within frequency intervals much larger than the damping bandwidth of the system.

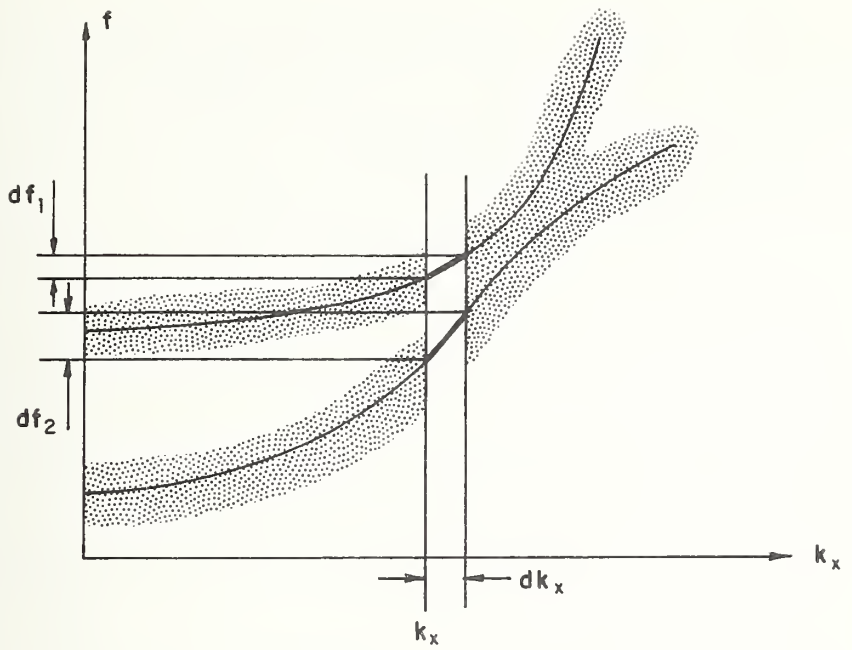

The magnitude of $|\frac{\hat{w}_n}{\hat{q}}|^2$ is indicated by the shading. The maxima of this function follow the dispersion curves of the coupled system modes. Within each interval, $[k_x, k_x+dk_x]$, the "spectral mass" is first resolved into the portions attributable to each mode and is then assigned to the corresponding dispersion curve. Finally each mass is projected onto the f line so as to be distributed within the intervals df_1 and df_2.

FIG. 2.11 ILLUSTRATION OF THE APPROXIMATION USED IN CALCULATING THE INTEGRATED SPECTRUM

When the above procedure is carried out, it is found that the integrated spectrum can be expressed in terms of the dispersion relations of the uncoupled rail and slab modes. The full result for light damping is as follows:

$$\Pi_F(\omega) = \sum_{n=1}^{\infty} \Pi_{F_n}(\omega) \tag{2.29a}$$

$$\Pi_{F_n}(\omega) = \frac{1}{2L}\left(\frac{\omega_{os}}{\omega_{or}}\right)^4 \psi_n^2 \left(1+\delta_s^2\right) S_q(\omega)\, \tilde{\Pi}_{F_n}(\omega) \tag{2.29b}$$

$$\tilde{\Pi}_{F_n}(\omega) = U\left(\frac{\omega^2}{\omega_{or}^2} - \Lambda_r\right)\left[\frac{dk_x}{d\omega}\,\frac{\omega_{or}^2}{\Delta_r\,\omega\left[(\Lambda_r-\Lambda_s)^2+4\beta\psi_n^2\right]+\left(\Delta_r+\Delta_s\right)^2}\right] \text{ at } \frac{\omega^2}{\omega_{or}^2} = \Lambda_r$$

$$+ U\left(\frac{\omega^2}{\omega_{or}^2} - \Lambda_{sn}\right)\left[\frac{dk_x}{d\omega}\,\frac{\omega_{or}^2}{\Delta_s\,\omega\left[(\Lambda_r-\Lambda_s)^2+4\beta\psi_n^2\right]+\left(\Lambda_r+\Lambda_s\right)^2}\right] \text{ at } \frac{\omega^2}{\omega_{or}^2} = \Lambda_{sn} \tag{2.29c}$$

where

$$\Lambda_r = \frac{1}{\kappa_1}\left(k_x^4 + \kappa_1\right) \tag{2.30a}$$

$$\Lambda_s = \frac{1}{\kappa_2}\left(k_x^4 + \gamma_n^4 + \kappa_2\,\frac{\omega_{os}^2}{\omega_{or}^2}\right) \tag{2.30b}$$

$$\Delta_r = \frac{1}{2}\left(\delta_s + \delta_r\beta\frac{\omega_{or}^2}{\omega_{os}^2}\psi_n^2\right)\frac{\omega_{os}^2}{\omega_{or}^2}\left[1-|\tau|\right] + \frac{1}{2}\delta_r[1+|\tau|] \tag{2.30c}$$

$$\Delta_s = \frac{1}{2}\left(\delta_s + \delta_r\beta\frac{\omega_{or}^2}{\omega_{os}^2}\psi_n^2\right)\frac{\omega_{os}^2}{\omega_{or}^2}\left[1+|\tau|\right] + \frac{1}{2}\delta_r[1-|\tau|] \tag{2.30d}$$

$$\tau = |\Lambda_r - \Lambda_s|\left[\Lambda_r - \Lambda_s)^2 + 4\beta\psi_n^2\right]^{-\frac{1}{2}} \tag{2.30e}$$

$$\left[\left(\frac{dk_x}{d\omega}\right)\right]_{\text{at } \frac{\omega^2}{\omega_{or}^2} = \Lambda_r} = \frac{1}{2}\kappa_1^{\frac{1}{4}}\frac{\omega}{\omega_{or}^2}\left(\frac{\omega^2}{\omega_{or}^2} - 1\right)^{-3/4} \tag{2.31a}$$

$$\left[\left(\frac{dk_x}{d\omega}\right)\right]_{\text{at } \frac{\omega^2}{\omega_{or}^2} = \Lambda_s} = \begin{cases} \frac{1}{2}\kappa_2^{\frac{1}{4}}\omega_{or}^{-\frac{1}{2}}\left(\omega^2 - \omega_{os}^2\right)^{-3/4}\omega \text{ (1st mode)} \\ \frac{\omega\kappa_2}{2\omega_{or}^2}\frac{1}{\alpha\sqrt{\alpha-\left(\frac{n\pi}{L}\right)^2}} \text{ (2nd, 3rd, ... modes)} \end{cases} \tag{2.31b}$$

$$\alpha = \left[\left(\frac{n\pi}{L}\right)^4 - \left(\frac{\pi}{2L}(2n-1)\right)^4 + \frac{\kappa_2}{\omega_{or}^2}(\omega^2-\omega_{os}^2)\right]^{\frac{1}{2}},\ n = 2, 3 \ldots \tag{2.31c}$$

Here $\omega^2/\omega_{or}^2 = \Lambda_r$ and $\omega^2/\omega_{or}^2 = \Lambda_s$ are the dispersion curves of the uncoupled rail and slab modes and U is a unit step function;

$$U(x) = \begin{cases} 1, & x \geq 0 \\ 0, & x < 0 \end{cases} \tag{2.32}$$

The value of ψ_n in Eqs. 2.29 and 2.30 is to be at $y = y_o$, where y_o is the distance of the rail from the edge of the slab, see Fig. 2.1.

Each term in Eq. 2.29c shows a peak at the rail and slab resonant frequencies due to the dependence on $\frac{dk_x}{d\omega}$. This result reflects the fact obtained in section 2.4, that overall slab response is maximum near rail and slab resonance. Below these frequencies each term has a cutoff due to the fact that bending waves do not propagate. Also, as might be expected the overall levels of Π_F are inversely proportional to the damping.

Figs. 2.12 and 2.13 show the contribution of the first mode, Π_{F_1} averaged over 5 Hz bands for two different cases. The rail used in the first case is that shown in Fig. 2.3 with $\omega_{or}/\omega_{os} = 10$. Here no coincidence occurs and the reduced spectrum falls off rapidly for frequencies above the rail resonance. In the second case, the bending rigidity of the slab has been increased by ∿40% and a coincidence occurs at ∿200 Hz. Although the power levels of the rail and slab peaks are not appreciably affected, above $\omega = \omega_{or}$, the reduced spectrum shows a wide hump centered at ∿180 Hz. The level here is some 10 dB above what it was in the non-coincident case. The contributions of the higher modes show similar characteristics.

From the above we conclude that if the excitation

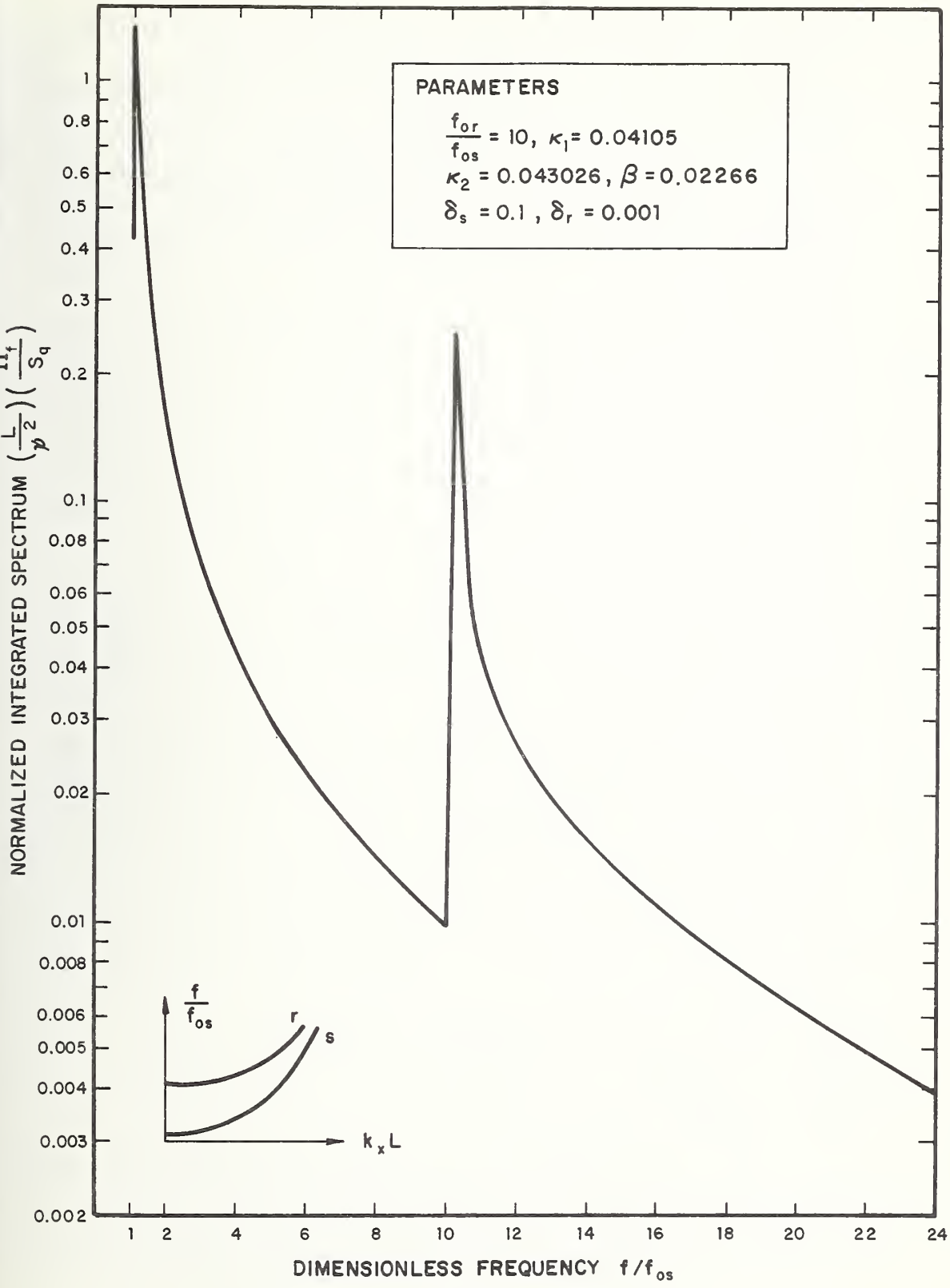

FIG. 2.12 INTEGRATED SPECTRUM OF TUNNEL FLOOR FORCE - NO COINCIDENCE

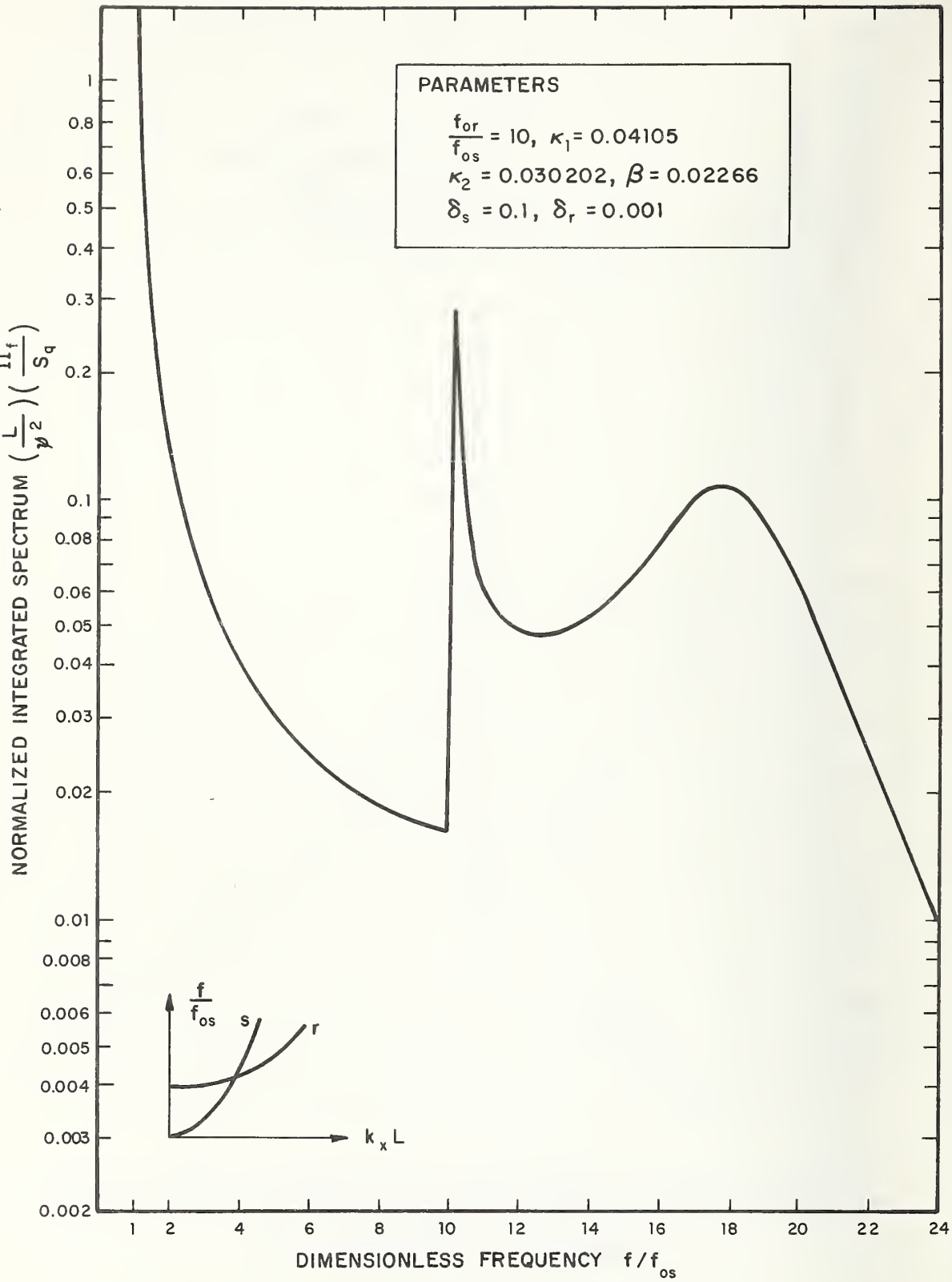

FIG. 2.13 INTEGRATED SPECTRUM OF TUNNEL FLOOR FORCE - WITH COINCIDENCE

spectrum is broad band and constant for all frequencies, the overall magnitude of the tunnel floor force is greatest near the uncoupled rail slab resonances. The occurrence of coincidence can significantly deteriorate slab effectiveness.

The spectrum of excitation due to the rolling of wheels on track is not constant for all frequencies. Thus, in section 2.7 the integrated spectrum will be calculated for an excitation spectra obtained from the micro-roughness model of the wheel-rail interaction [5].

2.6.2 High Damping

For high values of damping the response of the constant k_x oscillators is predominantly nonresonant. Thus, the integrated spectrum given by Eq. 2.29c will be in error, since it includes only the contribution from resonant oscillator vibration. If we include the nonresonant response, the integrated spectrum should be a sum of two terms.

$$\Pi_F(\omega) = \Pi_F^{\text{resonant}}(\omega) + \Pi_F^{\text{nonresonant}}(\omega) \tag{2.33}$$

where the first term is given by Eqs. 2.29.

To calculate the nonresonant contribution to the integrated spectrum, we refer back to Eqs. 2.24, 2.26 and 2.28 which give the integrated spectrum in terms of the wavenumber components for each slab mode,

$$\Pi_F(\omega) = \sum_{n=1}^{\infty} K_s^2(1+\delta_s^2)\ L \quad \frac{1}{2\pi}\int_{-\infty}^{\infty} dk_x\ S_{w_n}(k_x,\omega) \tag{2.34}$$

where $S_{w_n}(k_x,\omega)$ is the spectral density of the response of the n^{th} oscillator at wavenumber k_x. As noted previously, the spectral density for light damping exhibits large maxima at values of k_x and ω near those given by the dispersion curves for the uncoupled rail and slab modes. For large damping the spectral density does not exhibit large maxima so that all values of k_x must be considered in the integration of Eq. 2.34. To proceed we can assume that wavenumber coincidence effects are not important with regard to the nonresonant response since they occur only at a single value of wavenumber. In this case we can use a chaining approach, i.e., we can calculate the rail response assuming the slab to be rigid and then use the computed rail response to calculate the forces on the slab, the slab response, and the forces transmitted to the tunnel floor. Following this approach we find

$$\frac{S_{w_n}(k_x,\omega)}{S_q(\omega)} = \frac{\omega_{or}^4(1+\delta_r^2)}{\rho_s^2} \quad \frac{\psi_n^2(y_o,k_x)}{\left|\omega_{or}^2(1-j\delta_r)+\frac{E_r I_r}{\rho_r}k_x^4-\omega^2\right|^2} \cdot \tag{2.35}$$

$$\frac{1}{\left|\omega_{os}^2(1-j\delta_s) + \frac{E_s I_s}{\rho_s}(k_x^4 + \gamma_n^4) - \omega^2\right|^2}$$

where y_o is defined in Fig. 2.1. The summation and integration required in Eq. 2.34 can only be carried out numerically. This would represent a reasonable approach in detailed studies of one specific design. However, our objectives for the present study are to develop engineering design guidelines. Therefore, we proceed to simplify Eq. 2.35 so that the integration can be carried out analytically in closed form. Toward this end we deal only with cases where $\omega_{os} << \omega_{or}$ and where frequencies are in the range $\omega_{os} < \omega < \omega_{or}$.

The rigid body slab resonance, ω_{os}, is typically below 125 radians per second (20 Hz) and the rigid body rail resonance, ω_{or}, is above 785 radians per second (125 Hz). Thus, the frequency range ω_{os} to ω_{or} encompasses frequencies of greatest importance in calculating slab effectiveness, since the vibration transmitted to nearby buildings is greatest in this frequency range. Furthermore, we deal only with cases where the cutoff frequency of the n=2 crossmode, ω_{2s}, is well above ω_{or}. In this case we can limit the summation in Eq. 2.34 to a single term with n=1 and; from Eq. 2.4, γ_n=0, Eq. 2.34 becomes

$$\frac{\Pi_F(\omega)}{S_q(\omega)} = \left(\frac{\omega_{os}}{\omega}\right)^4 (1+\delta_s^2)(1+\delta_r^2)\, L \qquad (2.36)$$

$$\frac{1}{2\pi} \int_{-\infty}^{\infty} dk_x \frac{1}{\left[\left(1+\frac{k_x^4}{\kappa_1}\right)^2 + \delta_r^2\right]^2 \left[\left(1-\frac{\omega_{or}^2}{\omega^2}\frac{k_x^4}{\kappa_2}\right)^2 + \frac{\omega_{os}^2}{\omega^2}\delta_s^2\right]^2}$$

where we have set $\psi_n^2 = \psi_1^2 = 1$. As previously discussed we take the damping of the slab, δ_s, to be sufficiently high that the contribution to the integral from values of wavenumber greater than $(\kappa_2\omega^2/\omega_{or}^2)^{1/4}$ is negligible. Thus, as long as the condition

$$\frac{\kappa_1}{\kappa_2} < \left(\frac{\omega}{\omega_{or}}\right)^2 \qquad (2.37)$$

is held and $\delta_r < 1$, the integral can be evaluated as

$$\int_{-\infty}^{\infty} dk_x \frac{1}{\left(1+\frac{k_x^4}{\kappa_1}\right)^2} \qquad (2.38)$$

This gives

nonresonant

$$\frac{\Pi_F(\omega)}{S_q(\omega)} \simeq \left(\frac{\omega_{os}}{\omega}\right)^4 (1+\delta_s^2)(1+\delta_r^2)\left(\frac{\kappa_1}{64}\right)^{1/4} L \qquad (2.39)$$

We see from Eq. 2.39 that the resonance frequency of the slab should be kept as low as possible to prevent the transmission of forces to the tunnel floor by nonresonant slab motion. In addition, the damping should also be kept low. However, if it is too low the resonant slab response will degrade the slab performance.

2.7 Integrated Spectrum for Microroughness Excitation

Here we consider a more precise model of the excitation of the rail by the wheels. Actual wheels and rails deviate from perfect smoothness. Assuming uninterrupted rolling contact, the rails will be excited by the relative velocity of the contact point of the center of the wheel and a rail reference axis. The resulting spectrum of the force on the rail is [5]

$$S_q(\omega) = \frac{\omega^2}{S} \left| \frac{z_r z_w}{z_r + z_w} \right|^2 \Phi_r(k) \quad \text{with} \quad k=\omega/S \tag{2.40}$$

where z_r and z_w are the rail and wheel impedances respectively, S is the train speed and $\Phi_r(k)$ is the wavenumber spectrum of the relative velocity of wheel and rail due to their combined roughness. Z_r has already been obtained. For frequencies above roughly 50 Hz, a reasonable approximation for z_w is found to be

$$z_w \simeq -j\omega M \tag{2.41}$$

where M is the mass of the wheel, bearing and an equivalent axle mass.

To illustrate the effect of rail impedance on the characteristics of the reduced spectrum of tunnel floor force, we shall assume M to be so large that for all frequencies of interest,

$$S_q(\omega) \simeq \frac{\omega^2}{S} |z_r|^2 \Phi_r(k = \omega/S) \tag{2.42}$$

Thus, the wheel/rail interaction is modeled as a velocity source. The effectiveness of slab performance might now be judged by referring Π_F to $\Phi_r(k)$; i.e., by evaluating $\Pi_F/\Phi_r(k)$. The variation of $|z_r|^2$, as determined by Eq. 2.18, radically alters the character of the integrated spectrum associated with the resonant slab vibration. Figs. 2.14 and 2.15 show the first slab mode contribution to the reduced spectrum divided by $\Phi_r(k)$ for the cases considered in Figs. 2.12 and 2.13. The presence of resonant minima in $|z_r|^2$ at ω_{os} and ω_{or} completely eliminates the sharp peaks in Π_{F_1} due to a flat excitation spectrum. The effect of coincidence, however, remains the same, i.e., to increase the reduced spectrum about 10 dB over a broad frequency band centered at $\sim$180 Hz. Above that frequency, both spectra have a very wide hump (not shown in the figures) with a maximum at $\sim$500 Hz.

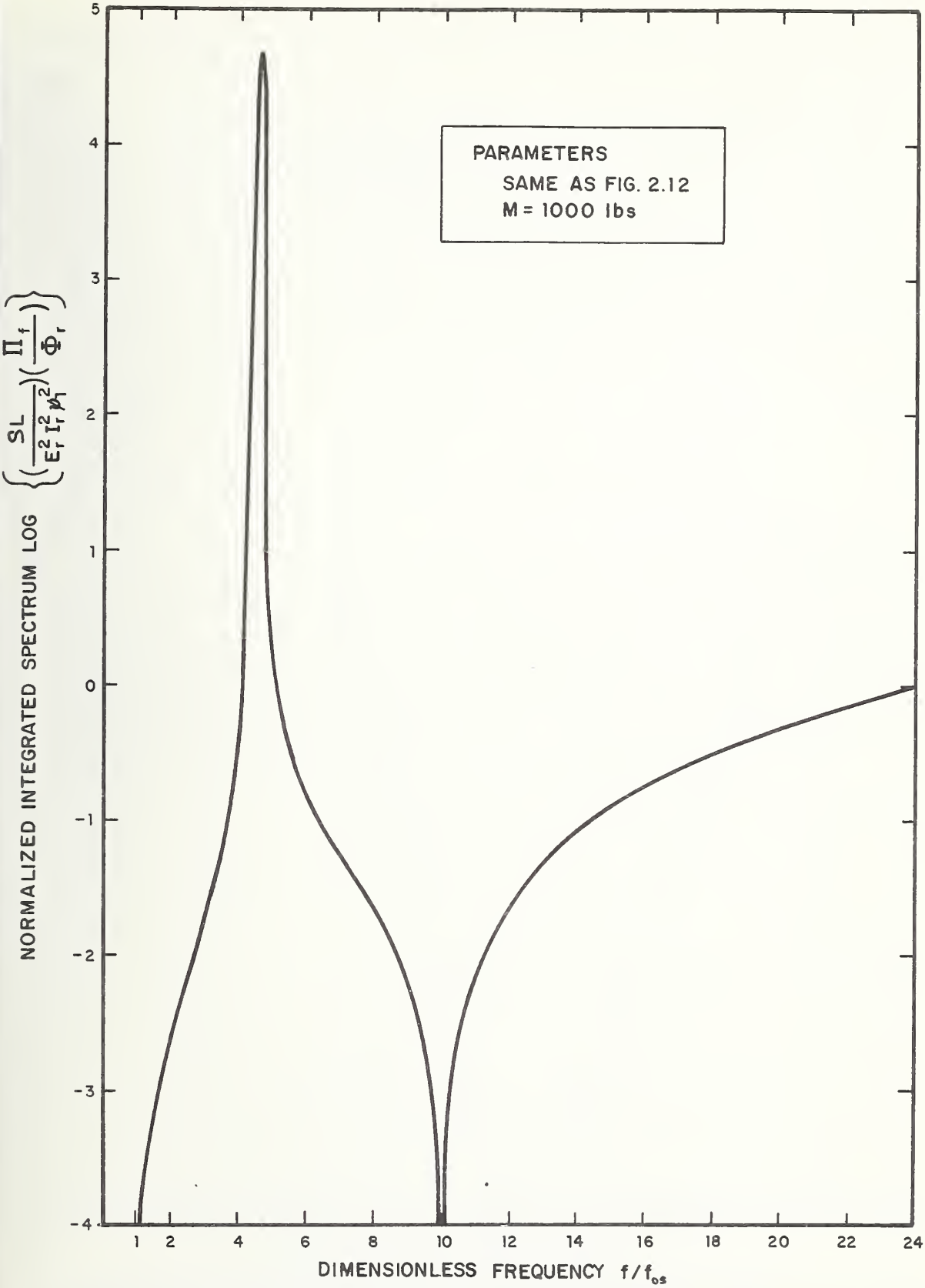

FIG. 2.14 INTEGRATED SPECTRUM FOR THE MICROROUGHNESS MODEL — CASE 1

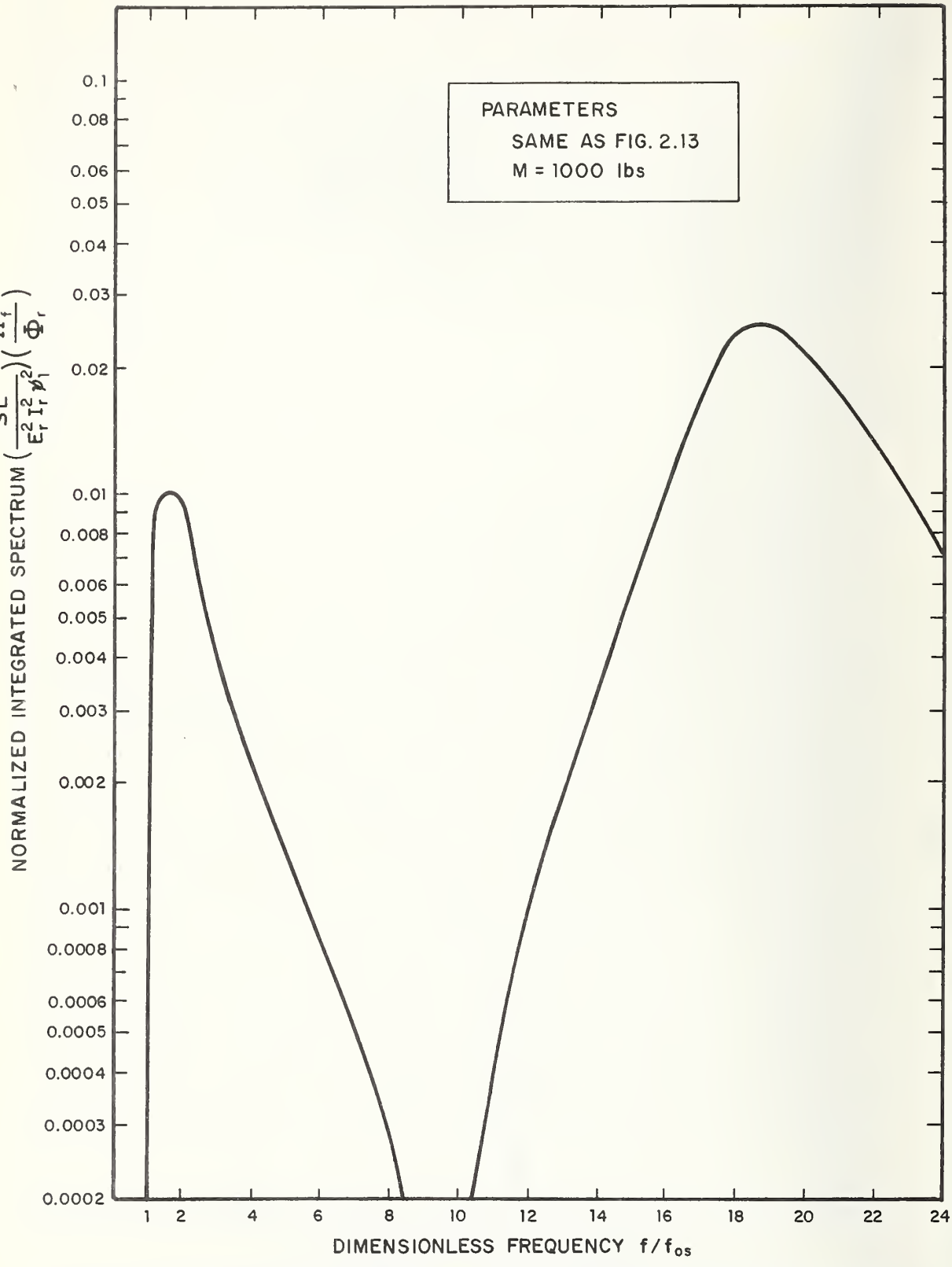

FIG. 2.15 INTEGRATED SPECTRUM FOR THE MICROROUGHNESS MODEL OF WHEEL-RAIL INTERACTION-CASE 2

It can be concluded that, in general, for a wheel/rail roughness excitation the reduced spectrum of the tunnel floor force exhibits no sharp resonant peaks near the rail resonant frequency or the slab mode cutoff frequencies. As in the case of a flat excitation spectrum, the occurrence of coincidence still has a significant effect on slab performance.

2.8 Total Acoustic Power Radiated by the Slab

Now consider the total acoustic power radiated by the slab. Only those wavenumbers smaller than the acoustic wavenumber ($k=\omega/c$) may radiate sound efficiently. But the significant response of rail and slab (looking at the k_x-ω plane) lies above the acoustic dispersion curve. Then, for forcing at a given ω, the total radiated power may be approximated by:

$$W_{rad}(\omega) \simeq \rho_o c_o \sigma_{rad} \int_0^L dy \int_{-\infty}^{\infty} dx \; |\dot{w}(x,y,t)|^2$$

$$= \rho_o c_o \sigma_{rad} \, \omega^2 \int_0^L dy \int_{-\infty}^{\infty} dx \; |\tilde{w}(x,\omega)|^2 \qquad (2.43)$$

$$= \rho_o c_o \sigma_{rad} \, L \, \omega^2 \sum_{n=1}^{\infty} \int_{-\infty}^{\infty} dx \; |\tilde{w}_n(x,\omega)|^2$$

where ρ_o and c_o are the density and velocity of sound in air, σ_{rad}

is the radiation efficiency of the slab, and use has been made of the modal expansion, Eq. 2.9, and the orthogonality properties of the slab modes. For a stationary random excitation, the spectrum of the total power radiated is therefore:

$$W_{rad}(\omega) = \sum_{n=1}^{\infty} W_{rad,n}(\omega) \tag{2.44a}$$

$$W_{rad,n}(\omega) = \rho_o c_o \sigma_{rad} \, L \, \omega^2 \, S_q(\omega) \int_{-\infty}^{\infty} dx \left| \frac{\tilde{\tilde{w}}_n}{\hat{q}} \right|^2 \tag{2.44b}$$

or, using Parseval's theorem:

$$W_{rad,n}(\omega) = \rho_o c_o \, \sigma_{rad} \, L \, \omega^2 \, S_q(\omega) \, \frac{1}{2\pi} \int_{-\infty}^{\infty} dk_x \left| \frac{\hat{w}_n}{\hat{q}} \right|^2 \tag{2.45}$$

Comparing this expression with Eq. 2.28 shows that

$$W_{rad,n}(\omega) = \frac{\rho_o c_o \sigma_{rad}}{K_s^2 \, (1+\delta_s^2)} \, \omega^2 \, \Pi_{F_n}(\omega) \tag{2.46}$$

where $\Pi_{F_n}(\omega)$ is the integrated spectrum of the force on the tunnel floor.

Apart from a factor of $\omega^2 \sigma_{rad}$ the total acoustic power radiated is proportional to the reduced spectrum of the force on the tunnel floor calculated above. Thus, the general characteristics of the total acoustic power are the same as those derived

for the reduced spectrum, except for a magnification by a factor of $\omega^2\sigma$rad. The radiation efficiency, σ_{rad}, can be taken to be equal to one for frequencies above 70 Hz [6].

2.9 Comparison of Prediction Procedure with State-of-the-Art Method

The analytical model developed in the preceding sections allows us to predict the vibration levels of the rail and slab and the dynamic forces on the tunnel floor. It is important now that we understand the significant differences between our results and those obtained using the state-of-the-art procedure.

The state-of-the-art procedure is to model the slab-track by an equivalent single-degree-of-freedom system as shown in Fig. 1.1. In this simple model the mass is taken to be the mass per unit length of the floating slab. It is implicitly assumed that the mass per unit length of the rail is small compared to that of the slab and therefore can be neglected. The spring constant in the single-degree-of-freedom model is set to be equal to the slab supports and the entrained air under the slab per unit length of track. With these definitions the resonance frequency of the single-degree-of-freedom system is simply the rigid body resonance of the slab, ω_{os}, as defined in Eq. 2.5b.

Finally, the damping coefficient for the single-degree-of-freedom model is set equal to the effective damping coefficient per unit length of the slab track, δ_s.

The performance of the floating slab is predicted in terms of the force transmissibility, $T_F(\omega)$, which is defined as the ratio of the amplitudes of the force applied through the spring and damping elements to the rigid support and the force applied to the mass [7]. This transmissibility, $T_F(\omega)$, is given by

$$T_F^2(\omega) = \frac{\omega_{os}^4(1 + \delta_s^2)}{(\omega^2 - \omega_{os}^2)^2 + \delta_s^2\omega_{os}^4} \tag{2.47}$$

where ω is the frequency in radians per second. The damping coefficient, δ_s, is a solid type of damping [8]. For a viscous damping mechanism it is more common to use a viscous damping coefficient, C_s, or a fraction of critical damping coefficient, ζ_s. These parameters are related by

$$\delta_s\omega_{os} = 2\zeta_s\omega = \frac{C_s}{M} \tag{2.48}$$

Thus, if the damping is viscous Eq. 2.47 becomes

$$T_F^2(\omega) = \frac{\omega_{os}^4 \left(1 + 4\zeta_s^2 \frac{\omega^2}{\omega_{os}^2}\right)}{(\omega^2 - \omega_{os}^2)^2 + 4\zeta_s^2\omega^2\omega_{os}^2} \tag{2.49}$$

The transmissibility for constant values of ζ_s are shown in Fig. 1.2

At high frequencies, Eq. 2.47 can be written approximately as

$$T_F(\omega) \simeq \left(\frac{\omega_{os}}{\omega}\right)^2 (1 + \delta_s^2)^{\frac{1}{2}} \text{ for } \omega >> \omega_{os} \qquad (2.50)$$

or in the case of viscous damping Eq. 2.49 can be written

$$T_F(\omega) \simeq 2\zeta_s \frac{\omega_{os}}{\omega} \text{ for } \omega >> \omega_{os} \qquad (2.51)$$

The force transmissibility for the single-degree-of-freedom system shows the following characteristics. At low frequencies below the rigid body resonance frequency of the slab, ω_{os}, the transmissibility is one--forces are transmitted without reduction in amplitude. At and near the resonance frequency the transmissibility is greater than one so that the forces are increased in amplitude by the addition of the slab. Finally, at high frequencies the force transmissibility is much less than one and decreases rapidly with increasing frequency. For solid type damping Eq. 2.50 shows that the transmissibility decreases with the second power of frequency and does not depend on the value of the damping unless δ_s is unusually large; i.e., near one. For a viscous damping mechanism Eq. 2.51 shows that the transmissibility decreases with the first power of frequency. In this case the

transmissibility also increases with increasing values of damping. Thus, a tradeoff occurs. Small values of viscous damping decrease the force transmissibility at high frequencies, but increases the amplitude of the peak in the transmissibility at the slab resonance frequency.

In the more precise analytical model developed in this report the force transmissibility must be defined for each cross-mode and as a function of both frequency, ω, and wavenumber, k_x; see Eq. 2.25. Combining Eqs. 2.24, 2.25, and 2.35 with the relationship,

$$S_{w_n}(k_x,\omega) = |\hat{w}_n(k_x,\omega)|^2 \tag{2.52a}$$

and

$$S_q(\omega) = |\hat{q}(\omega)|^2 \tag{2.52b}$$

we can find the transmissibility for each cross-mode. In the special case of the first mode with $k_x=0$ we find the transmissibility to be

$$T^2_{n=1,k_x=0}(\omega) = \frac{\omega_{or}^4 (1+\delta_r^2)}{(\omega_{or}^2-\omega^2)^2 + \delta_r^2\omega_{or}^4} \frac{\omega_{os}^4 (1+\delta_s^2)}{(\omega_{os}^2-\omega^2)^2 + \delta_s^2\omega_{os}^4} \tag{2.53}$$

For frequencies below the rail resonance frequency and for moderate to small values of rail damping the transmissibility given by Eq. 2.53 agrees with that given by the single-degree-of-freedom model.

The transmissibility for the first mode and for zero wavenumber indicates the transmission of forces that have a long wavelength. It is reasonable to argue that these long wavelength forces are more effective in exciting the tunnel into vibration than the forces with short wavelength, since the tunnel floor has a very high bending rigidity. Based on this argument it is also reasonable to conclude that the force transmissibility given by the single-degree-of-freedom model may give a good indication of the transmission of vibration to the tunnel. Further study of the tunnel response to different types of force excitation is needed to resolve the general validity of this conclusion.

The transmissibility given by the single-degree-of-freedom model also relates to the transmissibility for the integrated spectrum of forces due to nonresonant slab vibration. Comparison of Eqs. 2.39 and 2.50 shows that for high frequencies

nonresonant

$$\frac{\Pi_F(\omega)}{S_q(\omega)} = T_F^2(\omega) \quad (1 + \delta_r^2)\left(\frac{\kappa_1}{64}\right)^{1/4} L \quad \text{for } \omega >> \omega_{os} \tag{2.54}$$

where $\Pi_F(\omega)$ is the integrated spectrum from Eq. 2.39 and $T_F(\omega)$ is the force transmissibility given by Eq. 2.50. For typical conditions, RE 100 rail with a rail resonance frequency of 200 Hz (1257 rad/sec), Eq. 2.54 becomes

$$\frac{\Pi_F(\omega)}{S_q(\omega)}^{\text{nonresonant}} = T_F^2(\omega) \quad \frac{(1+\delta_r^2)\ L}{4.5} \tag{2.55}$$

where L is the slab width in feet. For single track slabs with a width of approximately 10 ft. and for typical values of rail fastener damping, the integrated spectrum divided by the spectrum of the forces applied to the rail at the wheel/rail contact point is very closely related to the force transmissibility given by the single-degree-of-freedom model.

A comparison of results from the precise model developed in this report with results from the state-of-the-art single-degree-of-freedom model shows that in a general case where forces over a broad range of wavenumber contribute to the tunnel response the simple single-degree-of-freedom model can overestimate the slab performance (underestimate the transmissibility) by over 10 dB. Thus, great caution must be must be used in applying the results of the simple model even though its use is valid under a number of conditions.

2.10 Extension of the Analysis to Floating-Tie Track

In previous sections we have carried out an analysis for floating slabs that are infinite in the direction along the track. In reality, of course, the slab is not infinite and in some cases is better modelled by a series of short segments. Floating tie systems must be included with these cases.

The floating-tie track consists of heavy concrete ties supported by resilient materials on the tunnel floor. The rail is fastened to the tie by means of conventional rail fasteners. To treat this system analytically we must model the ties by an orthotropic plate with the bending stiffness along the direction of the track being zero. Many of the fundamental concepts discussed earlier continue to be valid. To calculate the cross-mode resonance frequencies we use Eqs. 2.4 and 2.5 with $k_x=0$. The dispersion curves, shown in Fig. 2.3 for a floating slab, become straight lines with values of frequency being independent of wavenumber.

The mechanical oscillator analogy shown in Fig. 2.6 can also be used for the floating-tie track. Parameters are obtained by setting k_x equal to zero so that the oscillator masses and stiffnesses are no longer functions of wavenumber.

The assumptions and approximations leading to Eqs. 2.29 and 2.30 are no longer acceptable for the floating-tie system. However, if we restrict our attention to the frequency range below the rail resonance frequency we can use the chaining approach, which leads to an equation that is similar to Eq. 2.35.

$$\frac{S_{F_n}(k_x,\omega)}{S_q(\omega)} = \frac{\omega_{or}^4(1+\delta_r^2)\ \psi_n^2(y_o)}{\left|\omega_{or}^2(1-j\delta_r) + \frac{E_rI_r}{\rho_r}\ k_x^4-\omega^2\right|^2} \cdot \frac{\omega_{os}^4\ (1+\delta_s^2)}{\left|\omega_{os}^2(1-j\delta_s) + \frac{E_sI_s}{\rho_s}\ \gamma_n^4-\omega^2\right|^2} \tag{2.56}$$

Following the same approach used to derive Eq. 2.36 we find the integrated spectrum as

$$\frac{\Pi_F(\omega)}{S_q(\omega)} = \sum_{n=1}^{\infty} \frac{(1+\delta_s^2)(1+\delta_r^2)\ L\ \psi_n^2(y_o)}{\left(1-\frac{\omega^2}{\omega_{os}^2} + \frac{E_sI_s}{K_s}\ \gamma_n^4\right)^2 + \delta_s^2} \cdot \frac{1}{2\pi}\int_{-\infty}^{\infty} dk_x \left[\left(1+\frac{k_x^4}{\kappa_1}\right)^2 + \delta_r^2\right]^{-1} \tag{2.57}$$

For values of δ_r less than one we find

$$\frac{\Pi_F(\omega)}{S_q(\omega)} = \sum_{n=1}^{\infty} \frac{(1+\delta_s^2)\ L\ \psi_n^2(y_o)\ \left(\frac{\kappa_1}{64}\right)^{1/4}}{\left(1-\frac{\omega^2}{\omega_{os}^2} + \frac{E_sI_s}{K_s}\ \gamma_n^4\right)^2 + \delta_s^2} \tag{2.58}$$

If we limit the summation in Eq. 2.58 to the first mode, then

$$\frac{\Pi_F(\omega)}{S_q(\omega)} = \frac{1 + \delta_s^2}{(1 - \frac{\omega^2}{\omega_{os}^2})^2 + \delta_s^2} \; L(\frac{\kappa}{64})^{\frac{1}{4}} \tag{2.59}$$

The first term in Eq. 2.59 is identical to the square of the force transmissibility obtained from the single-degree-of-freedom model. The second term is approximately equal to two for typical floating-tie systems. Thus, we conclude that the simple model can be used for floating-tie systems as long as the resonance frequencies of the second and other higher cross modes are above the frequency range of interest. If this is not the case, then Eq. 2.58 can be used to provide a measure of performance for the floating-tie system.

2.11 Conclusions for Analytical Model

The analytical model developed in this section allows us to calculate the ratio of dynamic forces applied to the tunnel floor to those applied to the rail at the wheel/rail contact points. Ideally, we would like to calculate the vibration levels in buildings near the tunnel. However, to do this we require in addition models to calculate the dynamic forces at the wheel/rail contact points, the vibratory response of the tunnel, and the vibration transmission from the tunnel to nearby buildings.

Within the present state-of-the-art these models do not exist, although some relevant work has been carried out [2,9].

In spite of our inability to calculate the actual vibration levels in buildings, we can use the analytical model developed here to compare different floating slab designs. Designs which minimize the integrated spectrum of forces on the tunnel floor in the important frequency range from approximately 10 to 175 Hz are desired.

3. FIELD STUDY

3.1 Introduction

With the assistance of the New York City Transit Authority, Cambridge Collaborative, Inc. has undertaken a detailed field study of the floating slab track section located between the Parsons Boulevard and the 169th Street stations of the IND line. The purpose of the study was to gather comprehensive data that would exhibit the slab's performance in reducing the vibration transmitted to neighboring buildings. Data collected consists primarily of vibration measurements at several points on the slab, on the tunnel walls, and on the tunnel floor. Measurements of the acoustic levels in the tunnel were also taken.

Because the vibration levels arising from a train passage vary from passby to passby due primarily to differences in wheel condition and train speed, it was necessary to make simultaneous recordings of the vibration signals at many locations in the tunnel for each of several train passbys. With these simultaneous recordings it is possible to compare vibration levels near the floating slab track section with levels near a conventional section of track for the same passby. The comparison leads to a direct evaulation of the floating slab performance.

3.2 Tunnel and Slab Construction

The tunnel is of a typical four-track cut and cover construction with two express tracks at the center and two local tracks on either side as in Fig. 3.1. The floating slab is located on the inbound express track and is composed of four fifty-foot long sections which are connected together by steel reinforcing rods as shown in Section AA of Fig. 3.2. The slab is isolated from the tunnel structure by means of resilient rubber-encased glass fiber pads spaced as shown in Fig. 3.2. The increasing number of pads at both ends of the slab provides a gradual transition of support from the conventional track to the floating slab track. A cross section detail of the slab appears in Fig. 3.3.

The slab was constructed by removing the existing finished floor slab (shown in Fig. 3.1) and laying down a welded galvanized steel pan form with the resilient pads (Consolidated Kinetics Type KIP-8802) epoxied to the pan bottom. Steel reinforcing was installed and finally the concrete poured. Fiberboard spacers (Consolidated Kinetics Perimeter Isolation Board) were set between the slab and the tunnel piers to isolate the tunnel from any lateral motion of the slab. A soft mastic type compound was then poured on all edges and seams. The measured resonant frequency is about 16 Hz which indicates an overall resilient pad stiffness of 2.5×10^7 $lb_f/ft/foot$ of slab. The predicted resonance frequency using laboratory measurements of pad stiffness was 14 Hz (not including the weight of the train and the stiffness of the air enclosed under the slab).

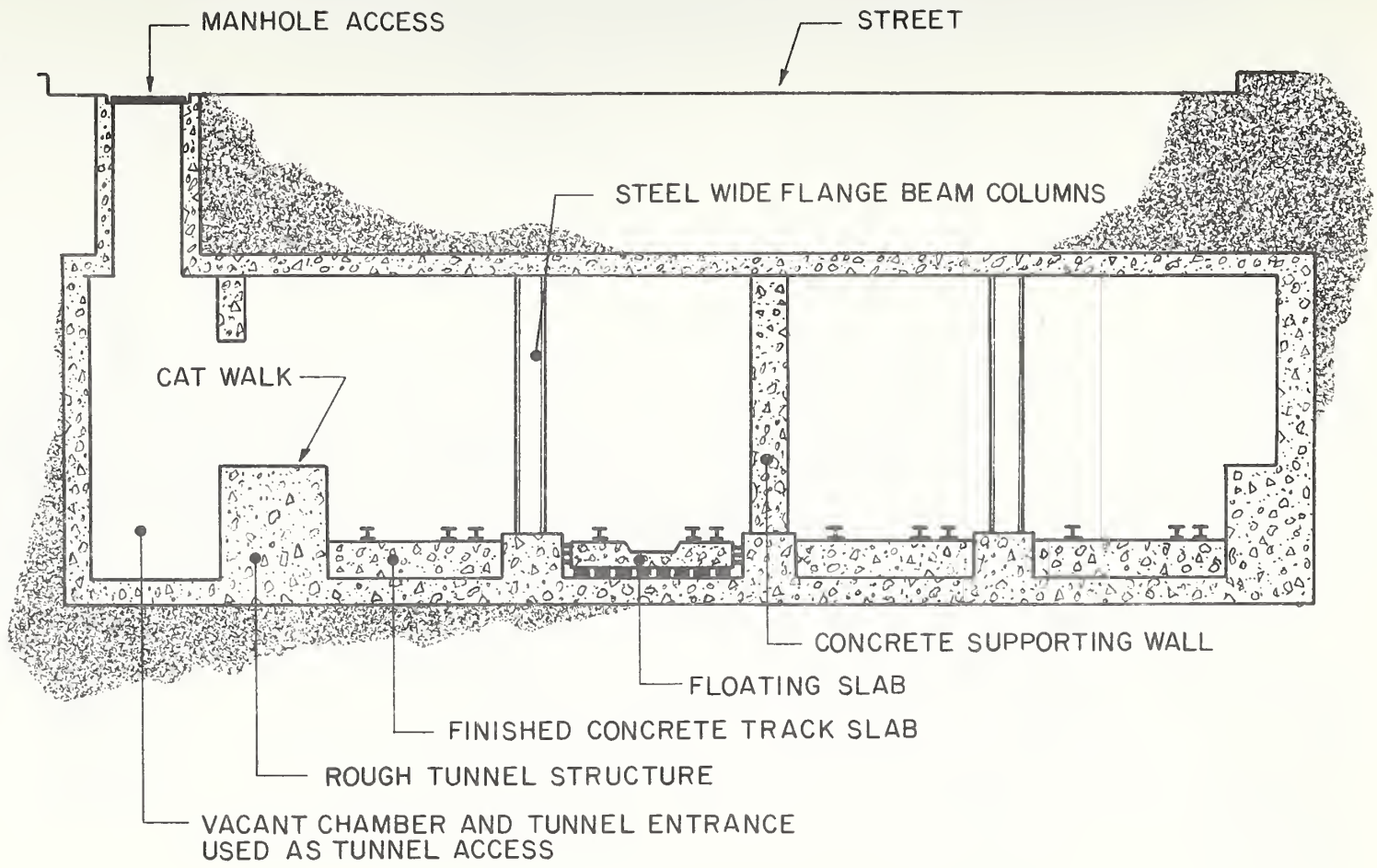

FIGURE 3.1 IND LINE TUNNEL CROSS SECTION SHOWING FLOATING SLAB AND TUNNEL ACCESS.

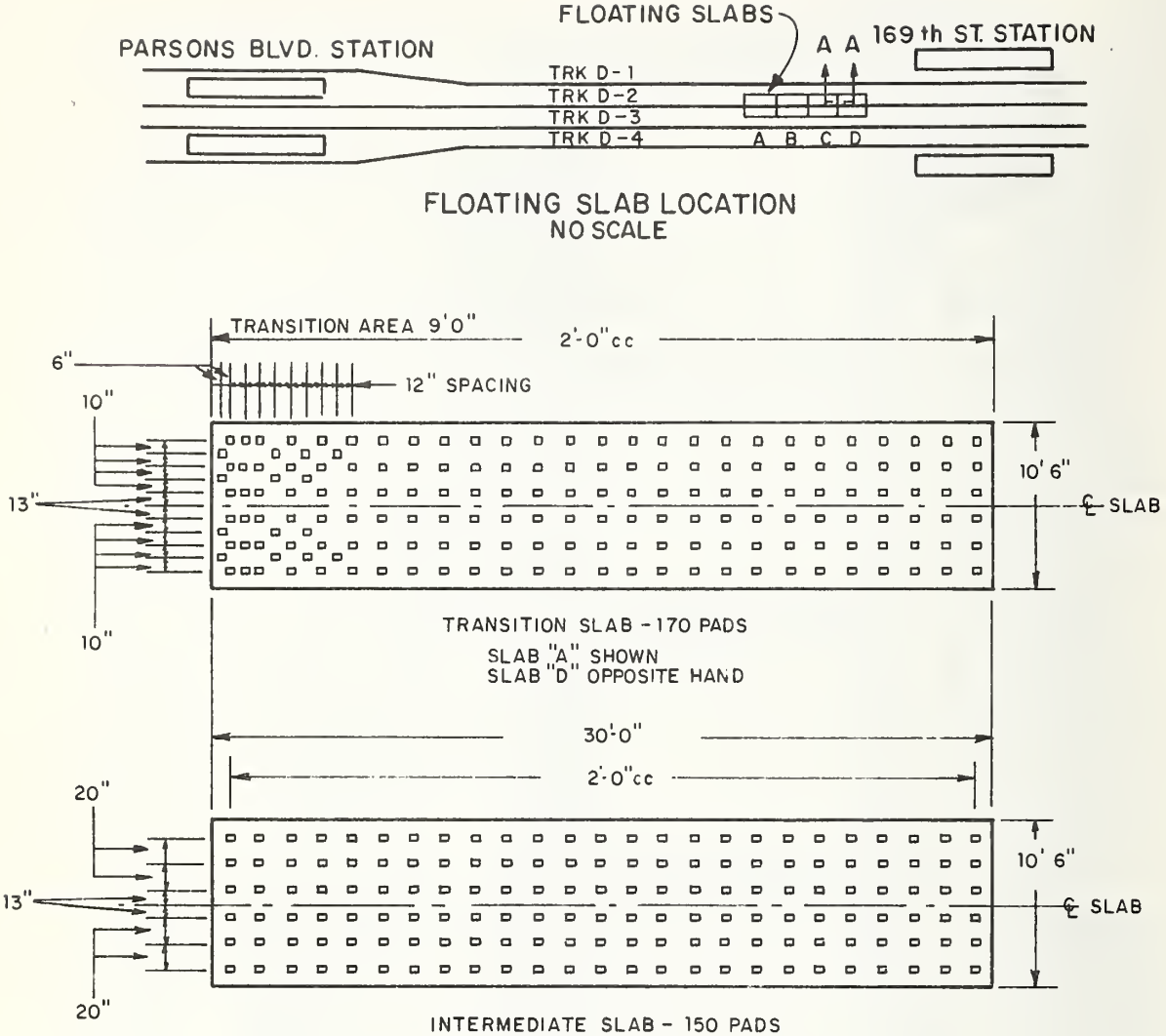

FIGURE 3.2 FLOATING-SLAB LOCATION ISOLATION PAD ARRANGEMENT, AND FLOATING-SLAB SECTION INTERCONNECTION SCHEME.

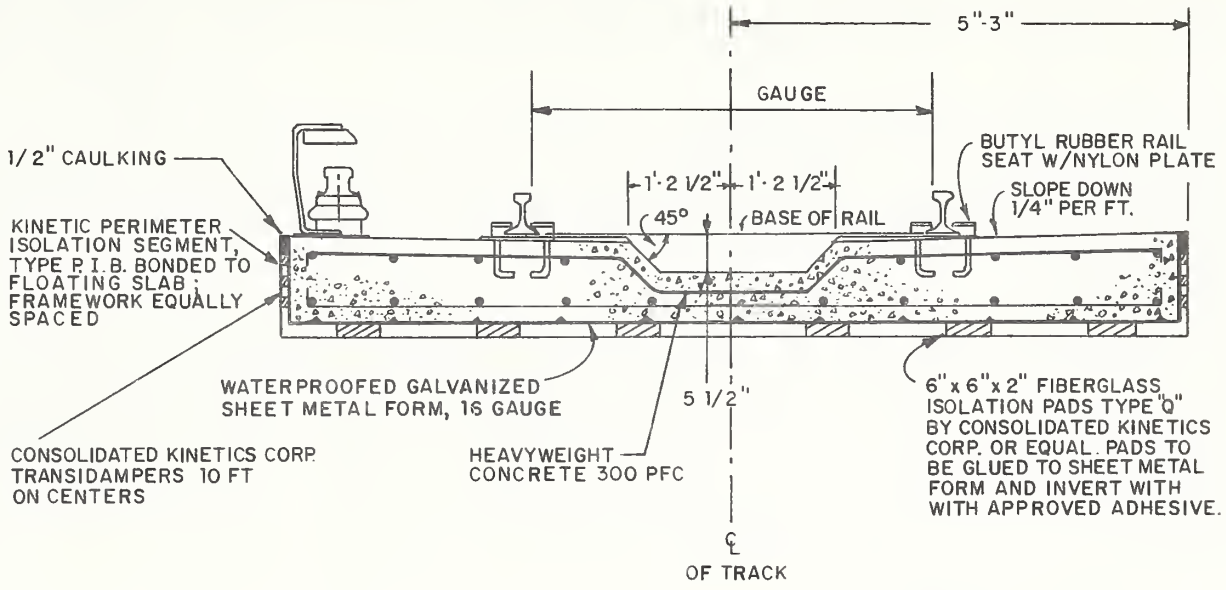

FIGURE 3.3 FLOATING-SLAB CROSS SECTION.

3.3 Measurement Scheme and Purpose

The purpose of the measurement scheme was to determine the floating slab's ability to reduce vibration transmission to neighboring buildings. The concept of Insertion Loss was used as a measure of the slab's performance. By Insertion Loss it is meant: the reduction in vibration at a given point arising from the addition of the floating slab into the tunnel-track system.

Fig. 3.4 contains a diagram of the track layout and measurement point locations. Notice that the measurement points form two tunnel cross sections: one through the floating slab track section and the other through a conventional track section. Measurement locations were selected such that vibration measured at the floating slab section would be indicative of the vibration that would be observed if the floating slab were infinitely long. Similarly, measurements at the conventional track cross section were taken sufficiently far from the floating slab that they would be indicative of measurements near an infinitely long conventionally designed track.

It should be pointed out, however, that a New York train is normally 600 feet long and the slab is only 200 feet long, so that at any one instant in time most of the trucks are located on the conventional track. As a result, the vibration reduction that an infinitely long floating slab can provide will not be fully realized at buildings adjacent to the tunnel.

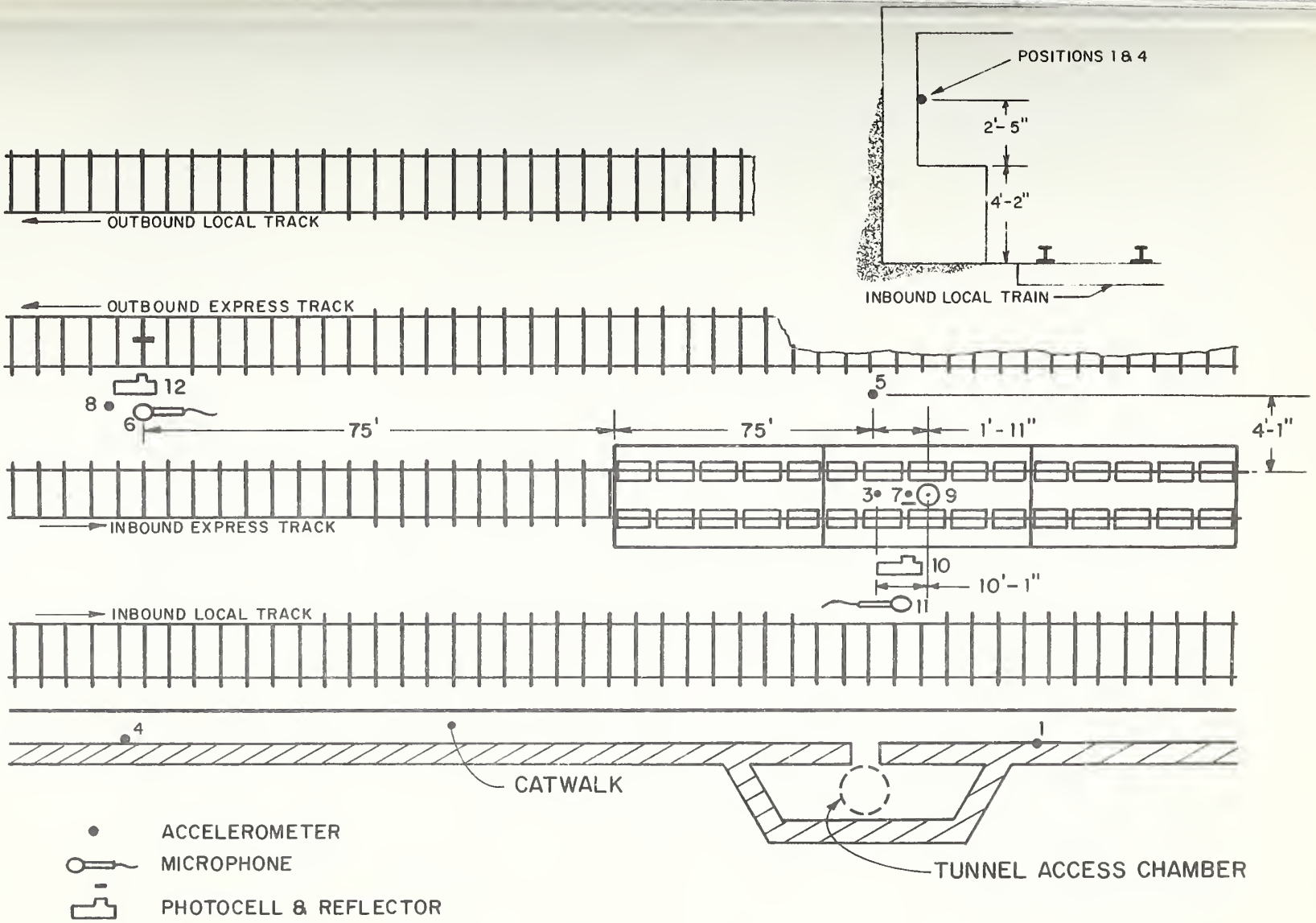

FIGURE 3.4 TRANSDUCER LOCATIONS IN TUNNEL.

One question that arises is whether, in fact, our measurements in the tunnel indicate the effect of an infinitely long slab. As mentioned above, most of the trucks are on the conventional track, however, it will be subsequently concluded from an examination of the data that the slab is long enough to give the same results as an infinitely long slab for measurements at the center island.

Insertion Loss is arrived at by subtracting the acceleration level measured at the floating slab track section from that measured at the same relative location of the conventional track tunnel cross section. The measure of Insertion Loss that has been considered is the difference in acceleration levels at the center island, positions 8 and 5 (Insertion Loss = $L_a^{(\text{Pos. } 8)} - L_a^{(\text{Pos. } 5)}$). When the vibration level at point 5 is less than that at 8, the Insertion Loss is positive, i.e., the effect of the floating slab is to reduce vibration transmitted to the tunnel floor and to adjacent buildings.

3.4 Instrumentation

Measurements were conducted by epoxying accelerometer stud mounts to the appropriate positions in the tunnel, mounting the accelerometers, and connecting the short microdot cables to

preamplifiers which acted as signal conditioners. The amplifying, monitoring, and recording equipment were located in a commercial van parked next to the access manhole on the street. Single conductor coaxial cables of lengths from 75 feet to 200 feet joined tunnel located transducers with the electronics in the van. Entrance to the tunnel was gained through a manhole at the street level which opened into a side chamber as shown in Fig. 3.1.

Since low frequency information was of prime importance, each acceleration signal was low pass filtered just prior to amplification in order to increase the signal-to-noise ratio in the lower frequency range. Acceleration levels below 125 Hz were of prime interest in view of the slab's low spring-mass resonance (16 Hz). Low pass filters used were single pole RC type and had a 3 dB down point at 180 Hz. The Insertion Loss down to about 31.5 Hz has been measured by Anthony Paolillo [10], Environment Staff Scientist for the NYCTA, and is in excellent agreement with that measured here in the frequency range 31.5 Hz to 125 Hz.

Because of noise floor limitations in the electronics, accurate levels at lower frequencies could not be determined from Paolillo's data. Particular attention has been paid to this problem in our measurements by selecting very low frequency roll-off devices. Typically, Insertion Loss spectra down to 0.63 Hz have been determined.

Only the most durable electronic system could be used because of the severe working environment in which measurements had to be taken. Much effort was put into collecting those components that would offer good low frequency resolution and high signal-to-noise ratio. Typically, B & K 4344 and 4333 accelerometers were attached to Ithaco 143 and 125 preamplifiers which provided a low impedance source to transmit data from the tunnel to A.C. coupled Ithaco or D.C. coupled DANA voltage amplifiers in the equipment van parked on the street. The signals were then recorded at 15 ips on a Honeywell 5600C, 14-channel, FM tape recorder which has a maximum linear input of 10 volt rms and a D.C. to 10 KHz flat frequency response. Amplifier gains were set to their maximum linear voltage output by monitoring passby signals on a storage oscilloscope. When all levels were set, data was then recorded.

In addition to acceleration signals, acoustic levels, photocell voltage, and an IRIG "B" time code were recorded. Acoustic signals were monitored and recorded using one inch GR microphones (with one inch wind screens) and GR 1933 Sound Level Meters. This acoustic information, though indicative of the effect of the slab on tunnel acoustic levels, was only used as a reference since the acoustic performance is not of great interest at this time.

The photocell, mounted beside the track in a position such that the car wheels broke its line of sight with a reflector, provided an FM recordable DC voltage shift upon each wheel passage. This provided us with both speed and position information.

3.5 Representative Passby Signals

The recorded data was processed at Cambridge Collaborative's laboratory facilities. Of particular interest are the filtered time histories that were acquired by playing back recorded signals into four GR 1933 Sound Level Meters and plotting the decibel level on a Gulton Four-Channel strip chart recorder. The photocell logic output was used to drive an event marker on the strip chart recorder which was activated at the passage of each wheel. Figs. 3.5 show a set of 125 Hz octave band level time histories and the associated photocell output. These time histories are useful in that they give evidence of the slab's performance.

In certain time histories the passage of neighboring truck pairs is very evident. Generally, the nearer the measurement position to the track, the more distinguishable are the

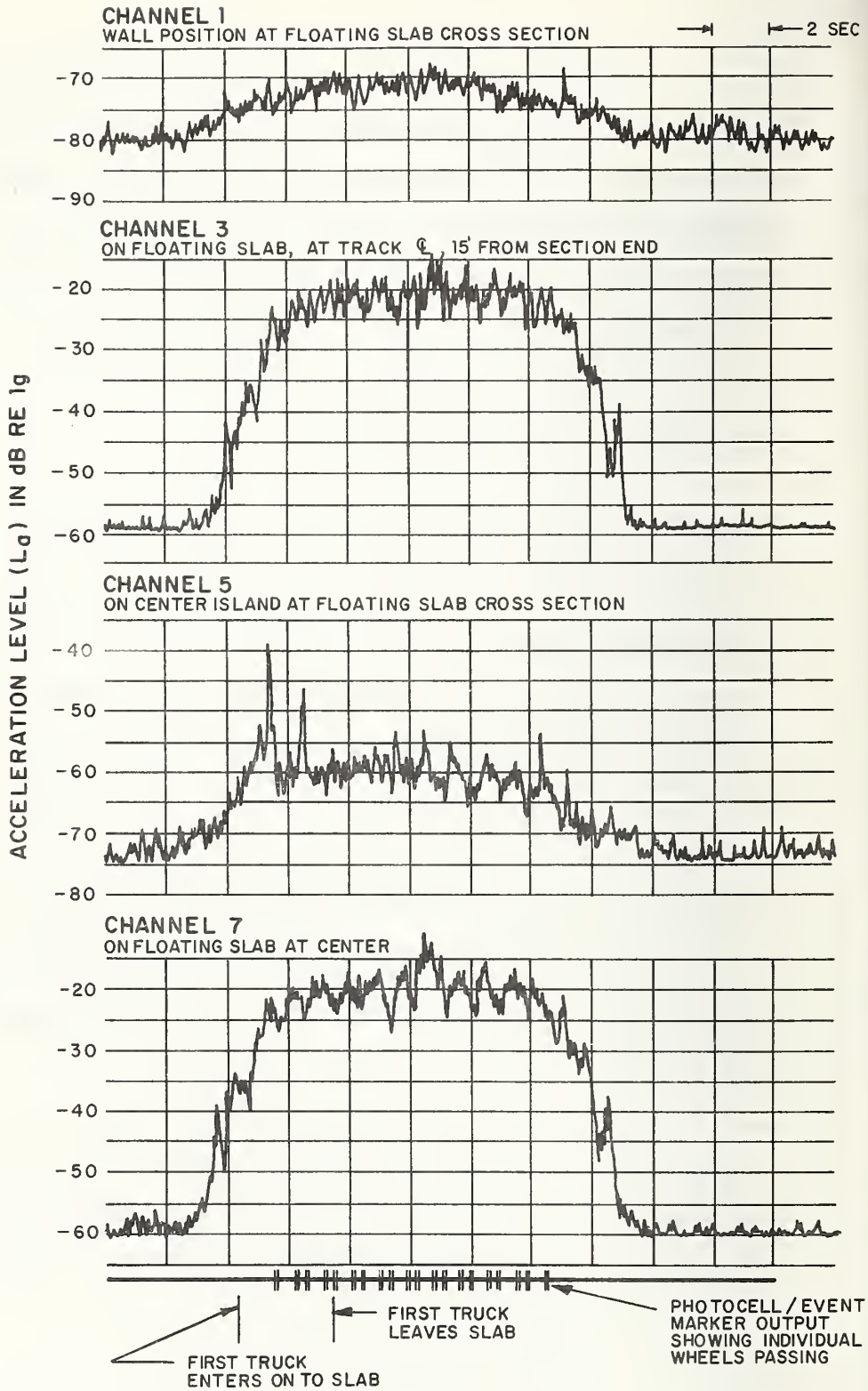

FIGURE 3.5A TYPICAL ACOUSTIC AND ACCELERATION LEVEL TIME HISTORIES FOR THE 125 HZ OCTAVE BAND AT ALL POINTS DURING 17:40 TRAIN PASSE

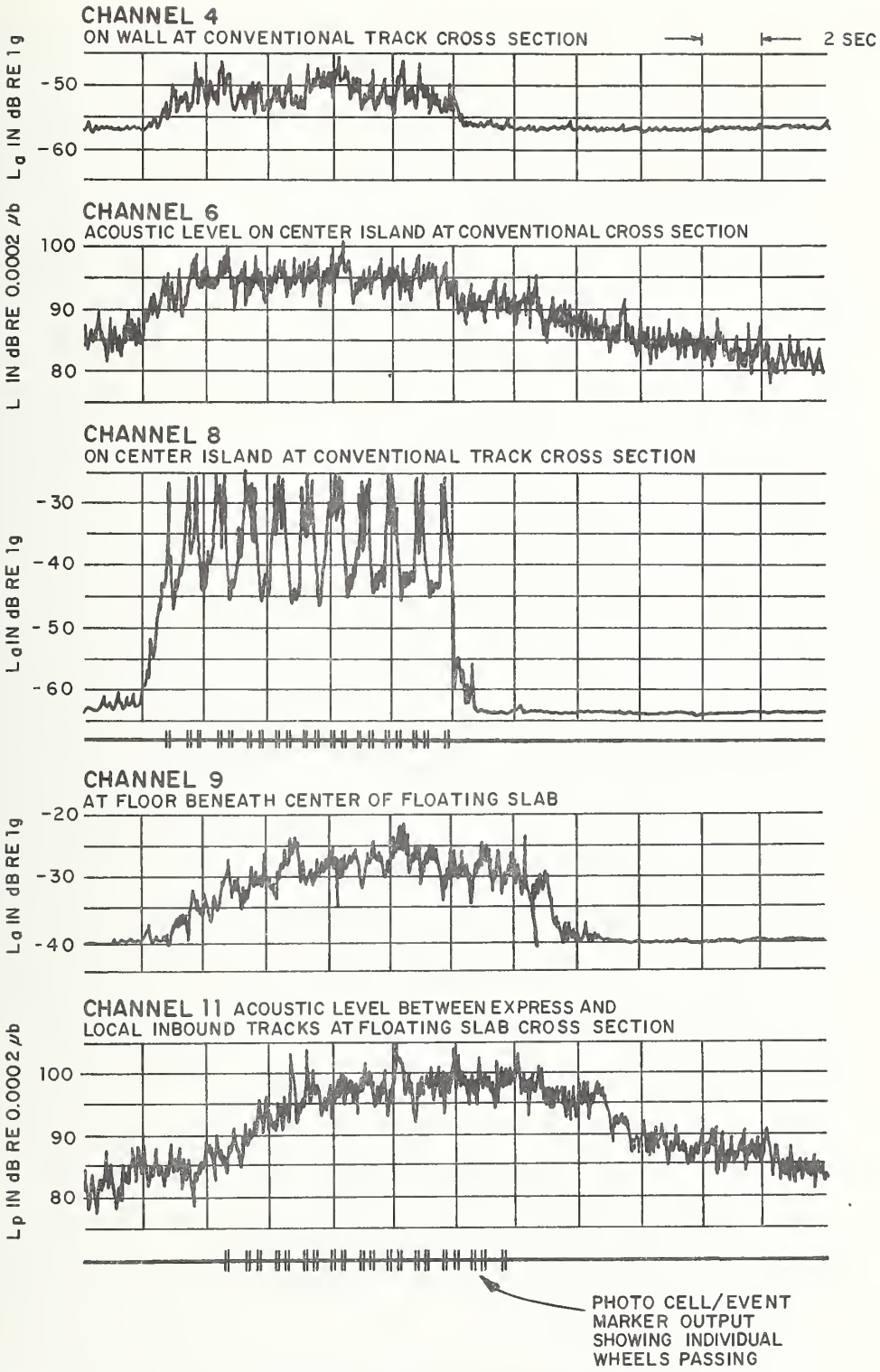

FIGURE 3.5B TYPICAL ACOUSTIC AND ACCELERATION LEVEL TIME HISTORIES AT ALL POINTS DURING 17:40 TRAIN PASSBY

associated time history peaks. The comparison of time histories for positions 4 and 8 indicates this to be very much the case. Also, the ability of the floating slab to distribute truck loading and truck vibration is illustrated through a comparison of time histories of channels 5 and 8; five being located on the center island near the floating slab section of track and eight being near the conventional track.

The effect of a finite length slab section can be seen by examining the acceleration time history for position 5. Knowing that the photocell is 75 feet from the approach end of the slab, it may be observed that the contribution of a vibration source at the approach end to the level at 5 is about 10 dB below that measured with trucks nearby on the slab, i.e., the contribution of off-slab sources is negligible. Similarly, the level at position 8, 75 feet from the approach end of the slab, is negligibly affected by sources at or near to the slab so that it may be inferred that the position 8 vibration is not influenced by the slab's presence. The conditions above have been and must be met before a valid measurement of Insertion Loss, in accordance with the earlier stated definition, can be made. Similarly, the difference in acceleration levels at points 1 and 4 constitutes a measure of slab Insertion Loss with regard to wall vibration. However, for these points, the above-mentioned condition that vibration should be from either slab or off-slab sources, but not both, is only marginally complied with. This would tend to result in a slightly conservative estimate of Insertion Loss because the

measured transmission from the slab includes small contributions from off-slab sources.

In plotting octave band spectra, steady-state levels are interpolated from time histories and used to evaluate various aspects of slab performance. Problems arise, however, when very low frequency analysis using time histories is attempted. The fast averaging time of the GR 1933 Sound Level Meter is too short to allow satisfactory confidence in the measurement; on the other hand, the length of the train passby is too short to allow sufficient time for an average level to be reached using the slow averaging sound level meter setting. Ideally, a much longer train passby time is needed for the sound level meter to reach a steady-state level. The effect of a longer train passby was obtained by storing an eight second portion of predominantly steady-state passby vibration levels in a B & K transient recorder. The transient recorder digitizes and stores a signal, and then outputs it repeatedly at an adjustable rate. The effect is to compress the signal time scale and raise its frequency content proportionally. For instance, eight seconds of data can be stored in the transient recorder and played back in as little time as 0.32 seconds, which constitutes a 25:1 time compression. Typically, data was recorded at 15 ips and played back from the tape recorder into the B & K transient recorder at 60 ips, and the transient recorder was adjusted to give a 10:1 time compression, thus effectively shifting the final playback frequency by a factor of

40 (16 one-third octaves) upwards.

Using these time-compressed signals, very low frequency one-third octave band levels were measured using a GR 1564 Sound and Vibration Analyzer set to the slow averaging time. Slow averaged one-third octave band levels were then read from the GR 1564 meter. The statistical confidence limits here in processing the random vibration signals are affected by both the meter averaging time and by the fact that only an eight-second data sample is used. A discussion of this will not be attempted here, but the resulting confidence limits appear in Fig. 3.6.

The technique of performing analog filtering and averaging on a long sample is identical to the way real time analysis is performed by certain real time analyzers. Among these are Spectral Dynamics and Federal Scientific which compress the time scale, sweep filter and average the data, and display the resulting frequency spectra. This process can be continuous, thus updating the spectra as the time domain signal changes. Essentially, the sweep filtering of a sample here is simply repeated on the same time sample rather than updating it by taking a new sample.

Other real time analyzers do not operate in this manner. These input the time domain signal into a bank of parallel

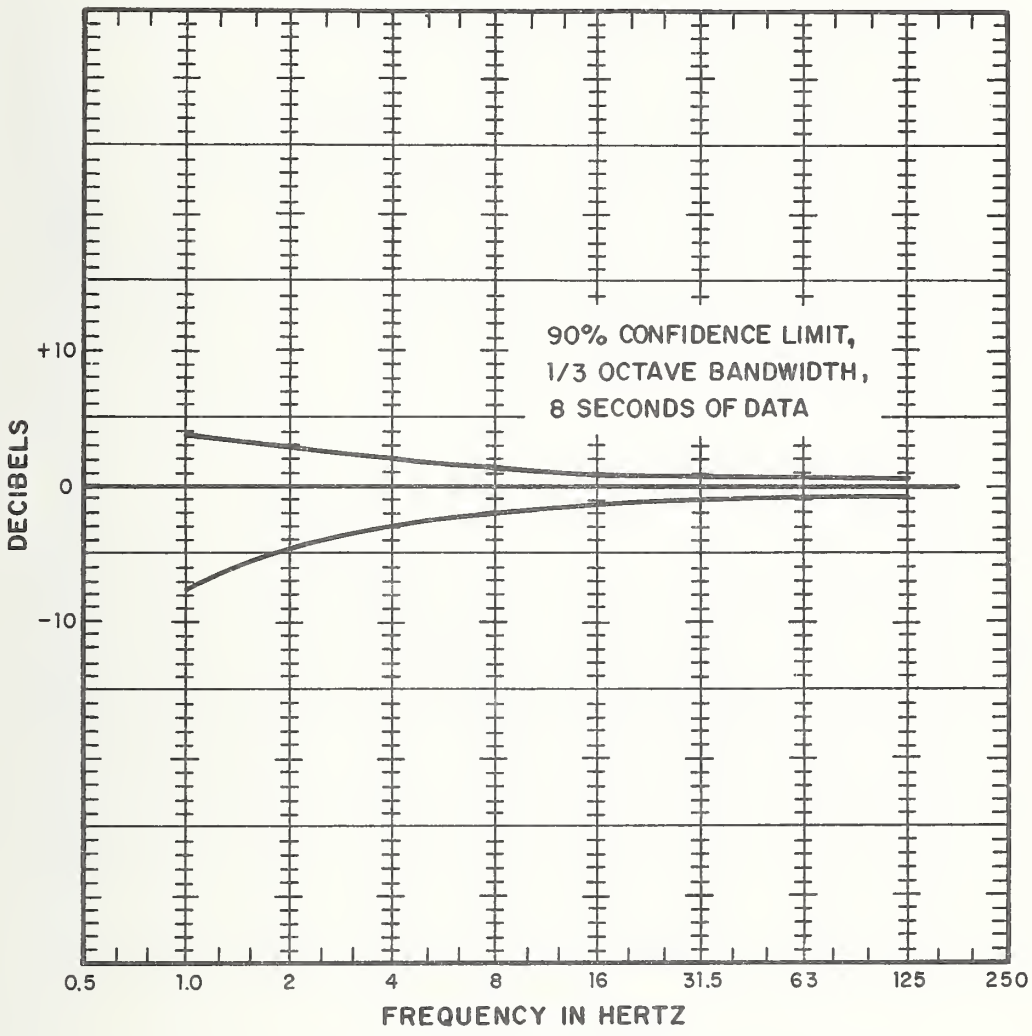

FIGURE 3.6 NINETY PERCENT CONFIDENCE LIMIT AS A FUNCTION OF FREQUENCY FOR AVERAGING OF AN EIGHT SECOND DATA SAMPLE.

filters and a short sample is taken from one randomly selected filter band, digitized, averaged with previous samples of the same band, and stored. This sampling occurs continuously, and an updated time averaged spectrum is generated. Note that this is not truly real-time analysis because spectral levels are not measured from the same time domain signal sample. For steady-state signals this is usually permissible, but for short transient signals erroneous spectra can result.

3.6 Measured Insertion Loss

Figs. 3.7a, 3.7b and 3.7c show acceleration levels in third-octave bands at measuring points 5 and 8 for three different passbys. Notice that at the floating slab's resonant frequency (16 Hz) the level on the tunnel floor near the slab track is higher than that at a conventionally designed tunnel section. Hence, the slab has a detrimental effect at low frequencies. Fig. 3.8 plots the corresponding Insertion Losses.

Also appearing in Fig. 3.8 is the Insertion Loss measured by Paolillo [10]. His levels extend up to 1600 Hz and show good agreement with our results down to about 31.5 Hz. The departure from our results below this frequency is due to a low signal-to-noise ratio in his measurements at low frequencies. The Insertion Loss measured by Paolillo is referenced to the

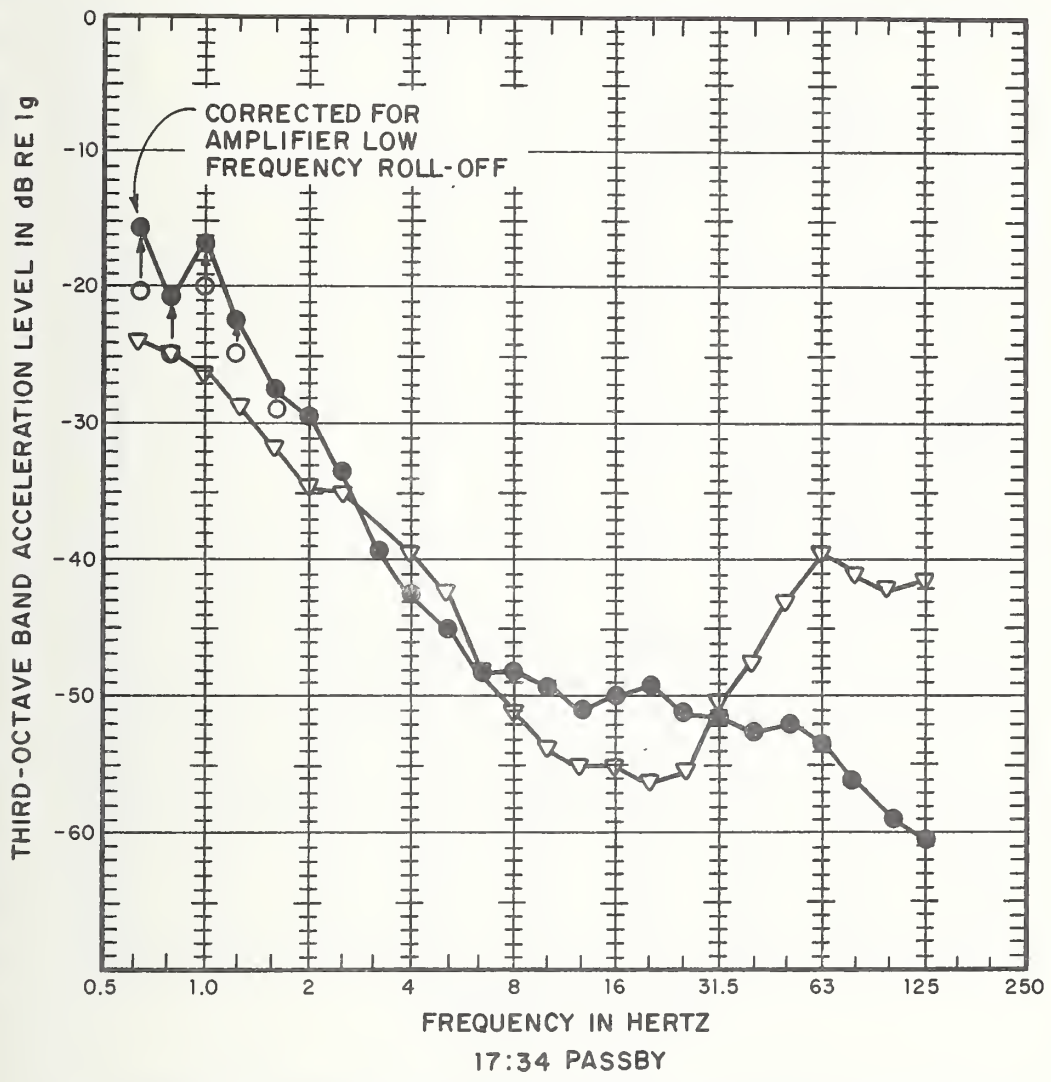

FIGURE 3.7A THIRD OCTAVE BAND ACCELERATION LEVELS AT CENTER ISLAND POINTS DURING 17:34 TRAIN PASSBY

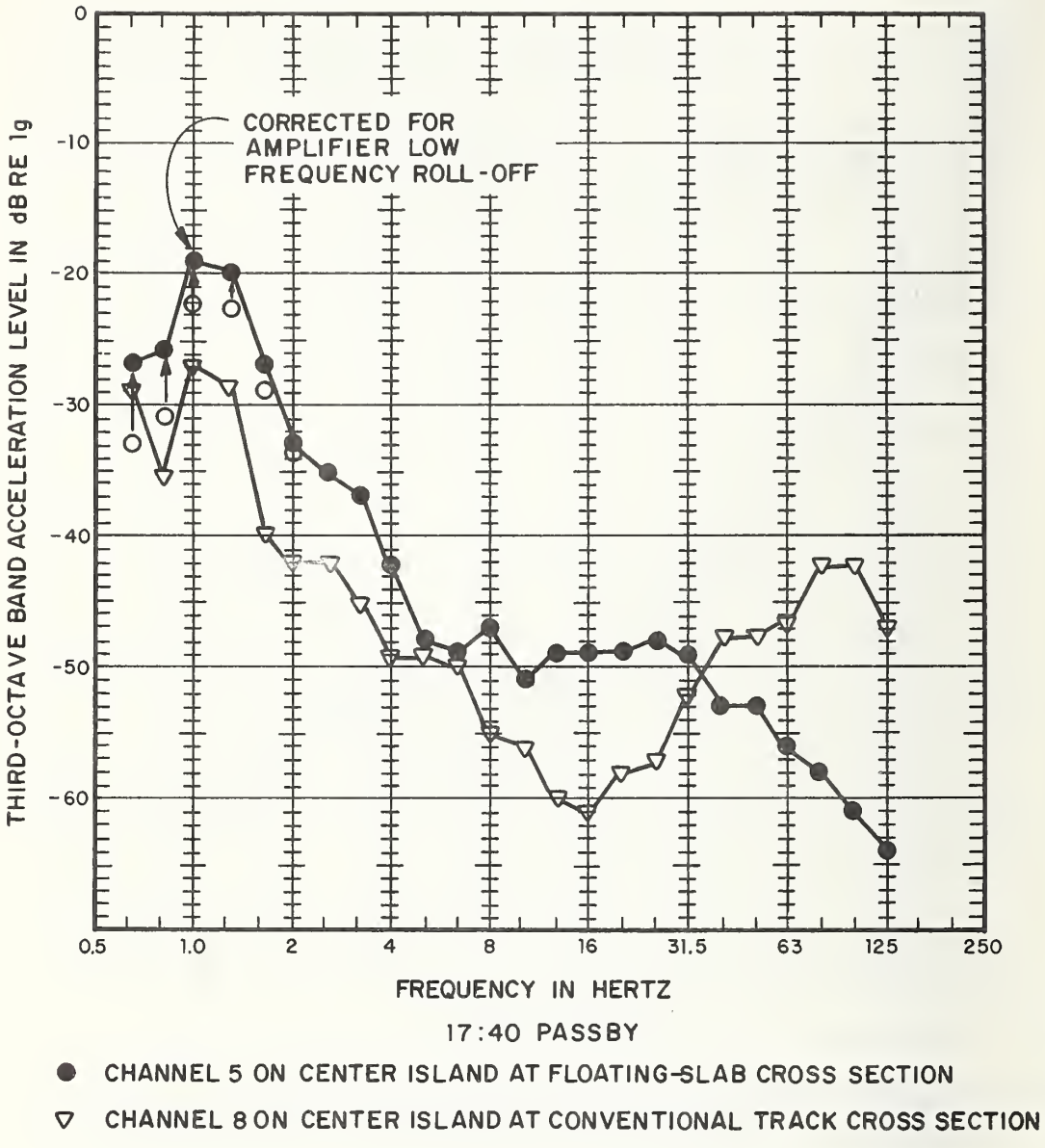

FIGURE 3.7B THIRD OCTAVE BAND ACCELERATION LEVELS AT CENTER ISLAND POINTS DURING 17:40 TRAIN PASSBY

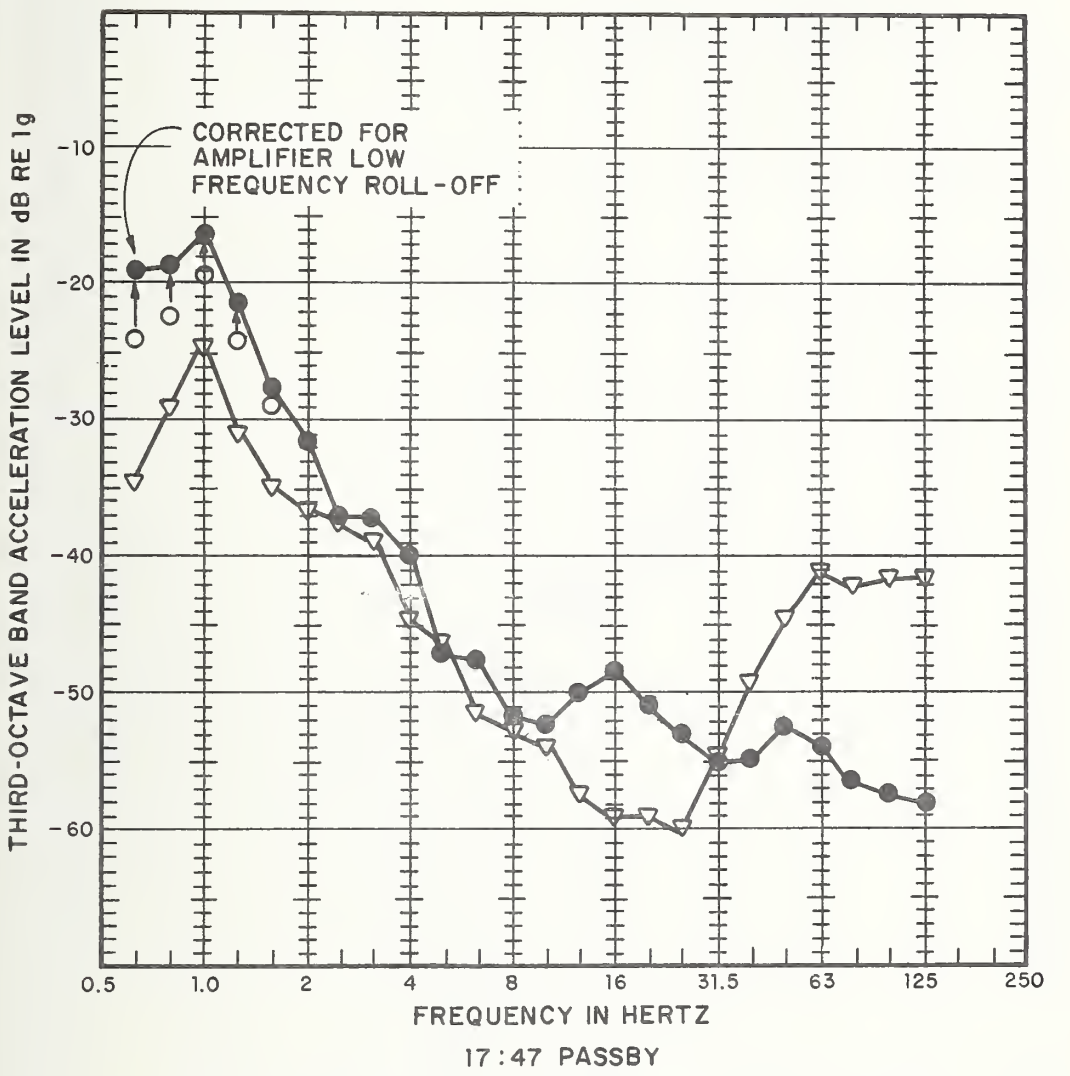

FIGURE 3.7c THIRD OCTAVE BAND ACCELERATION LEVELS AT CENTER ISLAND POINTS DURING 17:47 TRAIN PASSBY

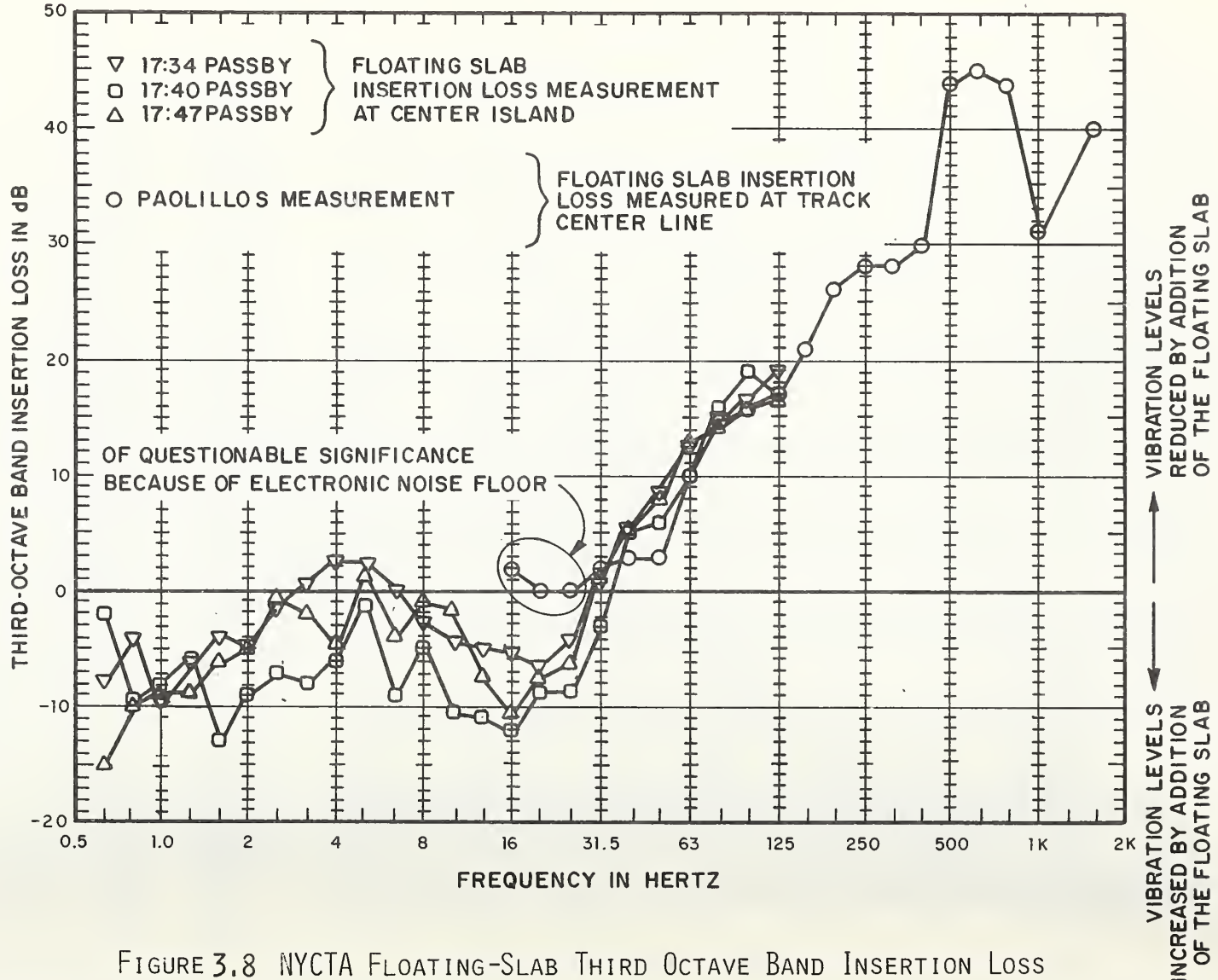

FIGURE 3.8 NYCTA FLOATING-SLAB THIRD OCTAVE BAND INSERTION LOSS

floor slab at the center of the track. It is understandable that this measure of Insertion Loss is quite close to that of the center island referenced Insertion Loss, but how either of these relates to the wall referenced Insertion Loss is not well understood within the present state-of-the-art.

Fig. 3.9 shows the difference between acceleration levels at points 5 and 8 for a train passage on the outbound express track (adjacent to the floating slab track). These measured levels indicate that the addition of the floating slab has altered the response of the tunnel to forces generated by a train on conventional track. This result may be due to the removal of the finished concrete track slab during installation of the floating slab, as shown in Fig. 3.1. The implication here is that the lightened tunnel structure in the area of the floating slab results in a generally higher vibration level. In any case, we can use the results shown in Fig. 3.9 to correct the measured Insertion Loss values so that they are applicable to the case in which a floating slab is added to a tunnel floor that is identical at both the floating slab track section and at the conventional track section. The corrected Insertion Loss values are shown in Fig. 3.10. For this case the floating slab has little effect on vibration levels at frequencies below the rigid body resonance frequency of the slab. At and near the resonance frequency, the vibration levels are increased by the addition of the floating slab. And, finally, at high frequencies

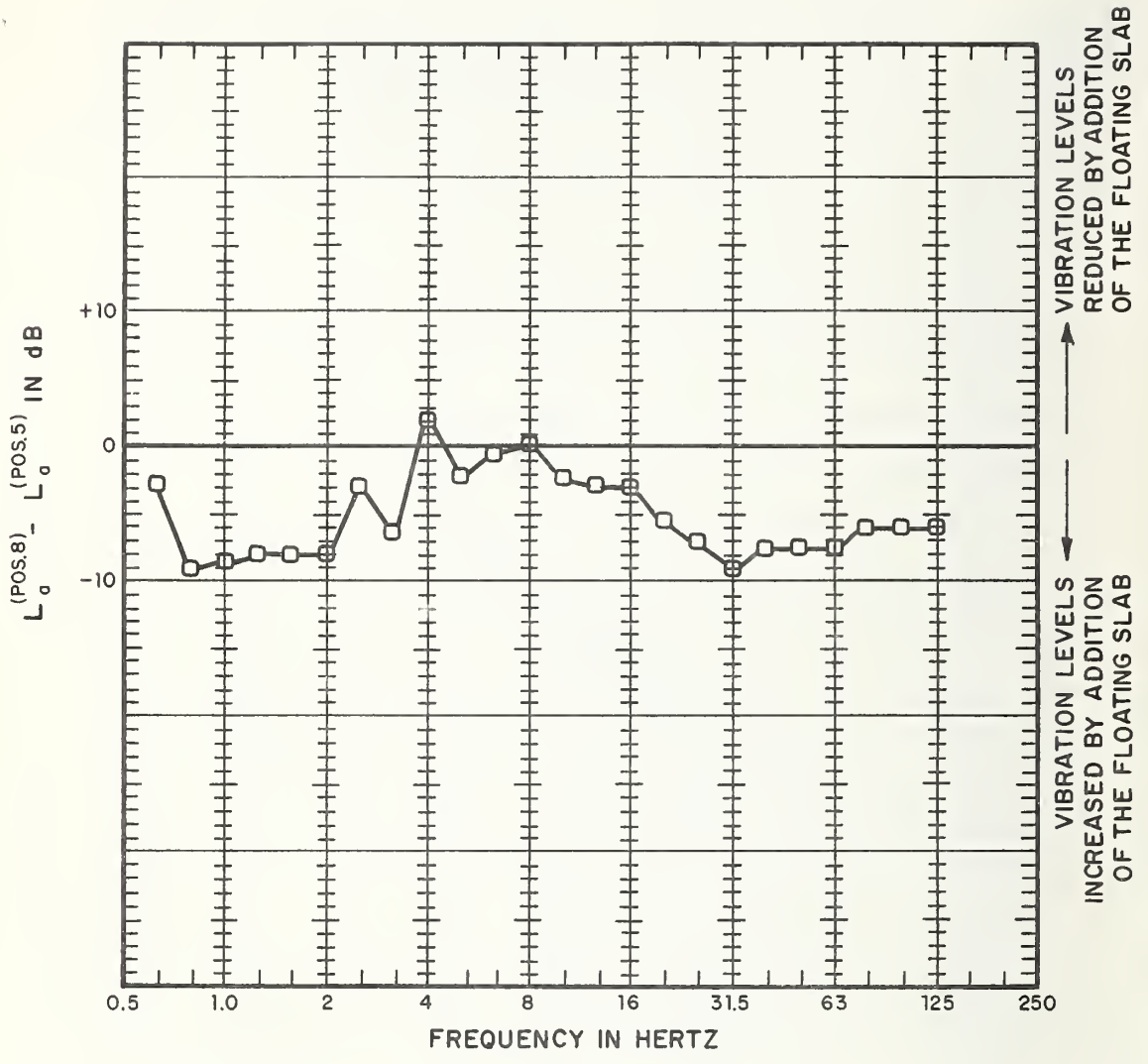

O DIFFERENCE IN ACCELERATION LEVELS
BETWEEN POSITIONS 8 AND 5,
17:34 PASSBY ON OUTBOUND EXPRESS TRACK

CHANNEL 5 ON CENTER ISLAND AT FLOATING SLAB CROSS SECTION
CHANNEL 8 ON CENTER ISLAND AT CONVENTIONAL TRACK CROSS SECTION

FIGURE 3.9 ACCELERATION LEVEL DIFFERENCE BETWEEN POINTS 8 AND 5 DURING THE PASSAGE OF AN OUTBOUND EXPRESS TRAIN.

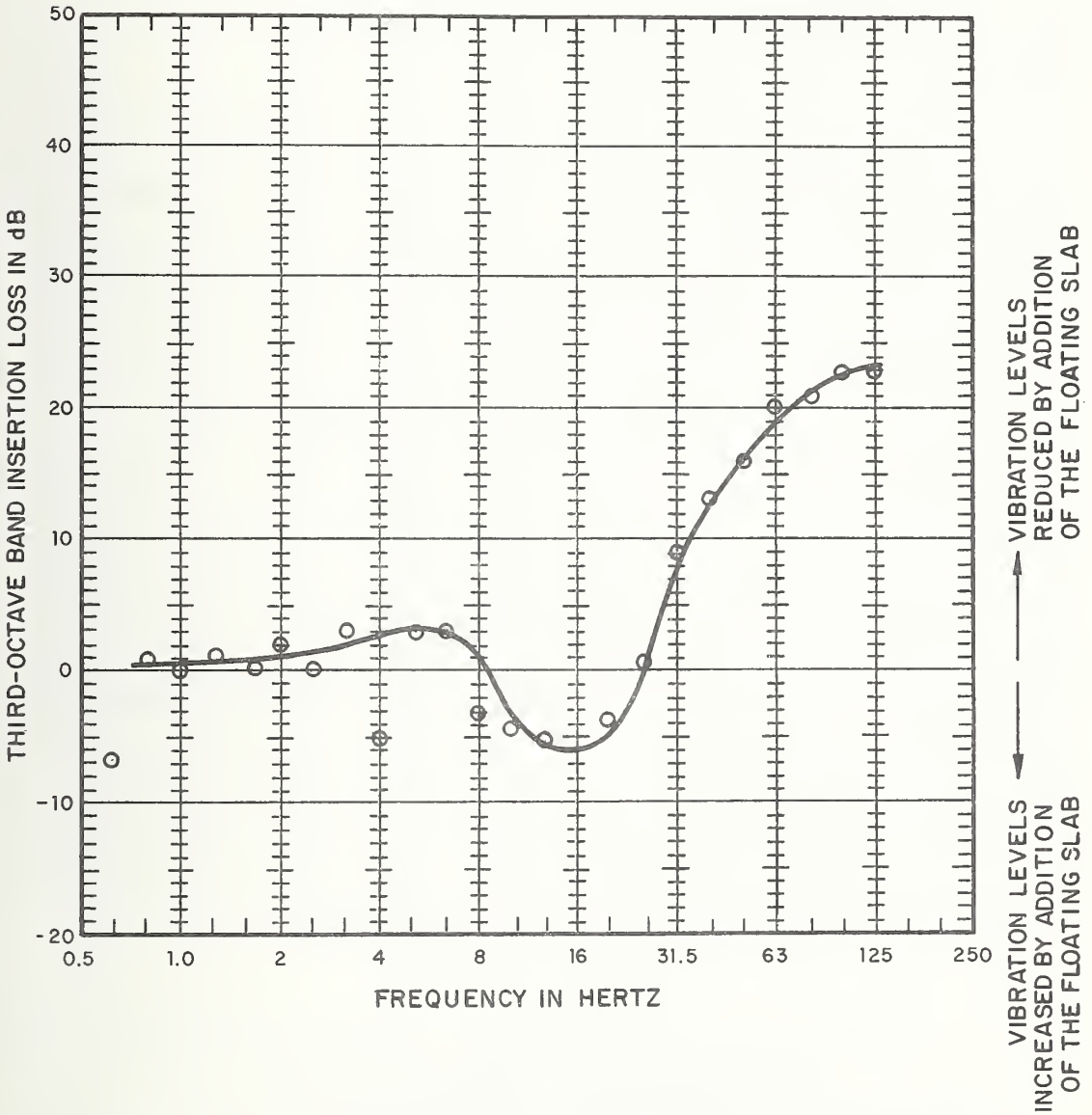

FIG. 3.10 INSERTION LOSS CORRECTED FOR DIFFERENCES IN TUNNEL STRUCTURE AT THE TWO MEASUREMENT POINTS ON THE CENTER ISLAND

the slab acts to significantly reduce the tunnel floor vibration levels. This behavior is very similar to that of a single-degree-of-freedom system, see Fig. 1.1. A discussion and comparison of the field results with prediction is presented in section 4.

The topic thus far has been the Insertion Loss measured at the center island. There is some question as to whether this Insertion Loss is the same as that which might be measured at the tunnel wall. The Insertion Loss based on measured vibration levels at two points on the tunnel wall--one near the floating-slab track and one near the conventional track--is shown in Fig. 3.11. Because of transducer failure we were forced to use a transducer and amplifier at one of the tunnel wall positions, channel 4, that did not have adequate low frequency performance. Thus, the Insertion Loss is plotted only for frequencies above 20 Hz. However, it is important to note that the Insertion Loss for wall vibration (for $f > 20$ Hz) is comparable to the "corrected" IL for center island vibration (Fig. 3.10). In spite of the relatively short length of the slab it appears to be effective in reducing vibration levels both of the tunnel floor and the tunnel walls.

The question as to whether the floor vibration or wall vibration is more significant in determining the vibration of nearby buildings is difficult to answer. We point out, however, that the floor vibration levels are at least 20 dB greater than wall vibration levels, as shown in Fig. 3.12. This suggests that the floor vibration levels may be more important with regard to vibration transmission to buildings than the wall vibration.

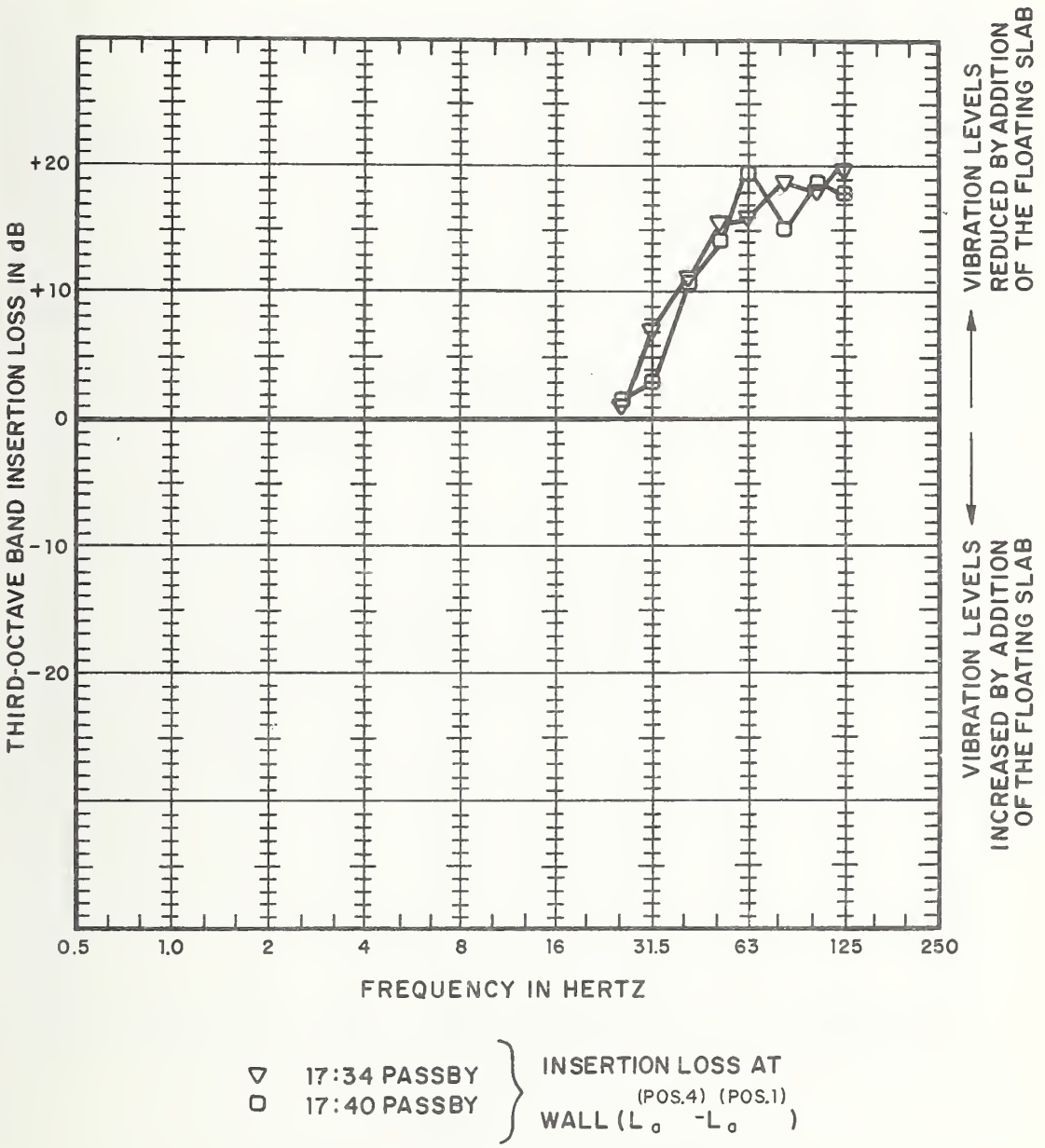

FIG. 3.11 INSERTION LOSS FOR VIBRATION OF THE TUNNEL WALL

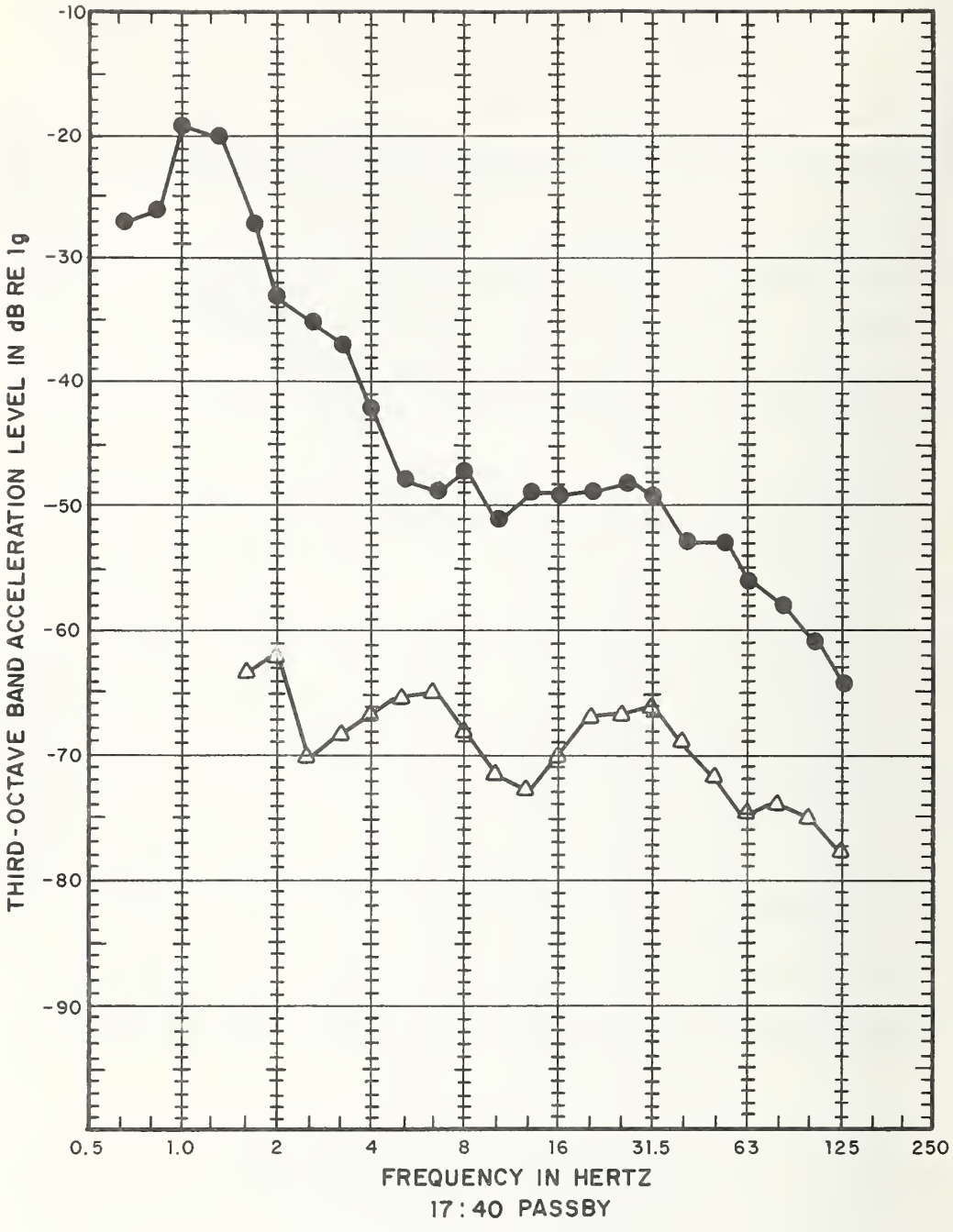

FIGURE 3.12 THIRD OCTAVE BAND ACCELERATION SPECTRA OF WALL AND CENTER ISLAND VIBRATION (POINTS 1 AND 5).

3.7 Vibration Due to Static Load

The measured vibrational acceleration levels at frequencies below approximately 10 Hz are quite high. The mechanism leading to this low frequency vibration is believed to be the passage of the static train load by the measurement point. Confirmation of this explanation was obtained by examining the spectral content of the photocell logic signal. This signal is a square wave which fluctuates between two voltages based on whether the light beam is blocked by a train wheel or not. The one-third octave band spectrum of the photocell signal is shown in Fig. 3.13. Also contained here are the one-third octave band acceleration spectra for three passbys at points 7 and 9. Notice that the peaks in the acceleration spectra are clearly identifiable with those in the photocell signal spectra. By knowing train speed and truck wheel bases, specific passage frequencies can be identified. The three that most significantly stand out are the car passing frequency, the passage frequency associated with the neighboring trucks on adjoining cars, and the wheel passage frequency associated with the distance between axles on a truck. These passage frequencies are identified in Fig. 3.13 for those trains involved. Data presented are from trains which have a truck wheel-to-wheel distance of 6' - 10", a car length of 60 feet, and neighboring truck distance of 15 feet. These dimensions are outlined in Fig. 3.14.

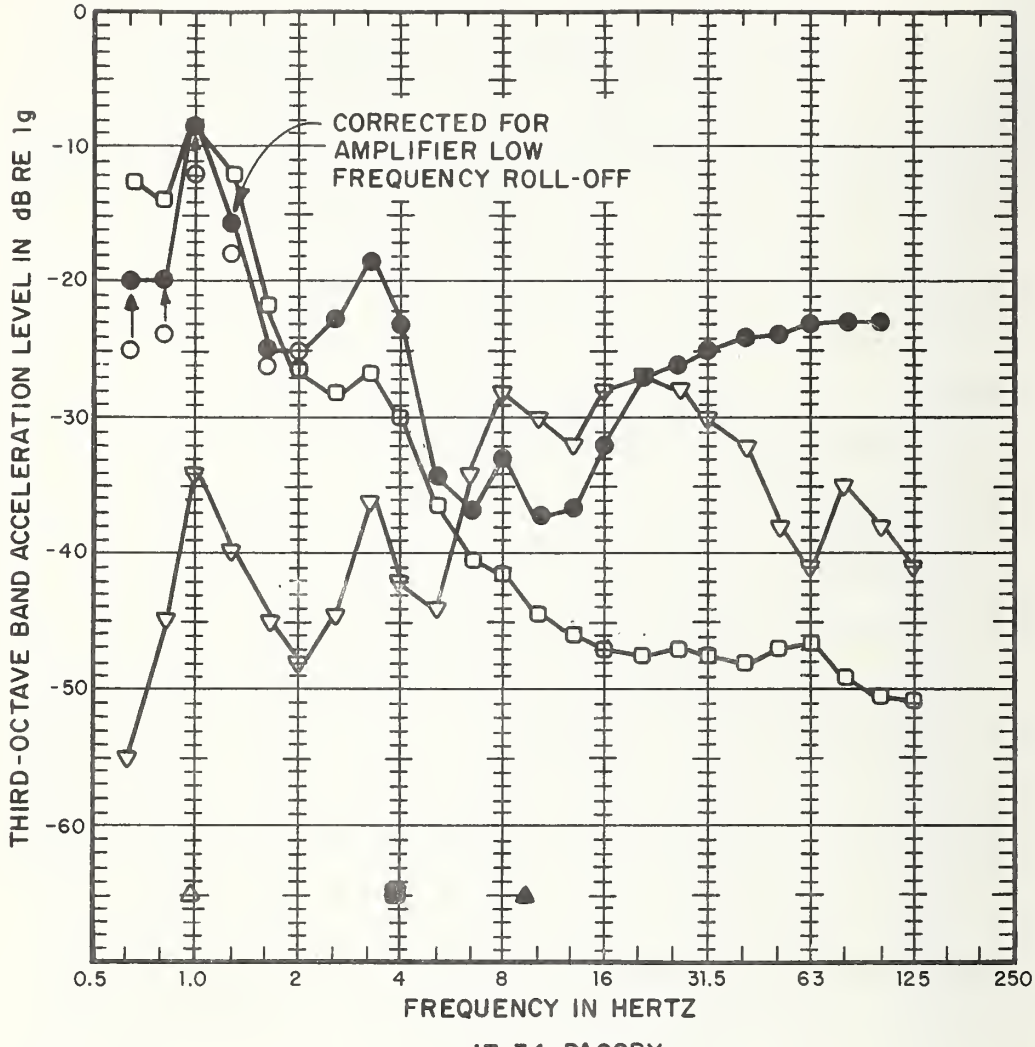

FIGURE 3.13A THIRD OCTAVE BAND ACCELERATION LEVELS AT CENTER OF FLOATING SLAB (7) AND BENEATH FLOATING SLAB (9) FOR 17:34 PASSBY

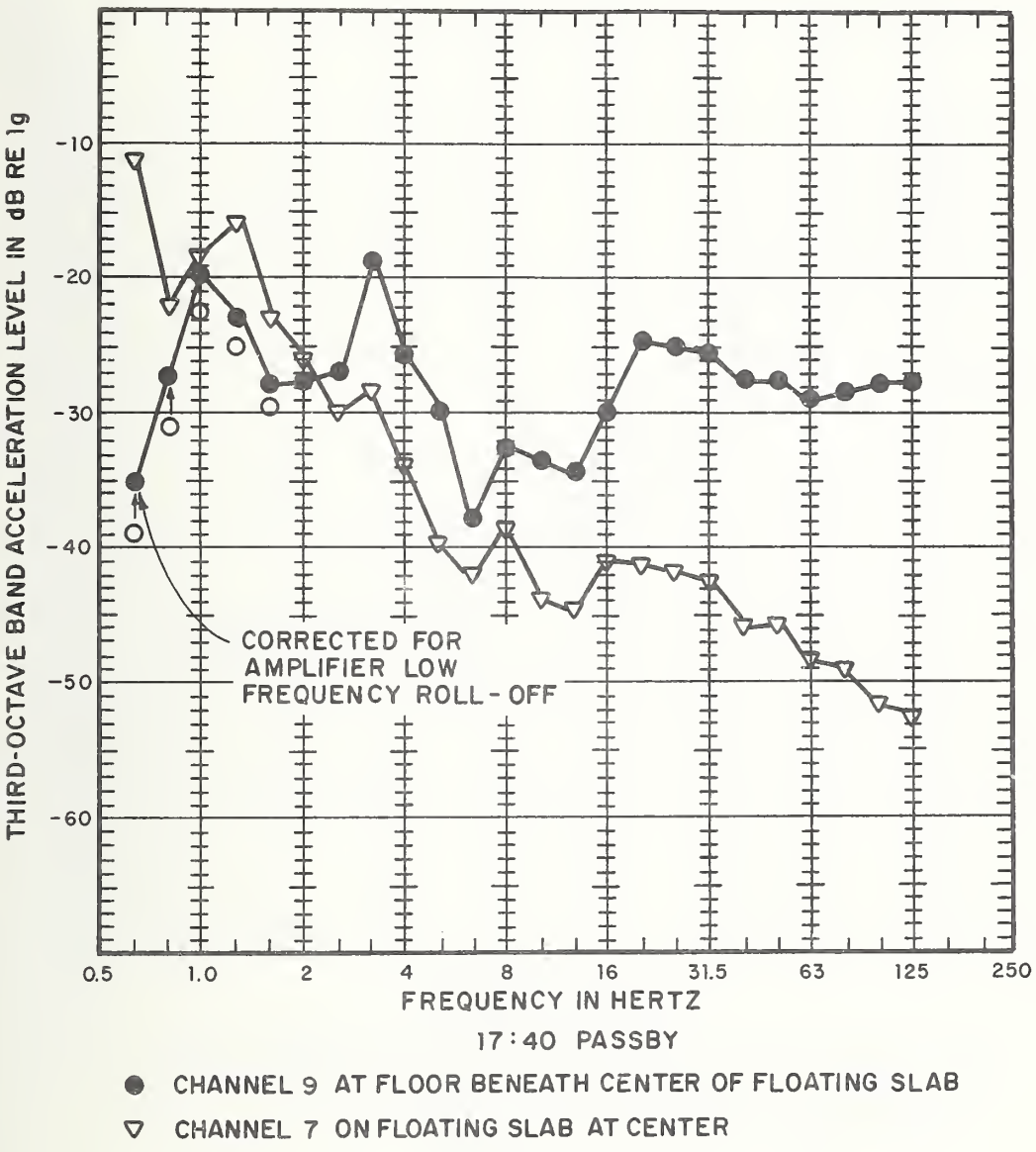

FIGURE 3.13B THIRD OCTAVE BAND ACCELERATION LEVELS AT CENTER OF FLOATING SLAB (7) AND BENEATH FLOATING SLAB (9) FOR 17:40 PASSBY

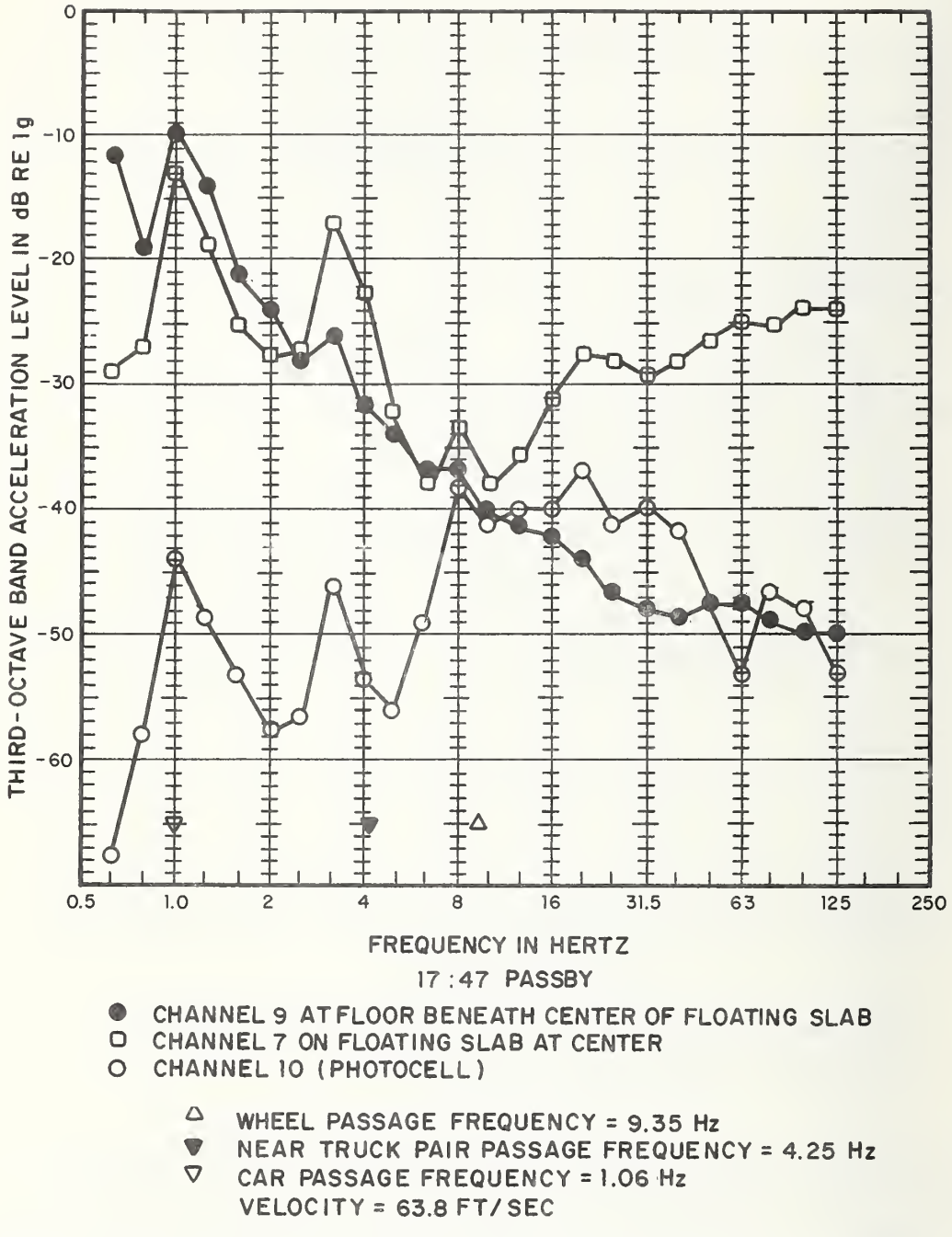

FIGURE 3.13c THIRD OCTAVE BAND ACCELERATION LEVELS AT CENTER OF FLOATING SLAB (7) AND BENEATH FLOATING SLAB (9) FOR 17:47 PASSBY

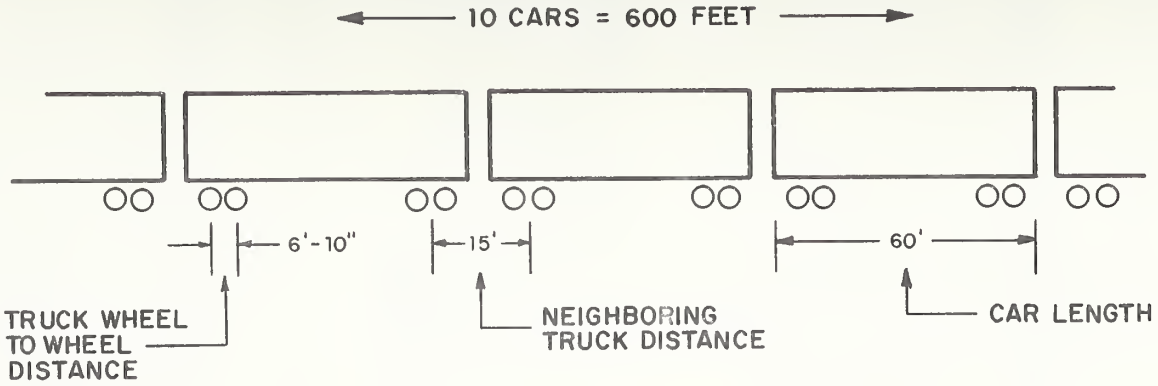

R1—R9, R38, R40 CAR DIMENSIONS

FIGURE 3.14 CAR/WHEEL ARRANGEMENT

It may then be concluded that the 1.0 Hz peak in the acceleration spectra results from the passage of the static train load. The importance of this peak with reference to propagation to neighboring buildings can be determined by examining signals coming directly from the recorded acceleration channels. Fig. 3.15 contains 0.5 Hz to 25 Hz band filtered acceleration signal time histories. They are predominantly of very low frequency and basically occur only when the train is in the immediate vicinity of the accelerometer positions. The implication here is that this low frequency excitation is non-propagating and is a decaying near field effect characteristic of rolling contact deflection.

Since the wall positions are some distance from the track, it is expected that the 1.0 Hz spectral peak would be less evident. Comparison of wall and center island acceleration spectra shown in Fig. 3.12 bears this out.

It should also be pointed out that the measurement of low passage frequency levels is not subject to the confidence limits of Fig. 3.6. These confidence limits apply to a stationary random process, whereas the passage frequency levels are from a deterministic excitation mechanism; i.e., the passage of various specific train components, and are exact within limits of small transducer and electronics errors. Only the wheel/rail roughness is assumed to be random and the confidence limits mentioned are applicable only insofar as Gaussian Statistics validly describe the excitation.

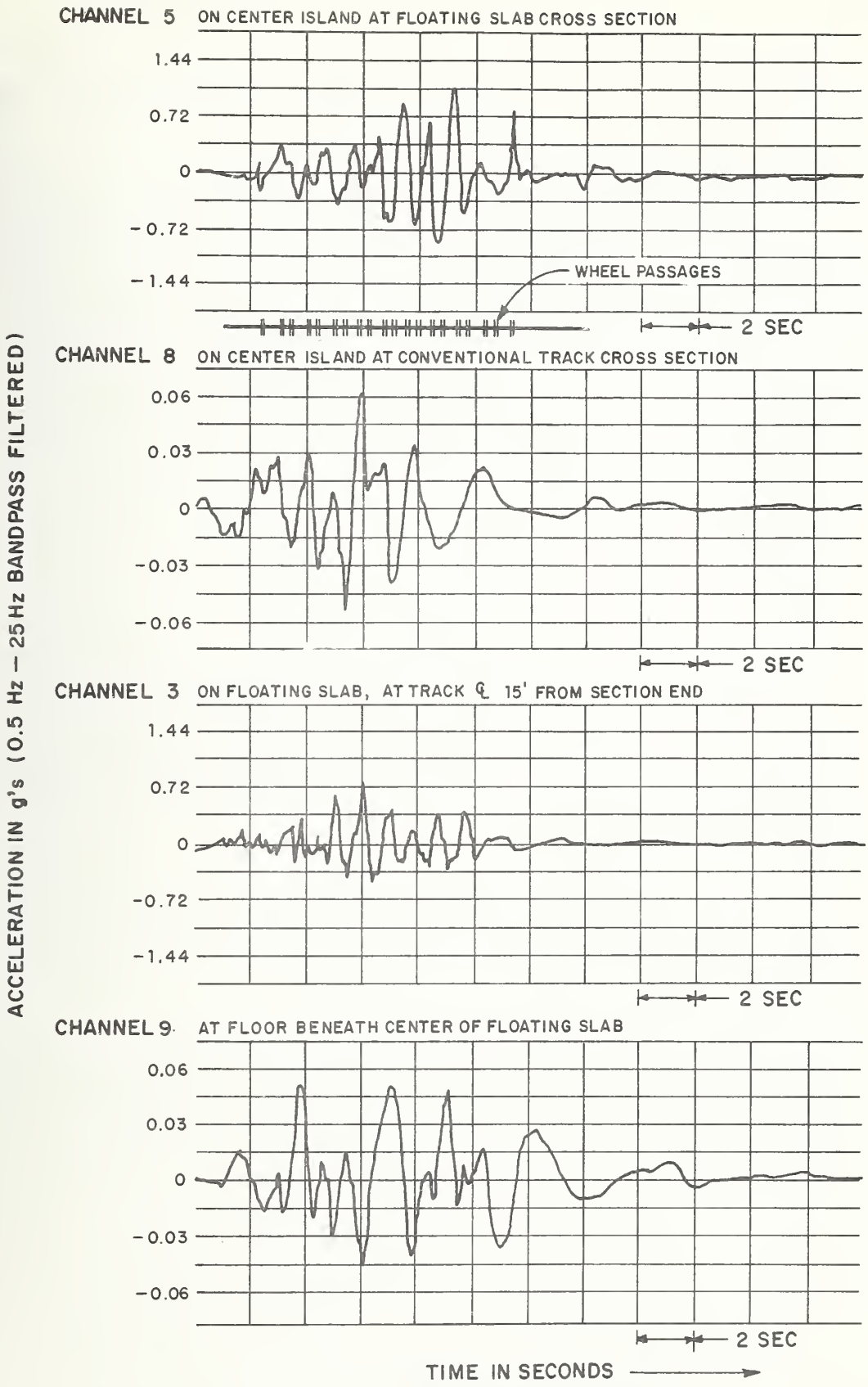

FIGURE 3.15 AC ACCELERATION SIGNALS MEASURED AT POINTS 5, 8, 3 AND 9.

3.8 Slab Support Damping

The damping of the slab supporting elements plays an important role in determining the forces transmitted to the tunnel floor. Prior to construction of the floating slab, tests were run to determine the stiffness and damping of the support pads [11]. The results showed the pad stiffness to be in the range 10,740 to 30,650 lbs/in depending on load. The stiffness for load corresponding to the slab weight is approximately 12,000 lbs/in. The damping of the pads was in the range 2 to 2.4% of critical damping.

The measured values of Insertion Loss show a negative peak of -6.3 dB at the slab resonance frequency. From the analytical model this would indicate a damping that is 30% of critical damping.

The discrepancy between these two damping values may be explained by the addition of Consolidated Kinetics Transidampers 10 ft. on centers at the edges of the slab. These were installed after the design shown in Figs. 3.2 and 3.3 and before our measurements. The damping of the Transidampers has not been measured as part of this study and data were not available.

3.9 Conclusions for the Field Study

The floating slab in NYC is quite effective in reducing the forces transmitted to the tunnel floor at frequencies above 25 Hz. However, the slab has a slightly detrimental effect near its resonant frequency (16 Hz). Fortunately this frequency is at a point where acceleration levels of the tunnel are at a minimum, as shown in Figs. 3.7 and 3.12. The Insertion Loss for vibration of the tunnel wall is similar to that for vibration of the center island above 20 Hz. Insertion Loss for wall vibration at lower frequencies was not determined because of limitations in the accelerometer electronics at the wall location near the conventional track section. However, at these low frequencies the wall levels at the floating slab track section were shown to be much lower than the floor acceleration levels. The question arises as to which contributes more to vibration transmission to neighboring buildings. In any case the Insertion Loss measured at the center island should be representative of the vibration isolation effect of an infinite slab.

The effect of the floating slab becomes less evident as the measurement position moves further from the track. The indication is that the vibration isolation of the slab is not fully realized in neighboring buildings because it is shorter than the trains. Further measurements would be necessary in order to formulate a slab length criteria for reducing vibration transmission to neighboring buildings.

The vibration levels at and near 1 Hz are quite high. These levels are believed to be due to the passage of the static load of the train at the car passing frequency, which is calculated to be 0.98 Hz. Vibration levels on the tunnel wall at and near 1 Hz are approximately 30 dB below the levels on the center island and are only slightly higher than levels at higher frequencies. The importance of these very low frequency (1 Hz) vibrations in terms of vibration transmission to neighboring buildings has not been determined.

4. CONCLUSIONS AND DESIGN RECOMMENDATIONS

The work described in this report has focused on a model to predict the vibration isolation (or reduction) provided by a floating slab or tie track. In Section 2 we have shown the development of a model which allows us to relate the forces acting on the tunnel floor to the forces applied at the wheel/rail contact points. Within the limitations of the present study, we did not extend the model so that the response of the tunnel floor could be predicted or so that the forces on the tunnel floor could be predicted without knowing the forces on the rail. Because of this limitation we could not use data from the field study to verify the analytical model. We had hoped to use rail and slab vibration data together with data on rail fastener and slab support pad stiffnesses to calculate the forces acting on the slab. However, we were unable to do this because we could not collect rail vibration data at a sufficient number of locations so as to specify the spatial distribution of the vibration levels.

A basic question that must be answered before the analytical model can be applied is how the tunnel responds to the dynamic forces applied by the slab supports. If we assume the tunnel floor to be much stiffer than the slab then the dynamic forces with a short wavelength in space (high wavenumber) will be less effective in exciting the tunnel than the forces

with long wavelength. In the limit, we can assume that forces due only to vibration of the slab in its 1st crossmode (n=1) and for k_x=0 are important. In this case the analytical prediction model yields the result that the force transmissibility, the ratio of the amplitudes of the force on the tunnel floor to the force on the rail, is given approximately by

$$T_F(f) = \left[\frac{(1 + \delta_s^2)}{\left(\frac{f^2}{f_{os}^2} - 1\right)^2 + \delta_s^2} \right]^{\frac{1}{2}} \qquad (4.1)$$

where δ_s is the slab support damping loss factor, f_{os} is the resonance frequency of the rigid slab on the support stiffness, and f is the frequency in Hertz. This result is identical to that given by the simple single-degree-of-freedom model shown in Fig. 1.1.

The expression given by Eq. 4.1 is for the case when the damping of the slab supports is of the 'solid' type. In many cases the damping mechanism is better modeled by a viscous damping factor, ζ_s, which is related to the solid type damping loss factor by [8]

$$2\zeta_s f = \delta_s f_{os} \qquad (4.2)$$

The force transmissibility for viscous damping is found by substituting Eq. 4.2 in Eq. 4.1.

In the most general case the damping coefficient is frequency dependent and cannot be modeled by either the solid type or the viscous type over the entire frequency range of interest. In this case, we let δ_s or ζ_s be a function of frequency. The force transmissibility is still obtained from Eq. 4.1.

The results of our field measurements in New York support the validity of the assumption that the force transmissibility given by the single-degree-of-freedom system can be used to predict the performance of a typical slab in reducing the tunnel vibration. However, it must be pointed out that in very lightly damped systems, the vibration induced by higher-order slab crossmodes and at higher wavenumbers may degrade the slab performance. The extent of the degradation can be formed by using the analysis presented in Section 2.

Floating tie systems should give the same or better performance as given by long slabs, since wave propagation down the slab is inhibited. If we consider only the rigid body response of the ties, i.e., no bending deformation across

the tracks, then the performance of the floating-tie system can also be predicted using the results from the single-degree-of-freedom model.

A number of design recommendations can be made based on the results of this study. The stiffness of the floating slab support elements* should be selected so that the deflection of the rail under anticipated train loads is within limits set by safety and ride comfort. The mass per unit length of the floating slab or floating-tie system should be set so that the resonance frequency of the slab on ties on their supporting elements is in the range 8 to 25 Hz. The performance of the 8 Hz system in reducing vibration will be 5 to 10 dB better than that of the 25 Hz system.

The resonance frequency should not be set below 8 Hz because of the possible amplification of the low frequency vibration which is caused by the passage of the static train load. On the other hand the resonance frequency should not be set above 25 Hz because of possible amplification of the vibration in the important 31.5 Hz octave band.

As a general rule the mass per unit length of the floating-tie system must be greater than that of a floating slab. This is due to the fact that the rail deflection under

*including the effective stiffness of the air trapped under the slab

the train load is reduced by the bending stiffness of the slab, thereby allowing the slab supports to have less stiffness. It follows that the mass required to achieve a given resonance frequency will be less for the slab than for the tie system.

Damping of the slab supports also plays an important role in determining the vibration reduction. The damping should be as high as possible to limit the amplification of the vibration at the resonance frequency. However, in many viscoelastic materials the damping modulus is frequency dependent and is best modeled by a viscous damping mechanism. Then, as shown in Fig. 1.2, high values of damping decrease the performance of the floating slab or tie system at frequencies above the resonance frequency. The designer should strive to use materials for which the damping modulus and the Young's modulus do not increase with increasing frequency.

REFERENCES

[1] Manning, J. E., et al, "Noise Prediction Models for Elevated Rail Transit Structures," Report No. UMTA-MA-06-0025-75-12, August 1975.

[2] Manning, J. E., Cann, R. G., and Fredberg, J. J., "Prediction and Control of Rail Transit Noise and Vibration — A State-of-the-Art Assessment," Report No. UMTA-MA-06-0025-74-5, April 1974, PB233363/AS.

[3] Bender, E. K., "Noise and Vibration of Resiliently Supported Track Slabs," J. Acoust. Soc. Am., Vol. 55, No. 2, 1974.

[4] Meisenholder, S. G. and Weidlinger, P., "Dynamic Interaction Aspects of Cable-Stayed Guideways for High Speed Ground Transportation," ASME, Paper No. 74-AUT-R, 1974.

[5] Bender, E. K. and Remington, P. J., "The Influence of Rails on Train Noise," J. Sound & Vib., Vol. 37, No. 3, p. 321-334, December 1974.

[6] See, for example, Section 3.4 of Reference 1.

[7] Crede, C. E., "Principles of Vibration Control," Chapter 12 of Handbook of Noise Control, edited by C. M. Harris, McGraw-Hill, New York, New York, 1957.

[8] Ungar, E. E., "Damping of Panels," Chapter 14 of Noise and Vibration Control, edited by L. L. Beranek, McGraw-Hill, New York, New York, 1971.

[9] Remington, P. J., et al., "Wheel/Rail Noise and Vibration Control," Report No. UMTA-MA-06-0025-73-15, May 1974.

REFERENCES (CONCLUDED)

[10] Paolillo, A., "Performance of Floating Track Slab Constructed Under Contract T-163," New York Transit Authority Inter-Office Memorandum, December 1973.

[11] Tests carried out by Columbus Testing Laboratory, Inc., for Consolidated Kinetics Corporation and Bonaco Construction Company, Inc., as specified by the New York Transit Authority, 1973.

APPENDIX A: REPRESENTATIVE VALUES OF PARAMETERS

Rail:

$$\rho_r = 34 \text{ lb/ft}$$

$$E_r = 4.32 \times 10^9 \text{ lb/ft}^2 = 30 \times 10^6 \text{ lb/in}^2$$

$$I_r = 49 \text{ in}^4 = 2.363 \times 10^{-3} \text{ ft}^4$$

Slab:

$$h = 1 \text{ ft}$$

$$L = 10 \text{ ft}$$

$$\rho_s = 1.0 \text{ lb/ft}^2$$

$$E_s = 3.5 \times 10^6 \text{ lb/in}^2 = 5.04 \times 10^8 \text{ lb/ft}^2$$

$$\omega_{os} = 62.8 \text{ rad/sec.}$$

In addition the values of various subsidiary parameters are as follows:

$$\kappa_1 \equiv \frac{K_r}{E_r I_r} = .0410 \text{ ft}^{-4}$$

$$\kappa_2 \equiv \frac{\rho_s \omega_{or}^2}{D} = .0430 \text{ ft}^{-4}$$

$$E_r I_r = 1.02 \times 10^7 \text{ lb-ft}^2$$

$$D = 4.3 \times 10^7 \text{ lb-ft}$$

$$\beta \equiv \rho_r/\rho_s L = .0226$$

$$\frac{\Delta_n}{\psi_n(y_o)} = 2\sqrt{\kappa_1 \kappa_2 \beta} = .0217 \text{ ft}^{-4}$$

APPENDIX B: ORTHOGONALITY OF THE SLAB MODES

The free, undamped motion of the slab is governed by

$$D\left[\frac{\partial^4}{\partial x^4} + 2\frac{\partial^4}{\partial x^2 \partial y^2} + \frac{\partial^4}{\partial y^4}\right] w + k_s w + \rho_s \frac{\partial^2 w}{\partial t^2} = 0 \qquad (B.1)$$

The free end conditions on the edges of the slab imply the following boundary conditions

$$\frac{\partial^2 w}{\partial y^2} + \mu \frac{\partial^2 w}{\partial x^2} = 0, \quad \frac{\partial^3 w}{\partial y^3} + (2-\mu)\frac{\partial^3 w}{\partial x^2 \partial y^2} = 0; \; y=0,L \qquad (B.2)$$

When Eq. 2.3 is substituted into the above, it is found that the ψ_n must satisfy

$$\frac{d^4\psi_n}{dy^4} - 2k_x^2 \frac{d^2\psi_n}{dy^2} = \gamma_n^4 \psi_n \qquad (B.3)$$

with the boundary conditions:

$$\frac{d^2\psi_n}{dy^2} = \mu k_x^2 \psi_n, \quad \frac{d^3\psi_n}{dy^3} = (2-\mu)\, k_x^2 \frac{d\psi}{dy} \qquad (B.4)$$

for $y = 0, L$

where

$$\gamma_n^4 = \alpha_n^4 - k_x^4 \qquad (B.5)$$

and α is given in terms of the frequency by Eq. 2.5a.

The essential question concerns the orthogonality of $\psi_n(y,k_x)$ and $\psi_m(y,k_x)$ for a given k_x. That is, k_x is a parameter which is fixed during the course of this discussion. The eigenvalue problem represented by Eq. B.3 and Eq. B.4 thus determines discrete values of γ_n^4 in terms of k_x, one γ_n^4 for each distinct ψ_n.

To investigate orthogonality, consider the quantity

$$\int_0^L \left(\frac{d^4\psi_n}{dy^4} - 2k_x^2 \frac{d^2\psi_n}{dy^2}\right) \psi_m \, dy$$

where $n \neq m$.

Integrating by parts, one has

$$\int_0^L \left(\frac{d^4\psi_n}{dy^4} - 2k_x^2 \frac{d^2\psi_n}{dy^2}\right) \psi_m dy = \left[\psi_m(\psi_n''' - 2k_x^2 \psi_n')\right]_0^2$$

$$- \left[\psi_m'(\psi_n' - 2k_x^2\psi_n)\right]_0^L + \left[\psi_n'\psi_m''\right]_0^L - \left[\psi_n\psi_m'''\right]_0^L$$

$$+ \int_0^L \psi_n(\psi_m'''' - 2k_x^2\psi_m'') \, dy \qquad \text{(B.6)}$$

where the primes denote differentiation with respect to y. Substituting the boundary conditions (Eq. B.4) for ψ_n into Eq. B.6 gives:

$$\int_0^L [(\psi''''_n - 2k_x^2\psi''_n)\psi_m - (\psi''''_m - 2k_x^2\psi''_m)\ \psi_n]\ dy$$

$$= [\ \psi'_n(\psi''_m - \mu k_x^2\psi_m)]_0^L - [\psi_n(\psi'''_m + k_x^2(\mu-2)\psi'_m)]_0^L \qquad (B.7)$$

First, note that from Eq. B.3 that the left hand side becomes

$$(\gamma_n^4 - \gamma_m^4) \int_0^L \psi_n\ \psi_m\ dy$$

Note also that ψ_m must satisfy the boundary conditions Eq. B.4 so that the right hand side of Eq. B.7 is identically zero. Hence, we obtain

$$(\gamma_n^4 - \gamma_m^4) \int_0^L \psi_n(k_x,y)\psi_m(k_x,y)\ dy = 0 \qquad (B.8)$$

which states that for each value of k_x, the corresponding set of eigenfunctions of Eq. B.3 are orthogonal.

APPENDIX C: PARTIAL DIFFERENTIAL EQUATIONS OF MOTION AND THEIR SOLUTION

Here we set forth the mathematical background for the work presented in Section 2. The basic idealizations used for this calculation are given on Page 14. In addition we limit our consideration here to the case in which the rail is excited by a point force, q(t). With these assumptions and the coordinates and conventions shown in Fig. 2.1, the equations of motion for the rail displacement, ξ, and slab displacement, w, are

$$E_r I_r \frac{\partial^4 \xi}{\partial x^4} + \rho_r \frac{\partial^2 \xi}{\partial t^2} + K_r^* [\xi - w(x,y_o,t)] = q(t)\ \delta(x) \qquad (C.1a)$$

$$D\left[\frac{\partial^2}{\partial x^2} + \frac{\partial^2}{\partial y^2}\right]^2 w + K_s^* w + \rho_s \frac{\partial^2 w}{\partial t^2} = K_r^* [(\xi - w)]\ \delta(y - y_o) \qquad (C.1b)$$

The stress-free condition on the edges y = 0, L of the slab give rise to the following boundary conditions:

$$\frac{\partial^2 w}{\partial y^2} + \mu \frac{\partial^2 w}{\partial x^2} = 0 \quad \text{at } y = 0,L \qquad (C.2a)$$

$$\frac{\partial^3 w}{\partial y^3} + (2 - \mu) \frac{\partial^3 w}{\partial x^2 \partial y} = 0 \quad \text{at } y = 0,L \qquad (C.2b)$$

where μ is Poisson's ratio for the slab material.

The total system response is formulated by expressing the equations of motion, Eqs. C.1, in terms of the Fourier transforms with respect to x of the rail and slab displacement,

$$\tilde{\xi}(k_x, t) = \int_{-\infty}^{\infty} dx\, e^{-jk_x x}\, \xi(x,t) \tag{C.3a}$$

$$\tilde{w}(k_x, y, t) = \int_{-\infty}^{\infty} dx\, e^{-jk_x x}\, w(x,y,t) \tag{C.3b}$$

Then, we note that $\tilde{w}$ may be generally expressed as

$$\tilde{w}(k_x, y, t) = \sum_{n=1}^{\infty} \tilde{w}_n(k_x, t)\ \psi_n(y) \tag{C.4}$$

where $\tilde{w}_n$ are the <u>modal coordinates</u> of the slab motion. Substituting Eq. C.4 into Eqs. C.1, multiplying both sides of Eq. C.1b by $\psi_m(y)$ (for some m) and integrating over y = 0,L gives us the equations of motion for the rail displacement and the slab modes. Finally, neglecting coupling terms due to damping, we find

$$\frac{\kappa_1}{\omega_{or}^2}\ddot{\tilde{\xi}} + [k_x^4 + \kappa_1(1-j\delta_r)]\,\tilde{\xi} - \kappa_1 \sum_{m=1}^{\infty} \tilde{w}_m \psi_m(y_o) = Q(t) \tag{C.5a}$$

$$\frac{\kappa_2}{\omega_{or}^2}\ddot{\tilde{w}}_n + \left[k_x^4 + \gamma_n^4 + \frac{\omega_{os}^2}{\omega_{or}^2}\kappa_2(1-j\delta_s) + \beta\kappa_2(1-j\delta_r)\ \psi_n^2(y_o)\right]\tilde{w}_n$$

$$= \kappa_2\beta\ \psi_n(y_o)\ \left[\tilde{\xi} - \sum_{m\neq n} \tilde{w}_m \psi_m(y_o)\right] \tag{C.5b}$$

where $Q(t) = q(t)/EI$

and $\beta = \frac{\rho_r}{L\rho_s}$

For floated slab systems it is realistic to assume both κ_1 and κ_2 are much less than 1 and that β is much less than 1. For β small, the total system behavior is determined primarily by the relative positions of uncoupled rail and slab dispersion curves shown for a typical case in Fig. 2.3.

Explicit solutions to Eqs. C.5 may be found by expressing these equations in terms of the space-time transforms of ξ and w. We define

$$\hat{\xi} = \int_{-\infty}^{\infty} dt\ e^{j\omega t}\ \tilde{\xi}(k_x, t) \tag{C.6a}$$

$$\hat{w}_n = \int_{-\infty}^{\infty} dt\ e^{j\omega t}\ \tilde{w}_n(k_x, t) \tag{C.6b}$$

$$\hat{Q} = \int_{-\infty}^{\infty} dt\ Q(t)\ e^{j\omega t} \tag{C.6c}$$

In terms of these quantities, Eqs. C.5 become

$$A\hat{\xi} - \kappa_1 \sum_{m=1}^{\infty} \hat{w}_m \psi_m(y_o) = \hat{Q}(\omega) \tag{C.7a}$$

$$b_n \hat{w}_n = \kappa_2 \beta \psi_n(y_o) [\hat{\xi} - \sum_{m=1}^{\infty} \hat{w}_m \psi_m(y_o)] \tag{C.7b}$$

where

$$A = k_x^4 - k_r^4 - j\delta_r \kappa_1 \tag{C.8a}$$

$$b_n = k_x^4 + \gamma_n^4 - \alpha^4 - j\kappa_2 \zeta_{sn} \frac{\omega_{os}^2}{\omega_{or}^2} \tag{C.8b}$$

$$\zeta_{sn} = \delta_s + \delta_r \beta \frac{\omega_{or}^2}{\omega_{os}^2} \psi_n^2 \tag{C.8c}$$

This infinite set of equations may be solved explicitly for $\hat{\xi}$, and each of the $\hat{w}_m$. From these results it can be shown that in the wavenumber and frequency region in which the uncoupled rail dispersion curve passes closer to the n^{th} slab mode dispersion curve than to any other mode, then $\hat{\xi}$ and $\hat{w}_n$ can be approximately obtained by considering the interaction of the rail with the n^{th} mode alone. This mode by mode interaction approximation allows relatively simple solutions to be obtained.

To find the spatial characteristics of response, it is assumed that only the first slab mode is significantly excited although qualitative results will hold in the general case.

First, we neglect all quantities except $\hat{\xi}$ and $\hat{w}_1$ in Eqs. C.7 to obtain

$$\hat{\xi} = \hat{H}_{\xi}(k_x, \omega)\ \hat{q} \tag{C.9a}$$

$$\hat{w}_1 = \hat{H}_{w1}(k_x, \omega)\ \hat{q} \tag{C.9b}$$

where

$$E_r I\ \hat{H}_{\xi} = B_1 \frac{1}{\mathcal{D}} \tag{C.10a}$$

$$E_r I\ \hat{H}_{w1} = \beta\kappa_2\psi_1 \frac{1}{\mathcal{D}} \tag{C.10b}$$

and where

$$\mathcal{D} = B_1 A - \kappa_1\kappa_2\beta\psi_1^2 \tag{C.10c}$$

$$A = k_x^4 - k_r^4 - j\delta_r\kappa_1 \tag{C.10d}$$

$$B_1 = k_x^4 - \alpha^4 - j\kappa_2 \frac{\omega_{os}^2}{\omega_{or}^2}\zeta_{s1} + \kappa_2\beta\psi_1^2 \tag{C.10e}$$

Expanding the denominator, $\mathcal{D}$, in k_x^4, it is found to be factorable in the form:

$$(k_x^4 - k_r^4 + \lambda_r - j\Delta_r)(k_x^4 - \alpha^4 + \kappa_2\beta\psi_1^2 - \lambda_r - j\Delta_s) \quad (C.11)$$

where

$$\Delta_r = \delta_r\kappa_1 - \lambda_I$$

$$\Delta_s = \kappa_2 \frac{\omega_{os}^2}{\omega_{or}^2} \zeta_s + \lambda_I$$

$$\lambda_r = \tfrac{1}{2}[\Lambda - \sqrt{\Lambda^2 + 4\kappa_1\kappa_2\beta\psi_1^2}]$$

$$\lambda_I = \tfrac{1}{2}[\delta_r\kappa_1 - \kappa_2 \frac{\omega_{os}^2}{\omega_{or}^2} \zeta_{sl}] \frac{\sqrt{\Lambda^2 + 4\kappa_1\kappa_2\beta\psi_1^2} - \Lambda}{\sqrt{\Lambda^2 + 4\kappa_1\kappa_2\beta\psi_1^2}}$$

$$\Lambda = k_r^4 - \alpha^4 + \kappa_2\beta\psi_1^2$$

Now consider the behavior of the time transforms of ξ and w_1; i.e.,

$$\tilde{\xi} = \frac{1}{2\pi} \int_{-\infty}^{\infty} dk_x \, e^{jk_x x} \hat{\xi}, \quad \tilde{w}_1 = \frac{1}{2\pi} \int_{-\infty}^{\infty} dk_x \, e^{jk_x x} \hat{w}_1 \quad (C.12)$$

For a given ω, Eqs. C.10 and C.11 show that the magnitudes of the integrands are sharply peaked at the intersections of uncoupled rail and slab dispersion curves with ω = constant. The parameters Δ_r and Δ_s represent the "spread" of these peaks about their maxima, while $|\Lambda - 2\lambda_r|$ is the separation b[illegible]

maxima and is always greater than $2\sqrt{\kappa_1\kappa_2\beta}\ \psi_1$. If damping is sufficiently small that $2\sqrt{\kappa_1\kappa_2\beta}\ \psi_1 >> \Delta_r$ or Δ_s (i.e., coupling forces are much larger than damping forces); then the time transforms of rail and slab response are approximately:

$$\frac{\tilde{\xi}}{\hat{Q}} = \frac{\Lambda - \lambda_r}{\Lambda - 2\lambda_r} I_r - \frac{\lambda_r}{\Lambda - 2\lambda_r} I_s \tag{C.13a}$$

$$\frac{\tilde{w}}{\hat{Q}} = \frac{\beta\kappa_2\psi_1}{\Lambda - 2\lambda_r} \{I_r - I_s\} \tag{C.13b}$$

where

$$I_r \simeq \begin{cases} \dfrac{\sqrt{2}}{4|\tilde{k}_r|^3} e^{-\frac{1}{\sqrt{2}}|\tilde{k}_r|x} \left[\cos \dfrac{|\tilde{k}_r|}{\sqrt{2}} x + \sin \dfrac{|\tilde{k}_r|}{\sqrt{2}} x\right]; \\ \qquad \tilde{k}_r^4 < 0 \ \& \ |\tilde{k}_r^4| >> \Delta_r \end{cases} \tag{C.14a}$$

$$\begin{cases} \dfrac{1}{4\sqrt{2}\Delta_r^{3/4}} \left[\left(1 + \dfrac{1}{\sqrt{2}}\right)^{1/2} + j\left(1 - \dfrac{1}{\sqrt{2}}\right)^{1/2}\right] \\ * e^{-\frac{1}{\sqrt{2}} \Delta_r^{1/4} \left[j\left(1 + \frac{1}{\sqrt{2}}\right)^{1/2} - \left(1 - \frac{1}{\sqrt{2}}\right)^{1/2}\right]} \\ \qquad + j\, e^{-x \frac{1}{\sqrt{2}} \Delta_r^{1/4} \left[j\left(1 - \frac{1}{\sqrt{2}}\right)^{1/2} + \left(1 + \frac{1}{\sqrt{2}}\right)^{1/2}\right]} \ ; \ |\tilde{k}_r^4| << \Delta_r \end{cases} \tag{C.14b}$$

$$\begin{cases} \dfrac{1}{4} \dfrac{1}{|\tilde{k}_r|^3} \left(-e^{-x|\tilde{k}_r|} + j\, e^{x\left(j|k_r| - \frac{\Delta_r}{4|\tilde{k}_r|^3}\right)}\right); \\ \qquad \tilde{k}_r^4 > 0 \quad |\tilde{k}_r|^4 >> \Delta_r \end{cases} \tag{C.14c}$$

$$I_s = I_r \text{ as } \tilde{k}_r \text{ approaches } \tilde{\alpha} \text{ and } \Delta_r \text{ approaches } \Delta_s \quad \text{(C.15)}$$

and where

$$\tilde{k}_r^4 = k_r^4 - \lambda_r, \quad \tilde{\alpha}^4 = \alpha^4 - \kappa_2 \beta \psi_1^2 + \lambda_r$$

Both rail and slab motions are seen to consist of two parts. One part, I_r, is akin to the response of the uncoupled rail-fastener system to a point force excitation and the other part, I_s, closely resembles the response of the uncoupled slab system. In $\tilde{\tilde{w}}$, these two parts make a nearly equal contribution, while $\tilde{\tilde{\xi}}$ consists mainly of I_r.

I_r is little affected by damping (which serves only to attenuate the propagating bending waves) except when ω is less than a damping bandwidth away from $\omega = \omega_{or}\sqrt{1 + \lambda_r/\kappa_1} \simeq \omega_{or}$. Near this frequency, the amplitude of I_r rises to a sharp maximum limited only by the damping. Similar remarks apply to I_s, except that its maximum occurs at

$$\omega = \omega_{os}\sqrt{1 + \frac{\omega_{or}^2}{\omega_{os}^2}(\beta\psi_1^2 - \lambda_r/\kappa_2)} \simeq \omega_{os}$$

Thus both $|\tilde{\tilde{\xi}}|$ and $|\tilde{\tilde{w}}_1|$ show resonant maxima near ω_{or} and at ω_{os}.

Another topic of interest here is the behavior at

structural wave coincidence. Strictly speaking, structural wave coincidence occurs when the dispersion curve of the rail motion with slab displacement blocked crosses the dispersion curve of the slab motion with the rail displacement blocked. The resulting condition for coincidence is

$$k_r^4 = \alpha^4 - \kappa_2\beta\psi_1^2 \quad \text{or} \quad \Lambda = 0 \tag{C.16}$$

For β small, this means that an approximate coincidence condition is simply the intersection of the uncoupled rail and slab dispersion curves determined above.

It is instructive to tie the coincidence condition to the general behavior of the coupled system mode dispersion curves. These are given by the zeroes of $\mathcal{D}$ in Eq. C.10 in the absence of damping. Denote the coincidence wavenumber and frequency by k_{xc} and ω_c. If we consider wavenumbers and frequencies far from k_{xc} and ω_c so that $|\Lambda| >> \kappa_1\kappa_2\beta\psi_1^2$ then λ_r in Eq. C.11 is of order $\kappa_1\kappa_2\beta/\Lambda^3$. Thus, in this case and for small β, the zeroes of Eq. C.11 are $k_x^4 \simeq k_r^4$ and $k_x^4 \simeq \alpha^4$, i.e., they are on the uncoupled system dispersion curves. The branch $k_x^4 \simeq k_r^4$ occurring for $\omega < \omega_c$ becomes $k_x^4 \simeq \alpha^4$ for $\omega > \omega_c$ and vice-versa. If coincidence occurs at all, Λ must achieve a minimum for some k_x and ω. From Eq. C.11 this occurs at $\Lambda = 0$; precisely the point of coincidence. This condition also implies the minimum separation (along

k_x) of the coupled system dispersion curves, equal to

$$|\Lambda - 2\lambda_r|_{min} = 2|\lambda_r|_{\Lambda=0} = 2\sqrt{\kappa_1\kappa_2\beta}\ \psi_1 \tag{C.17}$$

It then follows that the total kinetic energy of rail or slab (related to the integrals $\int dk_x|\hat{H}_{w1}|^2$, $\int dk_x|\hat{H}_{\xi}|^2$ is greatest at the coincidence frequency, since here the poles of $|\hat{H}_{w1}|^2$ or $|\hat{H}_{\xi}|^2$ are closest together.

Finally, we give the form of $\tilde{\tilde{\xi}}$ and $\tilde{\tilde{w}}_1$ at coincidence. For the present calculation, we assume that $|\tilde{k}_r^4|$ and $|\alpha^4|$ >> Δ_r and Δ_s. Then at coincidence:

$$\Delta_r = \Delta_s = \tfrac{1}{2}(\delta_r\kappa_1 + \kappa_2 \frac{\omega_{os}^2}{\omega_{or}^2}\ \zeta_s \tag{C.18a}$$

$$\lambda_r = -\sqrt{\kappa_1\kappa_2\beta}\ \psi_1 \tag{C.18b}$$

and, from Eq. C.15

$$\frac{\tilde{\tilde{\xi}}}{\hat{Q}} = \frac{1}{4}\frac{1}{|k_r|^3}\left\{-e^{-x|k_r|}\cosh\left(\frac{|\lambda_r|x}{4|k_r|^3}\right)\right.$$

$$\left. + j\, e^{x(j|k_r| - \frac{1}{4}\Delta_r/|k_r|^3}\cos x\left(\frac{|\lambda_r|}{4|k_r|^3} - j\,\frac{3}{16}\,\frac{\Delta_r|\lambda_r|}{|k_r|^7}\right)\right\} \tag{C.19a}$$

$$\frac{\tilde{w}_1}{\hat{Q}} = \frac{1}{4}\sqrt{\frac{\beta\kappa_2}{\kappa_1}}\ \frac{1}{|k_r|^3}\left\{e^{-x|k_r|}\sinh\left(\frac{|\lambda_r|x}{4|k_r|^3}\right)\right.$$

$$\left. -e^{x(j|k_r| - \frac{1}{4}\Delta_r/|k_r|^3)}\sin x\left(\frac{|\lambda_r|}{4|k_r|^3} - j\frac{3}{16}\frac{\Delta_r|\lambda_r|}{|k_r|^7}\right)\right\} \qquad \text{(C.19b)}$$

to within terms of order $|\lambda_r|/|k_r|^4$.

APPENDIX D : REPORT OF INVENTIONS

This report presents the development of a model to predict the performance of floating slab tracks. After a diligent review of the work performed under this contract, it was found that no new inventions, discoveries, or improvements of inventions were made.